universität wien

MASTERARBEIT / MASTER'S THESIS

Titel der Masterarbeit / Title of the Master's Thesis

„Screening of natural products and derivatives for their influence on intracellular cAMP-levels for immunomodulation“

verfasst von / submitted by

Dorothee Maria Michels, BSc

angestrebter akademischer Grad / in partial fulfilment of the requirements for the degree of

Magistra pharmaciae (Mag.pharm.)

Wien, 2022 / Vienna 2022

Studienkennzahl lt. Studienblatt / degree programme code as it appears on the student record sheet:	UA 066 605
Studienrichtung lt. Studienblatt / degree programme as it appears on the student record sheet:	Masterstudium Pharmazie
Betreut von / Supervisor:	Univ.-Prof. Dr. Verena Dirsch
Mitbetreut von / Co-Supervisor:	Mag. Dr. sc. ETH Alexander Franz Perhal

Abstract

The second messenger cyclic adenosine monophosphate (cAMP) plays a pivotal role in the innate as well as in the adaptive immune system. Hence, the modulation of the cAMP levels is the hub for several therapeutic strategies ranging from inflammatory to autoimmune diseases. The intracellular cAMP level can be affected via different mechanisms, for instance, the stimulation of G-protein coupled receptors (GPCRs) by ligands or the inhibition of the cAMP-metabolizing enzymes phosphodiesterases (PDEs). The discovery of new compounds which affect the cAMP levels would be a promising approach to examine further treatment strategies.

Numerous natural compounds from the DNTI project as well as synthesized substances were screened *in vitro* in modified HEK293 cells to determine their potential influence on the cAMP levels. Therefore, two different screening assays were performed. A target-based screening was conducted to assess a potential agonistic activity on the bile acid receptor TGR5, while a phenotypic screening served to examine substances for potential PDE inhibitory activity. A Epac-based FRET biosensor assay was used in both screenings. Several compounds could be identified which significantly increased the cAMP levels in the TGR5 target-based screening. In addition, CRE-luciferase assays were performed to confirm their effect on the cAMP/CRE pathway in another assay. A FXR-Gal4-luciferase assay was conducted to examine the selectivity for the TGR5 receptor. In previous phenotypic screenings an increase of the cAMP levels was observed with the magnolol derivatives LRK071 as well as AH-17 and the leoligin derivative 2743. To find out if these compounds have a potential PDE inhibitory activity, a kinetic cAMP measurement and a fluorescence polarization assay with the enzyme PDE4B2 were performed. Furthermore, the compounds' anti-inflammatory properties were tested in the Griess assay as well as in the NF-κB luciferase assay. Promising results were obtained in the Griess assay and in the kinetic cAMP measurement, while the results were not significant and difficult to interpret in the NF-κB luciferase assay as well as in the fluorescence polarization assay. Also, other mechanisms of action of LRK071 were tested, such as a potential PKA inhibitory activity with a CRE-luciferase assay, a potential receptor stimulation with a kinetic cAMP measurement as well as an adenylate cyclase stimulation in a phenotypic screening. The obtained results of these experiments support the theory that LRK071 might have a potential PDE inhibitory activity. However, further experiments are required to confirm this theory.

Zusammenfassung

Der sekundäre Botenstoff zyklisches Adenosinmonophosphat (cAMP) ist sowohl für das angeborene als auch das erworbene Immunsystem von zentraler Bedeutung. Verschiedene etablierte therapeutische Strategien gegen entzündliche Erkrankungen sowie Autoimmunerkrankungen bauen auf den immunmodulatorischen Eigenschaften des cAMP auf. Dabei gibt es verschiedene Ansätze, den cAMP-Spiegel zu beeinflussen, wie eine Erhöhung des Spiegels durch Rezeptorstimulation durch Liganden oder durch eine Inhibierung des cAMP metabolisierenden Enzyms Phosphodiesterase (PDE). So ist es von großer Relevanz, neue Substanzen zu identifizieren, die durch die Beeinflussung des cAMP-Spiegels neue therapeutische Möglichkeiten bieten.

Zahlreiche natürliche Substanzen vom DNTI-Projekt wie auch synthetisch hergestellte Verbindungen wurden *in vitro* in modifizierten HEK293 Zellen getestet, um deren Einfluss auf den intrazellulären cAMP-Spiegel zu bestimmen. Dabei wurden zwei Screenings mittels der FRET-basierten Fluoreszenzmessung durchgeführt, in welcher das Protein Epac als Biosensor für cAMP diente. Durch das Target-basierte Screening wurden Substanzen auf eine mögliche agonistische Aktivität am Gallensäurerezeptor TGR5 überprüft. Eine Erhöhung des cAMP-Spiegels im phänotypischen Screening wurde auf eine mögliche Hemmung des Enzyms PDE zurückgeführt.

Im TGR5 Target-basierten Screening konnten mehrere Substanzen identifiziert werden, die eine signifikante Erhöhung des cAMP-Spiegels hervorgerufen haben. Um diese Ergebnisse auf den cAMP/CRE-Signalweg zurückzuführen, wurden auch CRE-Luciferase-Assays durchgeführt, die diese Ergebnisse bestätigten. Weiters wurde ein FXR-Gal4-Luciferase-Assay gemacht, um die Selektivität der Substanzen für TGR5 zu überprüfen.

In früheren phänotypischen Screenings wurde bereits eine Erhöhung des cAMP-Spiegels durch die Magnolol-Derivate LRK071 und AH-17 als auch durch das Leoligin-Derivat 2743 beobachtet, welches auf eine mögliche Inhibierung des PDE-Enzyms zurückgeführt wurde. Um dieser Theorie nachzugehen, wurde eine kinetische cAMP-Messung und ein Fluoreszenzpolarisationstest mit dem Enzym PDE4B2 durchgeführt. Zudem wurden die Substanzen auch auf antiinflammatorische Eigenschaften mittels Griess-Assay sowie NF-κB-Luciferase-Assay überprüft. Sehr aussagekräftige Resultate brachten die kinetischen cAMP-Messung sowie der Griess-Assay, während nicht signifikante und unspezifische

Ergebnisse bei dem NF-κB-Luciferase-Assay und der Fluoreszenzpolarisationsmessung herausgekommen sind. Die Substanz LRK071 wurde auch auf mögliche andere Wirkmechanismen überprüft, wie eine mögliche PKA-Inhibierung mittels des CRE-Luciferase-Assays, eine mögliche Rezeptorstimulation mittels der kinetischen cAMP-Messung und eine mögliche Stimulation der Adenylatcyclase mittels des phänotypischen Screenings. Die Ergebnisse dieser drei Experimente untermauern die PDE-Inhibitor-Theorie. Aber dennoch sind weitere Experimente nötig, um den exakten Wirkmechanismus von LRK071 zu identifizieren.

Table of contents

A. Introduction

1 Immune system

Not only bacteria, parasites, or other pathogenic contaminants, which invade the human body, but also, degenerated cells such as tumor cells can be detected and eliminated by the immune system. It comprises a complex network, which consists of different cell types, organs, and soluble proteins. A distinction is made between the innate and the adaptive immune system, which will be described in more detail in the following. (1)

1.1 The innate immune system

The initial immune response to a source of infection involves the immigration of phagocytes, which encompass monocytes, macrophages, and neutrophile granulocytes. These cells are attracted by chemokines. (1) Monocytes differentiate to macrophages in the tissue. With receptors for antibodies and complement, macrophages and neutrophils recognize the opsonized pathogen and thus, phagocytic activity is induced. By exposing the engulfed contaminant to toxic intracellular molecules, like hydroxyl radicals, nitric oxide, superoxide anions, or lysozymes, phagocytes eliminate and destroy the pathogen eventually. Other cells of the innate immune system are natural killer (NK) cells and dendritic cells. (2) NK cells are lymphocytes, which destroy pathogenic cells by perforating the cell membrane. When an immune reaction starts, typical signs of inflammation occur, such as redness, heat, pain, and tumor. (1) Dendritic cells have a key function as antigen-presenting cells. Microorganisms have specific structures on their cell surface, which are known as pathogen-associated molecular patterns (PAMPs). The pattern-recognition receptors (PRRs) of dendritic cells are able to recognize PAMPs. Pattern-recognition receptors are mannose receptors, lipopolysaccharide (LPS) receptors, and members of the molecule family, which is denoted as toll. (2) The cell-mediated innate immune response is supported by the complement system, which belongs to the humoral immune system. It consists of twenty soluble plasma proteins. (1) The complement system can be activated by three different pathways: the classical pathway, the alternative pathway, and lastly, the lectin pathway. (2) Then, the activated complement system forms a membrane-attack-complex, which emerges on the surface of the bacterial cell membrane. The membrane-attack-complex causes the death of the pathogen by perforating its membrane. (1)

The innate and the adaptive immune system work closely together. After the phagocytosis of a contaminant, phagocytes activate the adaptive immune system by producing cytokines and by presenting antigen structures over major histocompatibility complex (MHC) -1 or -2 proteins to T-lymphocytes. (3) To specify this, MHC-1 proteins interact with cytotoxic T-cells, which are characterized by the cluster of differentiation (CD) 8, whereas MHC-2 proteins are recognized by T helper cells, which express CD4. Phagocytic cells initiate one of the first response of the adaptive immune system. (1, 2)

1.2 The adaptive immune system

While the innate immune system cannot induce a selective defense against a particular pathogen, the adaptive immune system can specifically adapt its defense against a particular pathogen. It can even remember the pathogenic antigen to instigate a faster secondary immune response. T- and B-lymphocytes play a fundamental role in the adaptive immune system. Lymphocytes are generated from stem cells in the bone marrow and mature either in the case of T-lymphocytes in the thymus or in the case of B-lymphocytes in the bone marrow. T-lymphocytes are responsible for the cell-mediated defense, whereas B-lymphocytes constitute the adaptive humoral defense. (1)

T-lymphocytes can be classified into T helper cells, cytotoxic T cells as well as regulatory T cells. Each of them has a specific function. T helper cells have specific T-cell receptors (TCR) to recognize antigens presented by MHC-2 proteins of antigen-presenting cells. The T helper cell binds to the complementary antigen-MHC-2 complex. (1, 2) As a result, the antigen-presenting cell secrets interleukin (IL)-1 and thus, the T helper cell is activated. The activation induces the clonal expansion of this specific T cell. Cytotoxic T cells are nearly likewise activated as the T helper cells. Pathogenic cells are selectively destroyed by CD8+ T cells by perforating the cell membrane, similar to the mechanism of NK cells. Regulatory T cells (Tregs) are crucial to stop the T cell immune response at the end of the immune reaction. (1)

B-lymphocytes are significant for the humoral defense since they produce antibodies. On the cell surface of every B- lymphocyte are immunoglobulins (Ig) of the type of IgM. Antigens bind to IgM and the emerged antigen-antibody complex is internalized by the B cell, which then presents a part of the antigen over MHC-2 proteins. Trough the interaction with T helper cells, B cells are activated to plasma cells, and produce different isotypes of antibodies, such as IgA, IgD, IgE, IgG and IgM. (1) The main function of antibodies encompasses the neutralization of

the antigen, the opsonization of the antigen for phagocytic cells of the innate immune system and the activation of the complement system via the classical pathway. To achieve a faster immune response and an alleviated course of disease after a secondary antigen contact, B cells ultimately differentiate to memory B cells. (1,3)

1.3 Inflammation

Inflammation is one of the central processes of the immune defense to eliminate pathogenic and foreign stimuli. (4, 5) Medicine generally distinguishes between acute and chronic inflammation. While acute inflammation is a short-term reaction, which can be caused by tissue damage, noxious substances as well as microbial invasion, chronic inflammation is defined as a long-term reaction, which can last only a few months or even years. Here, several possibilities exist which may cause chronic inflammation, such as pathogenic microorganism, which cannot be sufficiently combated by the immune system, industrial material like silica dust, or recurrent acute inflammation. Additionally, dysfunctions of the immune system itself can be responsible for chronic inflammation as well. To exemplify this, a specific component of the body may be recognized as pathogenic by the immune system due to a malfunction. The immune system then induces an immune response against this particular structure. Consequently, autoimmune disorders like rheumatoid arthritis evolve. (5)

Since chronic inflammatory diseases, such as diabetes, chronic obstructive pulmonary disease (COPD), or cardiovascular diseases like atherosclerosis, are the major causes for death worldwide (5, 6), it is significant to understand the processes of inflammation and to find effective treatments against it.

Inflammation is a dynamic and well-organized process, which consists of different mechanisms including enhanced vasodilatation and vascular permeability as well as migration of neutrophils and macrophages into the infected tissue, which is described by the term diapedesis. (4, 5) In the tissue, macrophages and dendritic cells secrete cytokines such as IL-1 and tumor necrosis factor α (TNFα) to stimulate the production of integrins and selectins in endothelial cells. This enables the diapedesis and migration of circulating leukocytes into the inflamed tissue. (5)

1.4 NF-κB signaling pathway

The nuclear factor kappa-light-chain-enhancer of activated B cells (NF-κB) is a transcription factor, which belongs to the immune system. It is crucial for the regulation of cell growth and survival by activating the immune system and inflammation. NF-κB is located in the cytoplasm of every cell. This transcription factor stands for a group of proteins, which are structurally similar and known as Rel-A (p65), Rel-B, c-Rel (Rel), NF-κB1 (p50) and NF-κB2 (p52). These proteins can build homodimers or heterodimers, which mostly serve to activate gene transcription. These transcription factors can be stimulated through different substances, including viruses, bacteria, stress, cytokines, and carcinogens. When activated, NF-κB translocates to the nucleus, where it regulates the expression of around 400 genes which encode for cytokines, chemokines, enzymes, adhesion molecules and many more. Since NF-κB is of paramount importance for the gene regulation, it certainly can be linked to different diseases, such as atherosclerosis, asthma, cancer, diabetes, AIDS and Alzheimer´s disease. (56)

The NF-κB signal pathway can be classified into the canonical and non-canonical pathway. While the non-canonical pathway is crucial for the development of B and T lymphocytes, the canonical pathway is important for the activation of the immune system and for the initiation of inflammatory processes to inhibit apoptosis. (56)

Toll-like receptors (TLR) are expressed on the cell surface of macrophages, dendritic cells and mucosal epithelial cells and are part of the innate immune system. These receptors detect microbial molecules, including nucleic acids and molecules of the bacterial cell membrane, such as LPS. (56) LPS binds to the LPS-binding protein (LBP) and this complex is recognized by the CD14 cell surface protein of phagocytes, which interacts with TLR-4. (3) After activation of TLR4, a signal cascade starts to combat the infection, whereby the NF-κB canonical signal pathway is stimulated. (56) To continue, because of the activation of TLR-4, this receptor can bind to the cytosolic adaptor protein MyD88, which interacts with the kinase IRAK. This kinase stimulates the kinase TRAF, which activates the IκB kinase (IKK). The cytosolic inhibitor IκB is bound to the transcription factor NF-κB. (3) Altogether seven members of the IκB family exists, namely, IκBα, IκBβ, IκBγ, IκBε, Bcl-3 and Rel-proteins p100 as well as p105. (56) Via the phosphorylation of IκB by IKK, NF-κB is released from IκB and translocates into the nucleus, where it modulates the immune system via altered gene expression. Among others, the production of inflammatory cytokines is increased, like TNFα and interferon-α. These

molecules stimulate macrophages, which perform a respiratory burst. Thereby, bactericidal substances are released, such as hydrogen peroxide (H_2O_2), nitrogen monoxide (NO*), superoxide anion (O_2^-), hypochlorite (OCl^-) and hydroxyl radical (OH^*). (3)

2 G-protein coupled receptor

G-protein coupled receptors (GPCRs) constitute one of the largest families of cell surface receptors. (3) With an impressively contingent of 50-60% of the drug targets, GPCRs play an important role in drug discovery. (7) These receptors channel an extracellular signal through the cell membrane that can ultimately affect gene expression or metabolism via different signaling cascades. (3) With their seven transmembrane helices, GPCRs are anchored in the cell membrane with alternating intracellular and extracellular loops. The extracellularly located NH_2-terminal domain provides docking sides for specific ligands (3,8), for instance hormones, neurotransmitters, or calcium ions. (7) Whereas the intracellular COOH-terminal domain includes phosphorylation sites, which are important for receptor desensitization. (9) The third and fourth intracellular loop connects the receptor directly with the guanine nucleotide-binding regulatory protein (G-protein). The G-protein is a heterotrimeric protein, which consists of three subunits designated as α, β and γ subunit. (3) Various subtypes of the α-subunit could be identified. To mention only a few of them, the α-subunit can be classified into Gαs, Gαi and Gαq. These are crucial for the further signaling pathway in the cell. (3)

When a ligand binds to a GPCR, the receptor changes its conformation and hence it becomes a guanine-nucleotide exchange factor (GEF). As a result, the intracellularly bound heterotrimeric G-protein lowers its affinity to guanosine diphosphate (GDP) and exchanges it with guanosine triphosphate (GTP). The heterotrimeric G-protein now dissociates in two subunits: the α-subunit with GTP and a βγ-dimer. (3, 10) The Gαq-protein activates the phospholipase C and consequently, inositol-1,4,5-trisphosphate (IP3) and Ca^{2+} are released, whereas the inhibitory $G\alpha_i$-protein and the stimulatory $G\alpha_s$-protein both affect the adenylate cyclase. In my master´s thesis the focus lies on the $G\alpha_s$-protein that activates the enzyme adenylate cyclase which is a membrane-bound protein. Due to its activation, it catalyzes the chemical reaction in which adenosine triphosphate (ATP) is converted into the second messenger cyclic adenosine monophosphate (cAMP). (3) To this group belong, among many others, the Gs-coupled beta-adrenergic receptors (11) as well as the EP_4 prostanoid receptor (12).

2.1 The second messenger cAMP and its effector proteins

The second messenger cAMP plays an important role in different physiological processes. The spectrum of those processes encompasses relaxation of airway smooth muscle cells (13), enhancement of inotropy in cardiomyocytes (14), immunomodulation in monocytes (15, 16) and many more. cAMP is a nucleotide derivative. As illustrated in **Figure 1,** the base adenosine, which is connected to the monosaccharide ribose, constitutes the central structure of cAMP. The phosphate group binds to the 3´- and 5´- hydroxy groups of the sugar. (3) The three main effector proteins of cAMP are the protein kinase A (PKA) (3), the exchange protein directly activated by cAMP (Epac) (17) and ion channels like the cyclic nucleotide-gated channels (CNG) or the hyperpolarization-activated cyclic nucleotide-gated channel (HCN) (18, 19). The different signaling pathways of cAMP are illustrated in **Figure 2**.

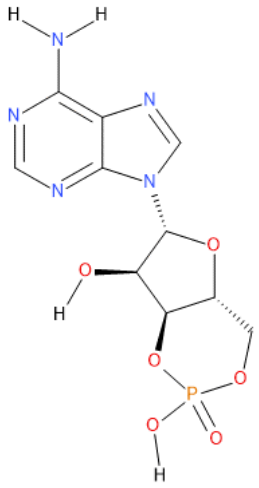

Figure 1: Structure of cAMP.

Through the interaction of cAMP with PKA, ultimately the gene expression can be affected. The heterotetrameric protein PKA consists of two regulatory and two catalytic subunits. When the cAMP level increases, two cAMP molecules bind to each regulatory subunit and induce an allosteric conformational change. Hence, the regulatory subunits are uncoupled and the catalytic subunits are activated. The activated subunits translocate into the nucleus, where they phosphorylate their target proteins on serine and threonine sides like the transcription factor cAMP response element-binding protein (CREB) and consequently, the target proteins are activated. The signaling pathway continues with the binding of the transcription factor to the cAMP responsive element (CRE) and this causes a change in the gene expression of target genes in the cell. In turn, the dephosphorylation of phosphorylated proteins by the protein phosphatases leads to the inactivation. (3)

A further effector protein of cAMP is called Epac, which was discovered two decades ago. (17) As a specific GEF for Rap1 and Rap2 (20), it plays an important role in cAMP signaling cascades, for instance, in memory (21), nerve growth and regeneration (22) as well as wound healing (23). A distinction is made between the isoforms Epac1 and Epac2. Both have a similar domain structure: the cAMP binding domain is located at the NH_2 terminal region, whereas the GEF domain is located at the COOH terminus. (20) A further difference lies in the expression

pattern. While Epac1 is expressed ubiquitously, Epac2 is solely expressed in the brain and adrenal gland. (24) De Rooij et al.[17] discovered that the Epac protein is directly activated by cAMP, but in a PKA independent-manner. (17) The inactive form of Rap1 and Rap2, which are small GTPases and homologues to Ras, bind GDP, whereas in the active conformation GTP is bound. Epac specifically activates Rap1 and Rap2 to the GTP bound form with its guanine exchange factor activity. (24)

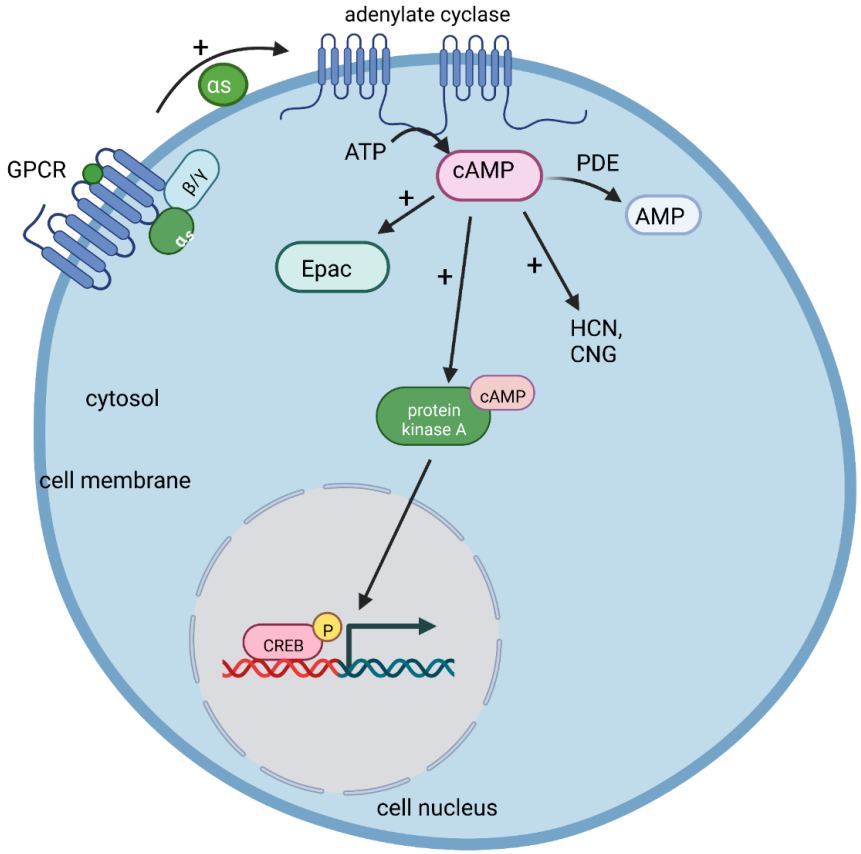

Figure 2: Cellular signaling of cAMP.

After activation of a Gαs-coupled receptor, the membrane bound adenylate cyclase catalyzes the reaction from ATP to cAMP. Then, the second messenger cAMP activates its effector proteins Epac, PKA as well as HCN and CNG channels. PKA affects the gene expression through the phosphorylation of the CREB protein. cAMP is metabolized to AMP by phosphodiesterases (PDEs). (3) Illustration created in BioRender.com

CNG and HCN channels are directly activated by cyclic nucleotides and are structurally classified to the superfamily of pore-loop cation channels. (19) After activation, the alkali ions Na^+ and K^+ and also the divalent cation Ca^{2+} can pass the channel. (19, 25) CNG channels are fundamental channels in photoreceptors and olfactory sensory neurons. However, they are

also expressed in nonneuronal tissues. cGMP and cAMP activate equally the channels in chemosensitive cilia in olfactory neurons, whereas the CNG channels in rods and cones are ligand selective and distinguish between cGMP and cAMP. (25) HCN channels are expressed in excitable cells, which encompasses neurons, photoreceptors, and even cardiac pacemaker cells. (26, 27, 28) Due to the interaction of cGMP and cAMP with the HCN channel protein, the activity of the channel is enhanced. (29)

2.2 Superfamily of phosphodiesterases

Phosphodiesterases (PDE) play a pivotal role in intracellular signaling by regulating the cyclic nucleotide levels. These enzymes metabolize cAMP or cGMP by hydrolysis to AMP or GMP and hence, reduce their concentration to basal levels. Because of that, cAMP has a very short half-life, which is important for an appropriate cellular reaction of new incoming signals. (3)

Nowadays, 11 gene families of PDEs are known and they are classified as PDE1 to PDE11. One to four genes are assigned to each family, which implies that more than 20 genes encode for many different PDE isoforms. (30) The PDEs have a common structure: the regulatory domain is located next to the NH_2- terminus followed by the catalytic domain. The carboxy as well as the amino domains differ in their structure between the PDE families and are of crucial relevance for the different functions of the PDE families. (31) To keep things in perspective, Joseph Beavo[32] evolved a classification system for PDEs. For instance, the acronym “PDE” plus the first number in “PDE4B2” stands for the gene family, the following letter “B” for the individual gene and finally, the number “2” for the splice variant. (32) PDEs are found ubiquitously in mammalian tissue, however, the expression of different gene families varies in their tissue expression pattern as well as in their subcellular localization. Even the substrate specificity depends on the family: PDE4, PDE7 and PDE8 metabolize cAMP selectively. The three families PDE5, PDE6 and PDE9 specifically hydrolyze cGMP and the remaining families are non-selective. (33)

Since the discovery of the huge impact of the PDE family in cell signaling by Butcher and Sutherland in 1962[34], PDE inhibition has been an important target for anti-inflammatory, anti-cancer or anti-neurodegenerative therapy, to mention just a few of them. (30) Nowadays, a variety of selective and non-selective PDE-inhibitors are applied in the treatment of different diseases. To exemplify this, Roflumilast is a selective PDE4 inhibitor (35), which is approved for the therapy of COPD (36). Sildenafil is a selective PDE5 inhibitor (37), which is applied in

the treatment of erectile dysfunction. (38) Also, non-selective PDE inhibitors are important in the therapy of some diseases, like caffeine in the treatment of apnea of premature infants. (34, 39)

2.2.1 PDE4

Especially the PDE4 family is of considerable relevance in the experimental part of this master´s thesis, because of its expression in macrophages and human embryonic kidney (HEK) cells, which are used in *in vitro* experiments. (40) However, to get an overview, PDE4 is also found in monocytes, lymphocytes, brain, cardiovascular (31) and smooth muscle cells (41). The PDE4 family consists of four genes, which are subclassified into PDE4A-D. Because of different mRNA splice variants 19 isoforms are currently known. These splice variants are grouped into long and short isoforms. The long isoform can be distinguished from the short isoform by an upstream conserved region (UCR). The UCR comprises an activation site, which can be phosphorylated by PKA or even by extracellular-signal regulated kinase (ERK) (42), which plays an important role in further signal pathways. Before this will be exemplified subsequently, it is to be added that PDE4A4, PDE4B2, PDE4D3 and PDE4D5 are mainly expressed in monocytes. After the differentiation to macrophages, the concentration of the isoform PDE4B2 increases, the concentration of PDE4D isoform decreases and PDE4A10 occurs. The effect of ERK phosphorylation of the UCR region can on the one hand activate the catalytic activity of the short isoform PDE4B or on the other hand inactivate the catalytic activity of the long isoform PDE4D. Hence, proinflammatory mediators can affect cellular mechanism by inhibiting PDE4D activity in monocytes and by increasing PDE4B activity in macrophages. To conclude, extracellular triggers can achieve different effects on long and short isoforms. (43)

2.3 GPCR desensitization

An overstimulation of the GPCR due to ligand binding can cause pivotal damage to the cell. Hence, mechanisms of short-term and long-term desensitization protect the cell from a signal overload. Short-term desensitization proceeds over minutes, whereas the long-term desensitization process takes hours or days. (44)

Short-term desensitization can be classified into heterologous and homologous desensitization. The heterologous desensitization process is agonist unspecific (44), which was demonstrated by an experiment of Sibley et al [(45)] in 1984. The results of this experiment

showed that cAMP and cAMP analogs activated PKA and thus, PKA phosphorylated the GPCR in the absence of ligands. (45) In contrast, the homologous desensitization is agonist specific. (44) This was also detected by the research of Sibley et al. one year later (46). Here, the receptor phosphorylation is conducted by G-protein coupled kinases (GRKs). (44) The βγ-dimer forms a platform, on which the GRK binds. This enzyme phosphorylates the receptor on its serine and threonine sides. Subsequently, β-arrestin binds to the phosphorylated receptor and prevents the interaction of the GPCR with the G-protein. (3)

Long-term regulation includes two mechanisms: Firstly, the receptor is phosphorylated by GRKs, gets internalized in vesicles, and can be degraded by lysosomes or be recycled to the plasma membrane. Secondly, mRNA levels of GPCRs are reduced by unknown mechanisms. (44) To be more precise, β-arrestin binds to the phosphorylated receptor and serves as an adapter for clathrin molecules. Many receptors to which arrestin has bound form a complex with clathrin molecules, the so called “coated pits”, which are, subsequently, separated in vesicles by the GTPase dynamin. After the loss of the clathrin molecules, the vesicles transform to endosomes. Because of the acidic surrounding, the ligand dissociates from the receptor and via phosphatases the receptor gets dephosphorylated. Now, the receptor can be either destructed via lysosomes leading to receptor downregulation or can be recycled to the cell surface and reacts again to new incoming signals. (3) To conclude, β-arrestin proteins are the hub of the short-term and long-term desensitization process.

Besides these two desensitization phases, also other processes have an impact on the desensitization and termination of cell signaling: the metabolization of the second messenger by PDEs or the intrinsic GTPase activity of the Gα-subunit. (3)

2.4 TGR5

The Takeda-G-protein-coupled receptor 5 (TGR5) is a G-protein-coupled bile acid receptor (Gpbar 1), which belongs to the GPCR superfamily. It is expressed in several tissues and cell types, including the intestine, adipocytes, muscles, gallbladder, the nervous system, and hematopoietic cells. TGR5 controls a wide variety of pathological and physiological processes through its influence on different signaling pathways. Thereby, the activation of this receptor has a positive effect on diet-induced obesity, glucose homeostasis, intestinal motility, liver steatosis (47) as well as atherosclerosis (48). More recently, the influence of TGR5 on inflammatory response, liver regeneration and cancer were detected in addition to the

already known metabolic regulation functions. Thus, TGR5 is an important drug target in different research fields. (49)

2.4.1 Ligands of TGR5

The endogenous ligands of TGR5 are bile acids. They can increase concentration-dependent the cAMP levels via TGR5, which was shown in TGR5-transfected CHO cells. The most potent activator of TGR5 is taurolithocholic acid (TLCA) with a half maximal effective concentration (EC_{50}) of 0.33 µM, followed by lithocholic acid (LCA; EC_{50}: 0.53 µM), deoxycholic acid (DCA; EC_{50}: 1.01 µM), chenodeoxycholic acid (CDCA; EC_{50}: 4.43 µM) and cholic acid (CA; EC_{50}: 7.72 µM). (50) Several natural products have been identified as ligands of TGR5. According to their structure these can be categorized in the group of triterpenoids, like oleanolic acid, ursolic acid, and betulinic acid (47), in the group of coumarins, like farnesiferol B and microlobidene (51), and lastly, in the group of limonoids, like obacunone. (52)

Bile acids are not selective for TGR5, but also bind to the farnesoid X receptor (FXR). Because of that, semisynthetic and synthetic ligands were developed to achieve a higher selectivity for one of those receptors. (49) An important discovery was the increased selectivity for TGR5 by methylation of the C-23(S) position of endogenous bile acids. By further optimization a potent TGR5 selective, semisynthetic steroid-like ligand called INT-777 was developed (**Figure 3**). A vast variety of nonsteroidal chemical structures of TGR5 ligands exists as well. (47) For instance, David Piotrowski et al. [53] discovered in 2013 tetrahydropyrido[4,3-d]pyrimidine amides as TGR5 ligands. (53)

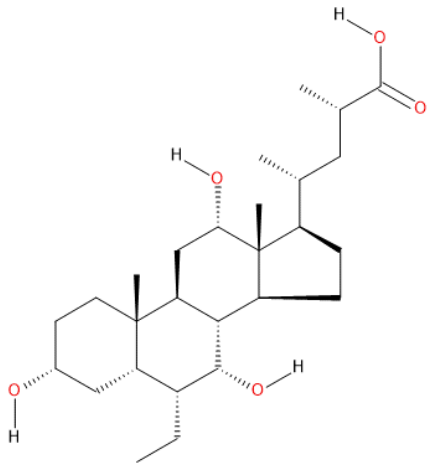

Figure 3: Structure of INT-777.

2.4.2 TGR5 affects atherosclerosis via immunomodulation

As mentioned before, TGR5 is crucial for numerous pathophysiological and physiological processes. The research of Kumar et al.[54] could show that the activation of TGR5 in pancreatic alpha cells increases the glucagon-like peptide 1 (GLP-1) secretion over an Epac-mediated pathway. This finding may point towards a new therapeutic approach to treat type 2 diabetes mellitus. (54) Additionally, a potential treatment strategy for gastric cancer could be the inhibition of the STAT3 pathway after the activation of TGR5, which suppresses cell

proliferation and migration of cancer cells. (55) Also, inflammatory processes of atherosclerosis can be inhibited via TGR5 activation, which is elucidated more precisely in the following. (48)

The working group of Thijs Pols has detected several effects after TGR5 activation, which led to the inhibition of atherosclerosis. The initial step to atherosclerosis is the uptake of LDL in macrophages and their transformation to foam cells. To examine a potential effect of TGR5 on these two mechanisms, macrophages were isolated from $TGR5^{-/-}$ and $TGR5^{+/+}$ mice. The mRNA levels of the scavenger receptor a (Sr-a) and CD36 were measured because both are involved in the LDL uptake in macrophages and their transformation to foam cells. The results show a lower mRNA level of Sr-a and CD36 in $TGR5^{-/-}$ mice compared to $TGR5^{+/+}$ mice. Furthermore, the treatment with INT-777 of $TGR5^{+/+}$ mice reduced the expression of Sr-a and CD36 and furthermore, decreased the oxidized LDL loading compared to $TGR5^{-/-}$ mice. (48)

Chronic inflammation represents a key factor in atherosclerosis and is triggered off through the secretion of different chemokines and cytokines by macrophages. To define the role of TGR5 in this process, Pols et al. treated RAW264.7 macrophages with or without INT-777 and subsequently stimulated the cells with LPS. While the mRNA levels of IL-6, IL-1β, TNFα and the monocyte chemoattractant protein 1 (Mcp-1) were enhanced in the LPS treatment alone group, the mRNA levels were decreased in the INT-777/LPS co-treatment group. To go into more detail, Pols et al. report that a strong attenuation of the NF-κB signal pathway through TGR5 activation takes place. So, the nuclear translocation of p65 is significantly reduced by activating TGR5 with INT-777. Furthermore, the IκBα phosphorylation through IKK and the p65 DNA binding activity declined. And even the NF-κB transcriptional activity was inhibited by TGR5 activation or overexpression in LPS-treated macrophages. (48)

The assumption that the TGR5-cAMP-NF-κB axis is pivotal in macrophages for the inhibition of cytokine production was confirmed by creating a TGR5 mutant called TGR5-A217P. This mutant cannot activate the cAMP-CREB pathway because the mutation is localized in a G-protein loop, which is important for interactions. CREB transcriptional activity was not increased by TGR5-A217P after INT-777 stimulation, which presumably led back to the inability of activating the cAMP pathway. The crucial result was the inhibition of the NF-κB pathway by the wildtype TGR5 protein, whereas the TGR5-A217P protein did not impede this pathway. (48) To sum up, cAMP potentially inhibits IKK, which belongs to the NF-κB signal

pathway, and thus, the phosphorylation of IκBα and the nuclear translocation of p65 is constrained (**Figure 4**). (47)

In a further experiment Pols et al. focuses on a potential effect of TGR5 activation that may lead to reduced atherosclerotic lesions. Therefore, an *in vivo* experiment with either $TGR5^{+/+}$ or $TGR5^{-/-}$ LDL-$receptor^{-/-}$ -mice was conducted. Because of the knockout of the LDL receptor, cholesterol levels were in both groups of mice equally high. The result was a significant reduction of vascular lesion in $TGR5^{+/+}$ mice, which were treated with INT-777. In $TGR5^{-/-}$ mice this effect was not observed. To conclude, the positive effect of INT-777 is reliant on the TGR5 receptor. Furthermore, also the mRNA levels of TNFα and IL-1β are declined in plaques of $TGR5^{+/+}$ mice, which were treated with INT-777 as compared to untreated $TGR5^{+/+}$ mice. Interestingly, also the number of macrophages was reduced in plaque from $TGR5^{+/+}$ mice treated with INT-777. (48)

To summarize, the activation of the TGR5 receptor through the specific agonist INT-777 has a huge antiatherogenic effect via immunomodulation. So, the oxidized LDL uptake in macrophages and the transformation of macrophages to foam cells is reduced. Chronic inflammation is attenuated by the inhibition of the NF-κB signal pathway by the cAMP-CREB axis and thus, the production of inflammatory cytokines such as IL-6, IL-1β, TNFα and Mcp-1 declines significantly. Moreover, less vascular lesion occurs, which is associated with reduced inflammatory cytokine production and a reduced number of macrophages in the plaques. (48)

2.5 cAMP as immunomodulator

The second messenger cAMP affects the innate as well as the adaptive immune response. Because of that the modulation of the cAMP levels is the hub for several therapeutic strategies for autoimmune and inflammatory diseases. For instance, the PDE4 inhibitor roflumilast is applied in the therapy of COPD and apremilast, also a selective PDE4 inhibitor, is used in the therapy of the autoimmune diseases psoriasis and psoriasis arthritis. (57)

2.5.1 cAMP as a regulator of the innate immune system

Cyclic AMP is pivotal for the regulation of innate immune functions. Specifically, it is a key regulator for immune functions of monocytes, macrophages and even neutrophils. (58) cAMP regulates the immune response through its influence on different effector functions, which are described in the following.

The treatment of human monocyte-derived macrophages with the prostaglandins PGE_2 and PGD_2 or different cAMP analogues elevates the intracellular cAMP levels and thus, the phagocytosis of apoptotic cells could be diminished. Furthermore, the increase of the cAMP levels affects the morphology of the macrophages, which change to a rounder shape and even structures which are important for interaction with actin or talin are reduced. These two changes in morphology have an enormous impact on the adhesive status of macrophages. The results concerning the phagocytosis and the change in morphology show that the elevation of the cAMP levels can limit inflammatory processes, which can potentially cause tissue damage. (15) In addition, cholesterol efflux was increased in J774.A1 macrophages after the treatment with the specific PDE4 inhibitors rolipram and cilomilast, which both enhance the cAMP levels. The cholesterol mobilization could have a positive effect in the treatment of atherosclerotic lesions because the progression from macrophages to foam cells is reduced. (59) Even the production of proinflammatory substances like NO is inhibited in macrophages due to increased cAMP levels. (60) Also the working group of Graziele Negreiros-Lima[61] detected that cAMP affects important proinflammatory functions of macrophages in a PKA-dependent manner. So, cAMP induces nonphlogistic monocyte recruitment, the reprogramming of macrophages to the M2 phenotype, and leads to an increase in efferocytosis of apoptotic neutrophils. The change of the phenotype goes hand in hand with the occurrence of certain cytokine types. While proinflammatory cytokines like TNFα and IL-6 are present with the M1 phenotype, anti-inflammatory cytokines like IL-10 are markers for the M2 phenotype. (61) To conclude, these results show that the elevation of the cAMP levels has different anti-inflammatory effects in macrophages, and that cAMP plays a pivotal role as immunomodulator.

2.5.2 cAMP as an inhibitor of the NF-κB pathway

Immune or inflammatory reactions initiate the synthesis of inflammatory proteins such as cell adhesion molecules, chemokines or proinflammatory cytokines. The synthesis of inflammatory proteins can amplify the primary pathogenic signal. To specify this, transcription factors such as the well-known NF-κB factor induce the gene expression of these proteins and lead to an inflammatory immune response. (62) Thus, an interruption of the NF-κB pathway can inhibit an inflammatory response.

As previously described, the author Pols and his working group [48] detected the inhibition of the NF-κB signal pathway through the cAMP-CREB pathway. Thereby, TGR5 was activated through its ligand INT-777. As a result, the phosphorylation of IκBα, the translocation of p65 as well as the NF-κB transcriptional activity were decreased in RAW264.7 macrophages. (48) Since the phosphorylation of IκBα is regulated by IKK, cAMP was suggested to have an inhibitory effect on IKK (**Figure 4**). (47) Also Minguet et al. [63] discovered that cAMP is indeed an inhibitor of the NF-κB signal pathway. In their experiments, the researchers activated the NF-κB pathway in splenic B lymphocytes via the B cell antigen receptor (BCR). They showed that the elevation of the cAMP levels through pre-treatment with forskolin and IBMX inhibited the activation of the NF-κB pathway. Furthermore, the decreased phosphorylation and degradation of IκBα was determined. Interestingly, by adding the PKA inhibitor H-89 the effect of the decreased IκBα phosphorylation was reversed. This suggests that PKA might be a responsible downstream effector of cAMP for these effects. (63)

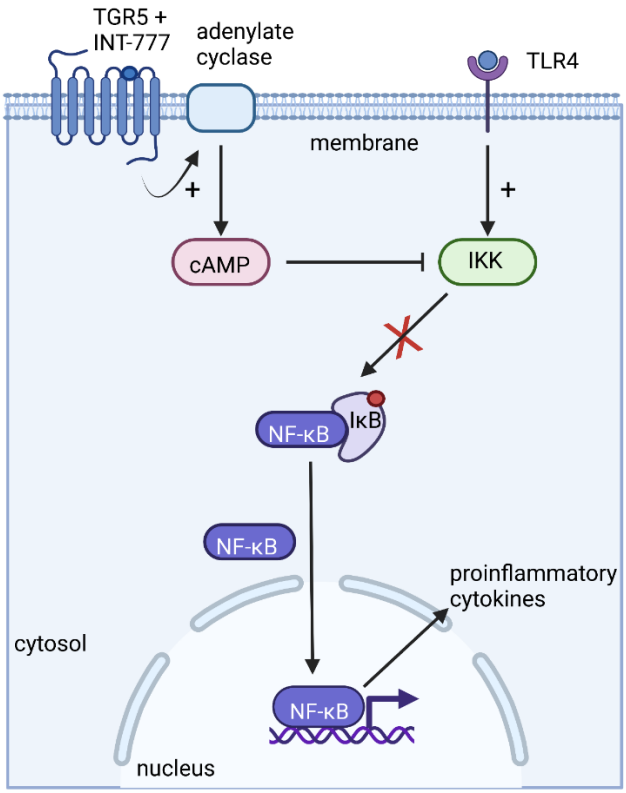

Figure 4: Inhibition of the NF-κB pathway via cAMP.

After activation of the TGR5 via its ligand INT-777, the second messenger cAMP is produced. cAMP inhibits the NF-κB pathway by inhibiting the kinase IKK. This prevents the phosphorylation of IκB and thus, the translocation of NF-κB into the nucleus is impeded. Furthermore, NF-κB does not promote the synthesis of inflammatory cytokines through gene expression. (48) Illustration created in BioRender.com

Another way of inhibiting the NF-κB pathway through the elevation of the cAMP levels, however, without preventing p65 translocation to the nucleus, is also modulated by PKA. This kinase phosphorylates the CREB protein, which then binds to the coactivator CBP. Also, the carboxy-terminal region of p65 aims to interact with the amino-terminal region of CBP. This competition leads to the inhibition of the NF-κB pathway suggesting that the activation of PKA is significantly involved. (64) To sum up, irrespective of which way cAMP inhibits the NF-κB signaling pathway, it consistently shows an immunosuppressive effect (62) and therefore, cAMP is important as an immunomodulator.

3 Natural products

Natural products are obtained from plants, microbes or even animals. Around 50% of drug substances, which have been approved since 1994, are based on natural products or at least

their derivatives. Different chemical structures can be found in this group. With new techniques such as high-throughput screenings, it is nowadays possible to screen many natural substances to find structures, which have a specific pharmacological effect. Numerous natural products with indications against cancer, inflammation, cardiovascular or gastrointestinal diseases are currently in different stages of research. (65)

3.1 Natural products and derivatives screened in this master´s thesis

3.1.1 Neolignane derivatives (compounds LRK071, LRK077, AH-17)

As traditionally used medicine, the magnolia bark extract belongs to the Chinese and Japanese medicine and is extracted from the bark of either *Magnolia officinalis* or *Magnolia obovate* (Magnoliaceae). The major constituents are the neolignanes magnolol and honokiol (**Figure 5**). The extract is well-known for its antioxidant, anti-inflammatory, sedative, antispastic and antibiotic effect. (66)

The compounds LRK071, LRK077 and AH-17 are derivatives of the natural products magnolol and honokiol. The three compounds differ in their functional group of the side chain of the phenyl ring: LRK071 has a meta-positioned nitro group (its structure is illustrated in **Figure 5** in comparison to magnolol and honokiol), LRK077 has a methyl ester, whereas AH-17 has a nitrile group. Previously, the master student Nourhan Elbeialy[67] of the working group of Univ.-Prof. Dr. Dirsch (University of Vienna) could detect in her research that the substance LRK071 increases the cAMP levels in an Epac-based FRET biosensor assay using Epac-HEK cells. (67) This result is an initial point for further research in this master´s thesis to elucidate the specific pathway of LRK071.

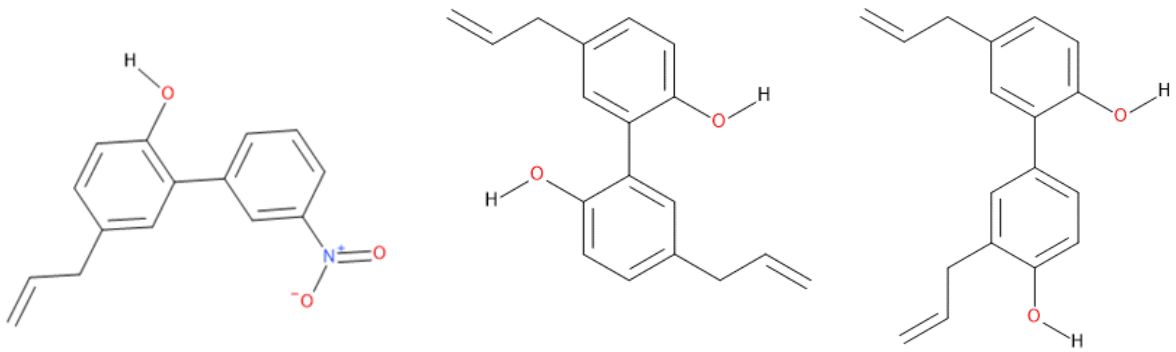

LRK071 Magnolol Honokiol

Figure 5: Structures of LRK071, magnolol and honokiol.

3.1.2 Leoligin derivatives (compounds 2743, 3162 and 3163)

Leoligin is a natural lignan, which is a constituent of the plant Edelweiss (*Leontopodium nivale ssp. alpinum* (Asteraceae)). (68, 69) In the alpine traditional medicine it is applied in the therapy of indigestion, abdominal aches, and fever. (70) Several effects of this lignan could already be detected. For instance, it induces cholesterol efflux in macrophages (68) or possess anti-inflammatory effects because of the inhibition of the NF-κB pathway (71). Leoligin consists out of a central tetrahydrofuran ring, which is coupled via an ester bond to an angelic acid on position 4. On each of the positions 3 and 5 are a dimethoxybenzene. The chemical structure is illustrated in **Figure 6**.

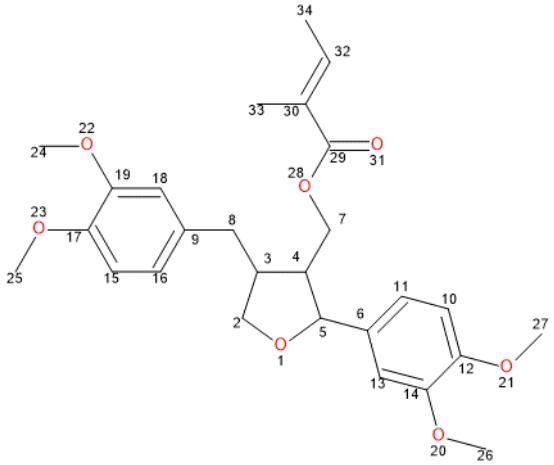

Figure 6: Structure of leoligin.

The compounds 2743, 3162 and 3163 are synthesized by Univ.- Prof. Dr. Marko Mihovilovic (Technical University of Vienna) and represents derivatives of leoligin. Their structures differ in the side chain of the central tetrahydrofuran ring on position 3. As regards the similarity of the side chain, all structures have a carboxylate group. The structures of the three compounds are shown in **Figure 6**. The chemical name of the side chain of the DNTI compound 2743 is 1-naphthoic acid. The side chain of DNTI 3162 is called ethyl-2-methylbut-2-enoate and the side chain of DNTI 3163, which is bound to a carboxylate group on position 3 of the tetrahydrofuran ring, is designated as 2-methylbut-2-enyl. Moreover, an increase of the cAMP levels in HEK293 cells in an Epac-based FRET biosensor assay could be determined of the DNTI substance 2743 by Nourhan Elbeialy. A toxic effect on the cells could be excluded by testing the compound in the Resazurin assay. (67) However, the pathway of the elevation of the cAMP levels is still unclear and is subject of further research.

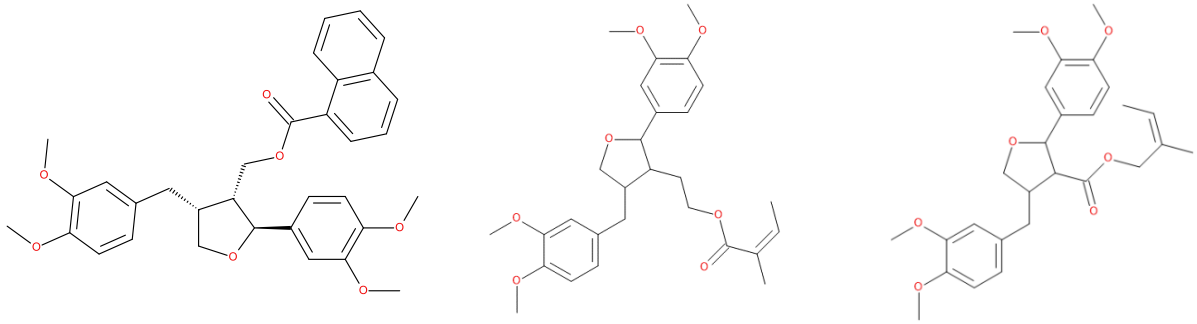

DNTI 2743 DNTI 3162 DNTI 3163

Figure 7: Structures of leoligin derivatives 2743, 3162 and 3163.

3.1.3 Helioxanthin, heliobuphthalmin and dehydroheliobuphthalmin

Helioxanthin (DNTI 2644) is a phenylnaphthalide lignan of *Ruta graveolens*. (72) This plant belongs to the family of the Rutaceae and has been well-known since the ancient times in the Mediterranean region. Various effects of this plant are described: among others, it has anti-inflammatory, antifungal, antitumoral and cytotoxic effects. Because of that it is applied in the treatment of pain, various inflammatory diseases, and dermatitis, for instance. (73) It is shown that a methanolic extract of this plant with its major component helioxanthin has immunomodulatory effects. In addition, it modifies the humoral immune response via the increase of the immunoglobulin production in a dose-dependent manner. (72) Furthermore, helioxanthin also inhibits the hepatitis B virus (HBV) and hence, it is a potent new drug in the treatment of hepatitis B. (74)

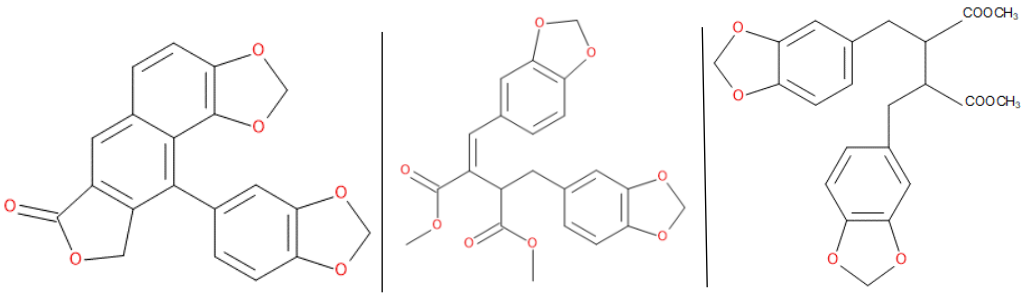

Figure 8: Structures of helioxanthin, dehydroheliobuphthalmin and heliobuphthalmin.

The natural products helioxanthin, heliobuphthalmin (DNTI 2640) and dehydroheliobuphthalmin (DNTI 2641) can also be isolated from *Heliopsis helianthoides var. scabra* (Asteraceae). They belong to the chemical group of lignans. (75) The center of the molecule heliobuphthalmin consists of a butanedioate structure and a benzodioxol is attached

to both sides of it. The structure of dehydroheliobuphthalmin differs from heliobuphthalmin because of a double bond on position 5.

3.1.4 The coumarin notopterol

The natural product notopterol (DNTI 1055), whose structure is illustrated in **Figure 9**, can be isolated from *Notopterygium incisum* (Apiaceae). (76, 77) It is traditionally used in the Chinese medicine as a treatment against rheumatism. Its anti-inflammatory effect can be traced back to a decreased production of inflammatory chemokines and cytokines through inhibition of the JAK-STAT signal pathway. (76) Various other effects of notopterol have been detected. *In vitro* and *in vivo* experiments show that this substance also ameliorates estrogen deficiency-induced osteoporosis (78), cognitive deficits in Alzheimer disease (79) and acute myeloid leukemia (80).

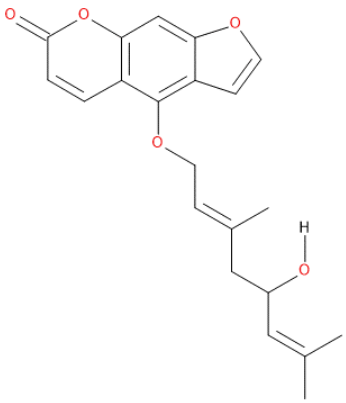

Figure 9: Structure of notopterol.

B. Aim of the study

The aim of the study was to identify new compounds which modulate the intracellular cAMP levels. The second messenger cAMP plays a pivotal role in the innate as well as in the adaptive immune system and hence, by affecting the cAMP levels by compounds a modulation of the immune functions is provided, which led to new therapeutic strategies. (57) Therefore, numerous natural compounds of the DNTI library as well as synthesized compounds were screened *in vitro* in two high-throughput screenings, namely, the TGR5 target-based and the phenotypic screening. In these screenings, the Epac-based fluorescence resonance energy transfer (FRET) biosensor assay was used to measure the intracellular cAMP levels directly.

While the TGR5 target-based screening was performed with stably transfected TGR5-Epac-HEK293 cells to determine compounds which are potential agonist of the bile acid receptor TGR5, the phenotypic screening was conducted with stably transfected Epac-HEK293 cells to identify potential PDE-inhibitors. To confirm the results of both screenings with a more sensitive method and to assess if the cAMP/CRE signal pathway was affected, also CRE-luciferase assays were performed. Additionally, to determine a selectivity of the compounds to TGR5, also a FXR-Gal4-luciferase assay was conducted.

In previous phenotypic screenings it was observed that the magnolol derivatives LRK071 and AH-17 as well as the leoligin derivative 2743 increase the intracellular cAMP levels in Epac-HEK293 cells. To determine which mechanism is exactly involved in the modulation of the cAMP levels, different assays were performed. To evaluate a potential PDE inhibitor activity, a kinetic cAMP measurement as well as a fluorescence polarization assay were conducted. Furthermore, to assess if these compounds might have anti-inflammatory properties as well as inhibitory activities against the NF-κB signal pathway, a Griess assay and a NF-κB- luciferase assay were performed. In addition, several CRE-luciferase assays were conducted to determine whether the compounds have potential PKA inhibitory or adenylate cyclase agonistic activities.

C. Materials and Methods

1 Compounds

The majority of the compounds screened within the scope of this master´s thesis was obtained in a previous project titled “Drugs from nature targeting inflammation” (DNTI). Additional compounds, which were not obtained from the DNTI project, will be mentioned separately. The DNTI compounds include plant extracts, isolated pure substances from plants and also synthesized pure substances. Several Austrian universities as well as external partners participated in the DNTI project, whose results were published from the year 2016 onwards. The aim of this project was to examine the effects of certain natural products on inflammatory processes. (81) Besides the substances of the DNTI project, also other substances were tested which were synthesized by the working group of Dr. Lukáš Rýček (Charles University in Prague) or the working group of Univ.- Prof. Dr. Marko Mihovilovic (Technical University of Vienna). The **Table 1** provides an overview of the origins of the different substances.

Table 1: The origins of the tested compounds are listed below.

Compound	**Provider**
Magnolol derivatives: LRK071, LRK077, AH-17	Dr. Lukáš Rýček (Charles University in Prague)
Leoligin derivatives: 2743, 3162, 3163	Univ.- Prof. Dr. Marko Mihovilovic (Technical University of Vienna)
Helioxanthin, heliobuphthalmin, dehydroheliobuphthalmin, notopterol	DNTI data bank (University of Vienna)

2 Cell culture

By working under a laminar air flow workbench HERAsafe®KS18 aseptic conditions were maintained to avoid microbial contamination of the cultured cells. To disinfect surfaces of the laminar air flow workbench, surfaces were cleaned at the beginning and at the end of each workflow with Hexaquart plus 1% (B. Braun, Melsungen, Germany) and ethanol 70%.

To ensure an optimal growth and a good viability of the cells, they were cultured in complete medium (CM) in culture flasks (T-175, Sarstedt) at 37 °C and 5% CO_2. CM consists of Dulbecco´s Modified Eagle´s Medium (DMEM) without phenol red, 10% fetal bovine serum (FBS), L-glutamine solution and of penicillin – streptomycin solution. For the compound treatments,

stripped medium (SM) was used. In this medium are the same components like in the CM with a difference in the use of charcoal stripped FBS (5% final concentration) instead of FBS. More detailed information on the composition of the used materials can be found in **Table 2**. To avoid confluence of more than 70 - 80% of the cell lines, cell passaging was conducted three times a week on Monday, Wednesday, and Friday. Information about the viability, density and a potential contamination of the cells was obtained by the optical examination of the cells under the Olympus CKX31 light microscope. To prevent damage to the cells, all used liquids were warmed up in the water bath Julabo® SW23 at 37°C before usage.

Table 2: Cell culture materials.

Material	Ingredients	Amount	Source
Complete medium (CM)	DMEM without phenol red, with 4.µg/l glucose	450 ml	Lonza (Basel, Switzerland)
	FBS	50 ml (10%)	Gibco (Lofer, Austria)
	L-Glutamine (2mM)	5 ml	Lonza (Basel, Switzerland)
	Penicillin (100 U/ml) Streptomycin (100 µg/ml)	5 ml	Lonza (Basel, Switzerland)
Stripped medium (SM)	DMEM without phenol red, with 4.5 g/l glucose	450 ml	Lonza (Basel, Switzerland)
	charcoal stripped FBS	25 ml (5%)	Gibco (Lofer, Austria)
	Penicillin (100 U/ml) Streptomycin (100 µg/ml)	5 ml	Lonza (Basel, Switzerland)
	L-Glutamine (2mM)	5 ml	Lonza (Basel, Switzerland)
PBS (pH 7.4)	ddH_2O	100 ml	
	NaCl	7.2 g	Carl-Roth (Karlsruhe, Germany)
	Na_2HPO_4	1.48 g	Carl-Roth (Karlsruhe, Germany)
	KH_2PO_4	0.43 g	Carl-Roth (Karlsruhe, Germany)
Trypsin/EDTA solution	Trypsin	0.5 g	Gibco (Lofer, Austria)
	EDTA	0.2 g	Carl-Roth (Karlsruhe, Germany)
	PBS	ad 1000 ml	

2.1 Cell lines

2.1.1 Wildtype HEK293 cells

The human embryonic kidney 293 (HEK293, ATCC CRL-1573™) cell line are cells extracted from the kidney of a human embryo. These cells are adherently growing and have a polygonal shape, which is good visible under a microscope. Because of the ease of use, HEK293 cells are optimal for the conduction of high-throughput screenings, like the target-based and the phenotypic screening, which are relevant in this master´s thesis. However, HEK293 cells were also used in the luciferase assay. Through stable transfection of wildtype HEK293 cells, new cell lines have been generated, which were essential for the experimental part of this master´s thesis and presented in the next chapter [2.1.2 Modified HEK293 cell lines].

2.1.2 Modified HEK293 cell lines

Three different adherent growing cell lines, which are derived HEK293 cells, were used either for the target-based screening, the phenotypic screening or the luciferase assay and are listed below:

- Epac-HEK cell line
- TGR5-Epac-HEK cell line
- HEK293/ NF-κB-luc cell line

One of the most intensively used cell line in this work was the Epac stably transfected HEK293 cell line, which are defined as Epac-HEK cells. Through stable transfection with the TGR5 cDNA also the TGR5-Epac-HEK cell line was established. The modified Epac protein is a biosensor protein, with which the high-throughput screenings, target-based and phenotypic screening, were conducted. The mechanism is based on the radiationless energy transfer between two fluorophores which are linked to the protein. (82) By applying this technique, the cAMP levels of the cells were measured. More detailed information is given in the chapter [3 Epac-based FRET biosensor assay]. For the experiments also HEK293/NF-κB-luc cells were used, which were obtained from Panomics (Fremont, CA, USA). Wildtype HEK293 cells were mostly used as control.

For the cell cultivation, the cell passaging was conducted. The CM in the culture flask was discarded and the cells were washed with 10 ml phosphate-buffered-saline (PBS). As regards the trypsinization, 4 ml solution of 0.5 g trypsin and 0.2 g EDTA solved in 1000 ml PBS was

added on the monolayer of TGR5-Epac-HEK293 cells and Epac-HEK293 cells for 5 min, the trypsinization time necessary for the cell detachment of the HEK293 cells and the NF-κB-HEK293 cells was about 2 min. During this time the cells were incubated at 37°C and 5% CO_2 in the HERAcell® 150 incubator for around 1-2 min due to the optimal activity of the enzyme under those conditions. Afterwards, trypsin activity was inactivated by adding 8 ml of CM. Then, the cell suspension was transferred to a 50 ml Falcon tube (Sarstedt) and was centrifugated (Heraeus™ Multifuge 1 S-R) for 4 min at 1400 revolutions per minute (rpm). In the next step, the supernatant above the cell pellet was discarded and the cells were resuspended in 11 ml CM. With the device ViCell™ XR Cell Viability Analyzer the cell count and viability of 1 ml cell suspension was determined. An amount of 6 x 10^6 cells was transferred to a new culture flask in 20 ml CM. Finally, the cells were incubated in the HERAcell® 150 incubator in a humidified atmosphere at 37°C and 5% CO_2.

2.1.3 Murine J774A.1 macrophages

Adherent growing J774A.1 cells (ATCC TIB-67™) are macrophages and are isolated from a mouse with reticulum cell sarcoma in 1968. In general, macrophages are important for the innate immune system. Via phagocytosis, bacteria or other contaminants are engulfed and eliminated through a microbicide cocktail of hydroxyl radicals, nitric oxide, superoxide anions, and lysozymes. (2) The J774.A1 macrophages are used for the Griess assay to determine potential anti-inflammatory effects of tested compounds, which are examined over measuring the NO production.

The passaging of the adherent growing J774A.1 cells is similar to the HEK293 cell passaging with one significant exception. Instead of the trypsinization, the cells got detached from the culture flask with a cell scraper. Therefore, the CM of the culture flask was removed, and 10 ml fresh CM was added. The cell scraper was slightly moved over the cell monolayer one time up and down. Afterwards, the cell suspension was transferred to a 50 ml Falcon tube. The further workflow is identical to the cell passaging, which was described in the previous chapter [2.1.2 Modified HEK293 cell lines].

Table 3: Devices used in the cell culture.

Device	Source
HERAsafe®KS18	Thermo Fisher Scientific Inc. (Waltham, CA, USA)
Julabo® SW23	Julabo GmbH (Allentown, PA, USA)
HERAcell® 150 Incubator	Thermo Fisher Scientific Inc. (Waltham, CA, USA)
Olympus CKX31 Light Microscope	Olympus Europa GmbH (Hamburg, Germany)
Centrifuge Heraeus™ Multifuge 1 S-R	Thermo Fisher Scientific Inc. (Waltham, CA, USA)
ViCell™ XR Cell Viability Analyzer	Beckmann Coulter (Fullerton, CA, USA)

3 Epac-based FRET biosensor assay

Förster or Fluorescence Energy Transfer (FRET) was first described in 1948 by Theodor Förster and is based on the radiationless energy transfer between two chromophores. (82) With an Epac-based FRET biosensor assay it is possible to obtain a qualitative, quantitative, and direct measurement of the cAMP levels in living cells with a high temporal resolution. (83) The Epac protein is an effector protein of cAMP and activates as GEF the GTPases Rap 1 and 2 and hence, different cellular processes are affected. (20) For the purposes of both high-throughput screenings, the target-based and the phenotypic screening, the FRET biosensor is suitable to perform fast and precise measurements.

In this assay, the Epac-based FRET biosensor is a unimolecular sensor (85), which is based on the Epac protein. The sensor consists of two fluorophores, the cyan fluorescent protein (CFP) and the Venus protein, which are both linked to Epac in a single polypeptide. The two chromophores differ in their emission spectra. So, it was observed that cyan is the color of CFP and yellow of Venus. (86) The distance between the two fluorophores is a key factor for the occurrence of the energy transfer and thus, should be in the range of 1-10 nm. (87) In the case of the Epac-based FRET biosensor, the distance between the two fluorophores is under 5 nm in unbound conditions. Due to the excitation wavelength of 420 nm, the donor chromophore CFP gets excited. The overlap of the emission spectrum of CFP with the excitation spectrum of Venus causes an energy transfer (88), which is detectable because of the wavelength of the emitted light of Venus at 520 nm. The FRET mechanism in this assay is based on the conformational change of the Epac protein due to the binding of cAMP and hence, the distance between the two chromophores increases. (86, 84) Therefore, after the

binding of cAMP, no energy transfer occurs, and the emitted light of CFP at 480 nm is detected. The FRET mechanism of the Epac-based biosensor is illustrated in **Figure 10**. The detection of the fluorescence was measured via the TECAN Spark® Microplate Reader.

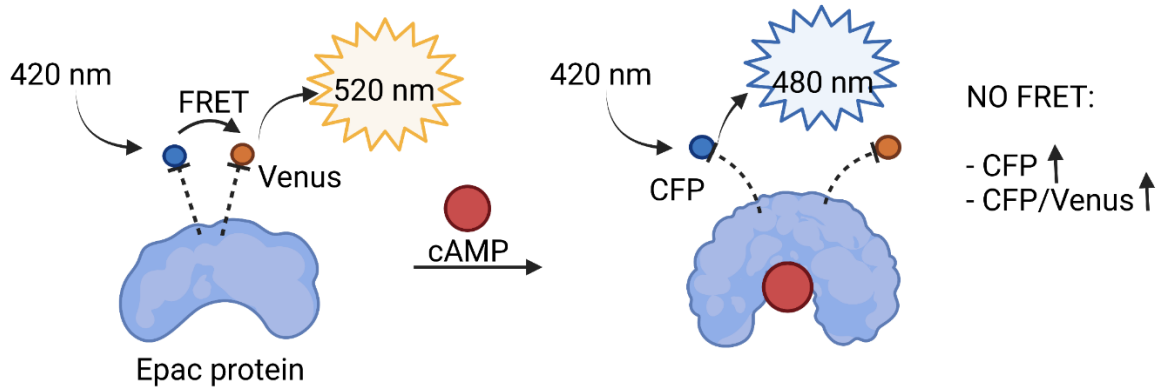

Figure 10: FRET mechanism of an Epac-based FRET biosensor.
Two fluorophores, CFP and Venus, are linked to the Epac protein. An excitation wavelength of 420 nm excites CFP and due to a small distance between the fluorophores in an unbound state, the energy transfer takes place. Hence, the emission wavelength of Venus at 520 nm can be detected. Due to the binding of the second messenger cAMP to Epac, the protein undergoes a conformational change and the distance between the fluorophores increases. The energy transfer cannot occur anymore and thus, the emission at a wavelength at 480 nm (CFP) can be measured. Illustration created in BioRender.com

3.1 Screening of compounds by the Epac-based FRET biosensor assays

On a 96-well plate cells were seeded in 200 µl CM at a density of 0.1 x 10^6 cells per well, except for the wells of the rows D and H. These were left empty for the determination of the autofluorescence of each tested substance. For the target-based screening the TGR5-Epac-HEK cells and for the phenotypic screening the Epac-HEK cells were seeded. The cells were incubated overnight at 37°C and 5% CO_2. **Figure 11** shows a schematic illustration of a 96-well plate used in both screenings.

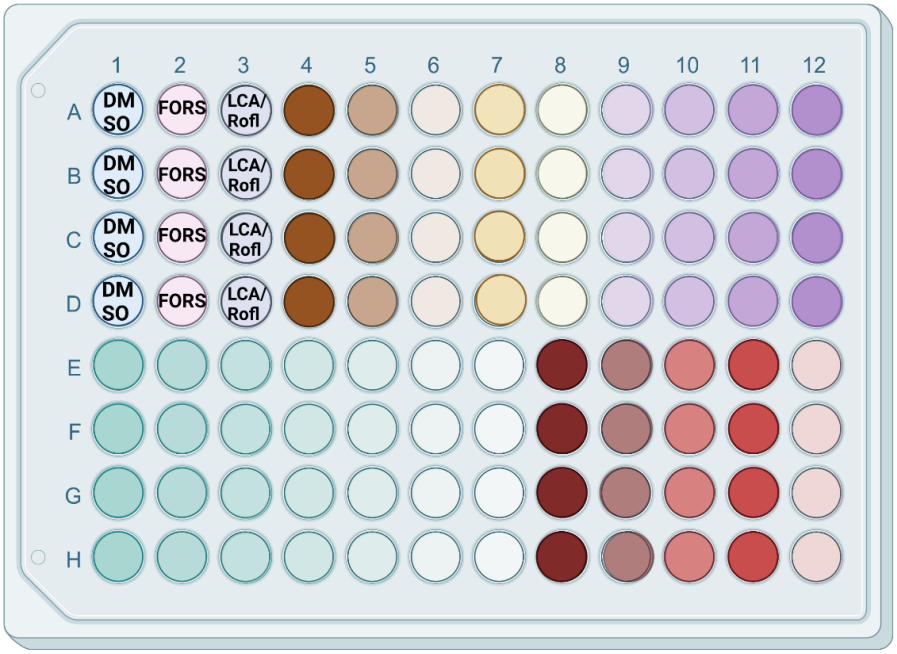

Figure 11: Schematic illustration of the 96-well plate after compound treatment used in both screenings.
This 96-well plate was used either for the target-based screening with TGR5-Epac-HEK cells or for the phenotypic screening with Epac-HEK cells. The cells were seeded in the rows A-C and E-G, because of the measurement of the autofluorescence of the tested compounds in row D and H. The vehicle control was dimethyl sulfoxide (DMSO) 0.1% and a positive control was forskolin 10 µM. In addition, a further positive control in the target-based screening was LCA 10 µM, whereas the positive control in the phenotypic screening was roflumilast 1 µM. FORS= forskolin; Rofl= roflumilast. Illustration created in BioRender.com

However, the compound treatment of the cells in the target-based and in the phenotypic screening differed and hence the conduction of both screenings is separately elucidated in the following. For a better understanding, the workflow of both screenings is compared in **Figure 12**.

3.1.1 TGR5 target-based screening

To start with, the complete induction buffer (CBI) was prepared. The CBI consisted of 50 ml 1x FURA buffer, 3-isobutyl-1-methylxanthine (IBMX) with the final concentration of 500 µM (Cayman Chemical (Ann Arbor, MI, USA); Cay13347) and rolipram (final concentration 30 µM) (Cayman Chemical (Ann Arbor, MI, USA); Cay10011132). The composition of the FURA buffer is listed in **Table 4**. The addition of the unspecific PDE-inhibitor IBMX as well as the specific PDE4-inhibitor rolipram served to stabilize the cAMP signal for the measurement due to the fast metabolization by PDE. (89) An amount of 999 µl CBI was pipetted to 24 x 1,5 ml Eppendorf tubes. 1 µl of the testing compounds stock solutions (mM concentration) were diluted (1:1000) in the tubes containing the CBI to obtain final micromolar concentrations.

Hereby, dimethyl sulfoxide (DMSO) 0.1% was used as a vehicle control. The endogenous ligand of TGR5 LCA 10 µM was utilized as the positive control and forskolin 10 µM, an activator of adenylate cyclase, was used as second positive control (**Figure 11**). The origin of the substances is listed in **Table 6**. The Eppendorf tubes were vortexed thoroughly. The compounds were pipetted to four wells below each other on a non-sterile 96-well plate. The first three wells served to receive technical triplicates in each measurement and the fourth well was to measure the autofluorescence of the respective compound. Then, the incubated 96-well plate was taken out of the incubator and the CM was removed from the cells. The cells were carefully washed with 150 µl 1x FURA buffer. The washing step is important, because the CM could distort the measurement by its autofluorescence. Finally, 100 µl of the compound dilutions were pipetted onto the cell layer. The fluorescence was measured after a 10 min incubation to obtain a maximum cAMP level in the cells step via a TECAN Spark® Microplate Reader (Tecan Group Ltd.).

3.1.2 Phenotypic screening

In the phenotypic screening, the compound dilutions were prepared under a laminar airflow workbench (HERAsafe®KS18) due to the heightened danger of contamination during a long incubation period. A volume of 999 µl SM was pipetted to 24 x 1,5 ml Eppendorf tubes and 1 µl of compound stock solutions were added. Hence the dilution factor was 1:1000. The selective PDE4 inhibitor roflumilast 1 µM was utilized as positive control and forskolin 10 µM was again the second positive control. DMSO 0.1% was used as vehicle control (**Figure 11**). Information about the origin of the substances is provided in **Table 6**. After the vortexing of the tubes, the compound dilutions were transferred to four wells of a sterile 96-well plate with an amount of 200 µl per well. The incubated 96-well plate was retrieved out of the incubator and the old CM was carefully discarded. 150 µl of compound dilutions were pipetted from the prepared plate onto the cell layer. The cells were incubated with the compounds for 30 min. In the meantime, the isoprenaline dilution was prepared in two dilution steps to obtain a final concentration of 10 nM isoprenaline (Cayman Chemical (Ann Arbor, MI, USA), Cay15592) in 10 ml 1x FURA buffer. This step was conducted in a non-sterile surrounding. Once the incubation time was over, the SM on the cells was discarded and a washing step with 150 µl 1x FURA buffer was conducted also in a non-sterile surrounding. 100 µl of the prepared isoprenaline dilution (10 nM) was pipetted onto the cells. Subsequently, the 96-well plate was measured via TECAN Spark® Microplate Reader after an initial incubation step of 30 minutes.

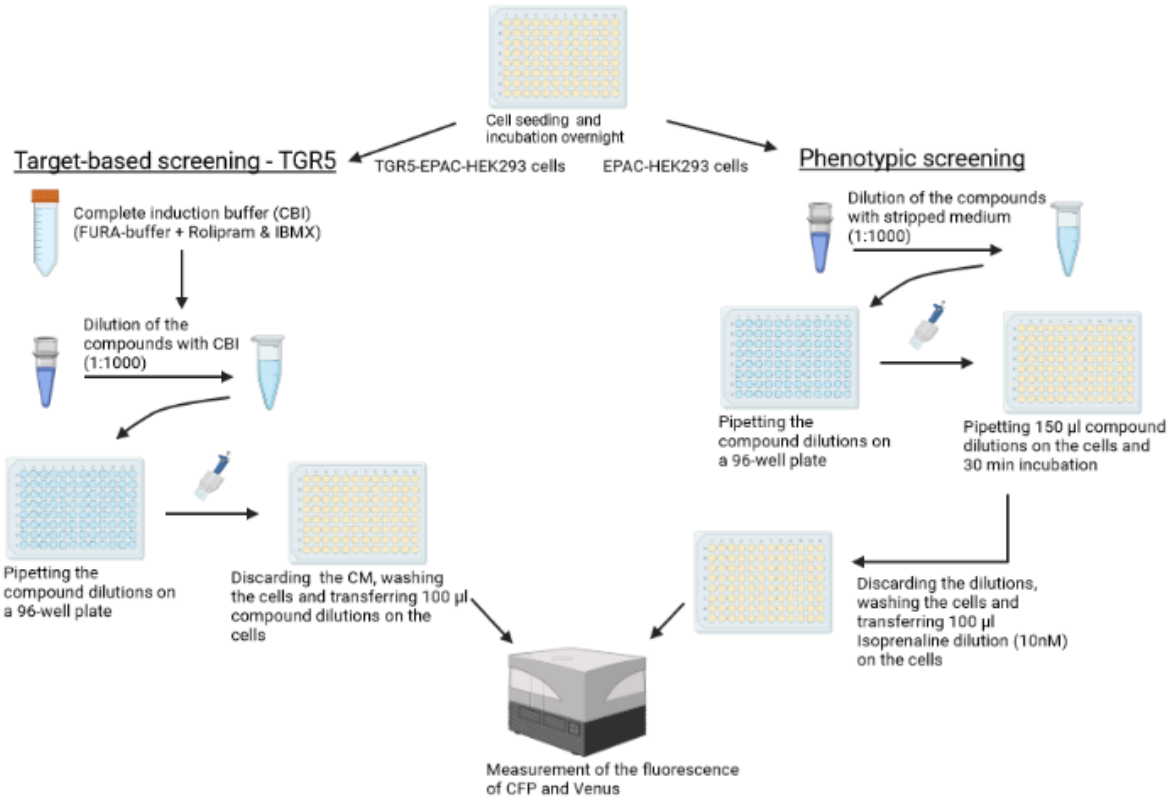

Figure 12: Schematic illustration of the workflow of the target-based and the phenotypic screening. The process started with the seeding of the TGR5-Epac-HEK cells in the target-based screening or the Epac-HEK cells in the phenotypic screening on a 96-well plate. Then, the 96-well plate was incubated overnight. On the next day, the compound dilutions were prepared differently in the screenings. Subsequently, the cells were treated with the compound dilutions. The cells were also stimulated with isoprenaline 10 nM in the phenotypic screening. The measurement was performed via a microplate reader. Illustration created in BioRender.com

3.1.3 Measurement and statistical analysis

A fluorescence intensity scan of the 96-well plate was conducted via TECAN Spark® Microplate Reader. In the measurement, the donor fluorophore CFP got excited with monochromatic light at 420 nm at room temperature. To examine the emission of both fluorophores CFP and Venus, an emission spectrum was measured from 460 nm to 550 nm with a bandwidth of 20 nm.

For the analysis of the data, the fluorescence ratio of CFP/Venus was calculated for the technical triplicates by using Microsoft Office Excel. Therefore, the autofluorescence was subtracted from the emissions at the emission peaks, which were at 480 nm for CFP and at 526 nm for Venus. After calculating the ratios of the triplicates, the mean of the ratios was normalized to the vehicle control DMSO 0.1%. The results were expressed as percentage of the increase in the fluorescence emission ratio of the basal levels. The data was transferred

to GraphPad Prism 6.01. With this program the statistical analysis was made by using one-way-ANOVA analysis followed by a Dunnett´s posthoc test. Also, IC_{50} values were calculated, and dose-response curves were created by non-linear regression.

3.2 Kinetic cAMP measurement via FRET assay

On a 6-well plate 1 x 10^6 cells per well were seeded in 3 ml CM and incubated overnight. In this experiment the Epac-HEK cell line was used. On the next day, the compound dilutions (1:1000) were prepared in a sterile surrounding by using SM. DMSO 0.1% served as vehicle control and roflumilast 1 µM as positive control. Afterwards, the old CM, which was on the incubated 6-well plate, was discarded and 3 ml of the compound´s dilutions were pipetted in each well. The cells were again incubated for 30 min. In the meantime, isoprenaline was diluted in two steps to an end concentration of 100 nM by using 1x FURA buffer in a non-sterile surrounding. After the incubation period, the compound dilutions were removed from the 6-well plate and the cells were washed with 1 ml 1x FURA buffer. Subsequently, 3 ml of 1x FURA buffer were pipetted in each well and the measurement with TECAN Spark® Microplate Reader was started. By the injection of 300 µl isoprenaline dilution (100 nM) into the 3000 µl 1x FURA buffer a further dilution with the factor 1:10 was achieved. So, the final concentration of isoprenaline was 10 nM.

The measurement was conducted at room temperature via TECAN Spark® Microplate Reader. Initially, 300 µl isoprenaline (100 nM) in FURA buffer was injected into a well via the injection module of the microplate reader and directly afterwards, the fluorescence intensity scan started. The scan lasted 15 min per well and 55 emission spectra were recorded. After that time, the same process started in the next well. The excitation wavelength was at 420 nm and the measured emission spectrum was from 460 nm to 550 nm with a bandwidth of 20 nm.

For the analysis of the data, the fluorescence emission ratio of 480 nm to 526 nm was calculated for every single timepoint by using Microsoft Office Excel. The statistical analysis was carried out by the same program that was used to illustrate the graphics, namely, the program GraphPad Prism 6.01. Here, the one-way-ANOVA analysis was used.

Table 4: Composition of the FURA buffer.

Material	Ingredients	Amount	Source
10x FURA buffer (pH 7.2)	NaCl (138 mM)	40.3 g	Sigma-Aldrich (Vienna, Austria)
	HEPES (20 mM)	23.8 g	Sigma-Aldrich (Vienna, Austria)
	Glucose (1 g/L)	5 g	Sigma-Aldrich (Vienna, Austria)
	KCl (5 mM)	1.86 g	Sigma-Aldrich (Vienna, Austria)
	$CaCl_2$ (1.6 mM)	1.17 g	Sigma-Aldrich (Vienna, Austria)
	$MgCl_2$ (1 mM)	0.47 g	Sigma-Aldrich (Vienna, Austria)
	ddH_2O	ad 500 ml	
1x FURA buffer (pH 7.2)	10x FURA buffer	50 ml	
	ddH_2O	450 ml	

Table 5: Devices used in the FRET assay and in the Griess assay.

Device	Source
HERAsafe®KS18	Thermo Fisher Scientific Inc. (Waltham, CA, USA)
Julabo® SW23	Julabo GmbH (Allentown, PA, USA)
HERAcell® 150 Incubator	Thermo Fisher Scientific Inc. (Waltham, CA, USA)
VM-3000 Mini Vortexer	VWR International (Radnor, PA, USA)
TECAN Spark® Microplate Reader	Tecan Group Ltd. (Maennedorf, Switzerland)

Table 6: List of the substances used as positive or negative controls.

Material	Source	Catalog number
DMSO 100%	Sigma-Aldrich (Vienna, Austria)	
Forskolin	Cayman Chemical (Ann Arbor, MI, USA)	Cay11018
Roflumilast	Sigma-Aldrich (Vienna, Austria)	SML1099
LCA	Sigma-Aldrich (Vienna, Austria)	L6250
Parthenolide	Sigma-Aldrich (Vienna, Austria)	P0667

4 Griess assay

To determine the nitric oxide (NO) production in J774A.1 macrophages *in vitro* the Griess assay was performed. Different compounds were tested to examine their effect on the NO production in macrophages. NO has a very short half-life which lasts maximal a few seconds.

Depending on the reaction conditions, NO oxidizes to nitrite or nitrate. Therefore, in this experiment the concentration of nitrite is measured. (90)

For the measurement, the Griess reagents sulfanilamide and N-naphtyl-ethylenediamine were sequentially added in an acidic solution to the testing liquid. Sulfanilamide reacts with nitrite to a diazonium salt, which changes over the coupling reaction with N-naphtyl-ethylenediamine to a pink-colored, stable azo compound. The absorbance of this compound is at 540 nm and is linear to the nitrite concentration. (91, 92) In **Figure 13** the Griess reaction is illustrated.

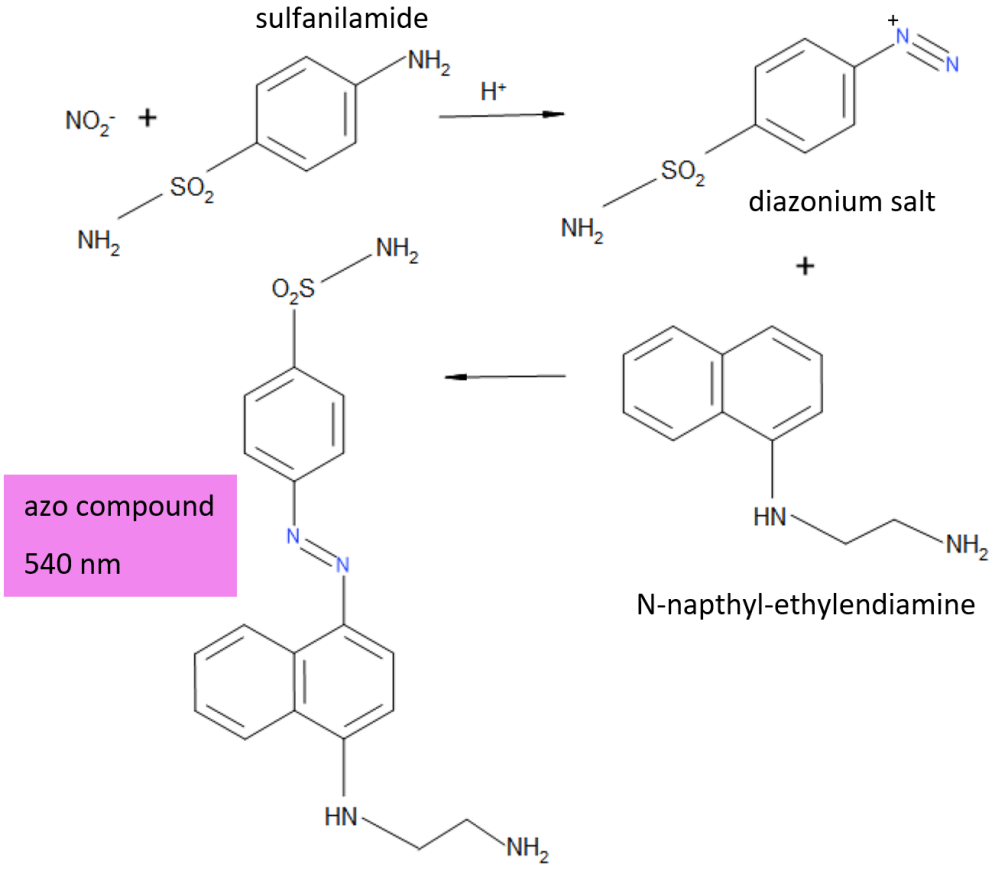

Figure 13: Illustration of the Griess reaction.

Nitrite reacts with sulfanilamide to a diazonium salt and subsequently, N-naphtyl-ethylenediamine reacts with the occurred diazonium salt to a stable azo compound, which has an absorbance at 540 nm. (91, 92)

4.1 Determination of the NO production in murine macrophages by the Griess assay

Adherent growing J774A.1 macrophages were seeded on a 12-well plate. An amount of 0,5 x 10^6 cells was placed per well in 2 ml CM. After the seeding process, the cells were incubated overnight at 37°C and 5% CO_2.

On the next day, dilutions of the compounds with the factor 1:1000 were prepared in SM. This work process took place under the laminar air flow workbench (HERAsafe®KS18). The old CM of the incubated 12-well plate was discarded and 2 ml of the compound´s dilutions were added to the cells. After 30 min incubation time, 2 µl LPS (final concentration 1 µg/ml in PBS) (Fluka Analytics (Vienna, Austria), 62326) were pipetted to each well, except for the well with the negative control (DMSO 0.1% plus PBS). In this well 2 µl PBS were added instead of LPS. To compare the basal NO production of the cells without LPS stimulation to the stimulated NO production by LPS, the negative controls DMSO 0.1% plus PBS and DMSO 0.1% plus LPS were mandatory. Parthenolide 1 µM, a NF-κB inhibitor (97), served as positive control. Then, the 12-well plate was incubated overnight at 37°C and 5% CO_2. A schematic illustration of the 12-well plate is shown in **Figure 14**.

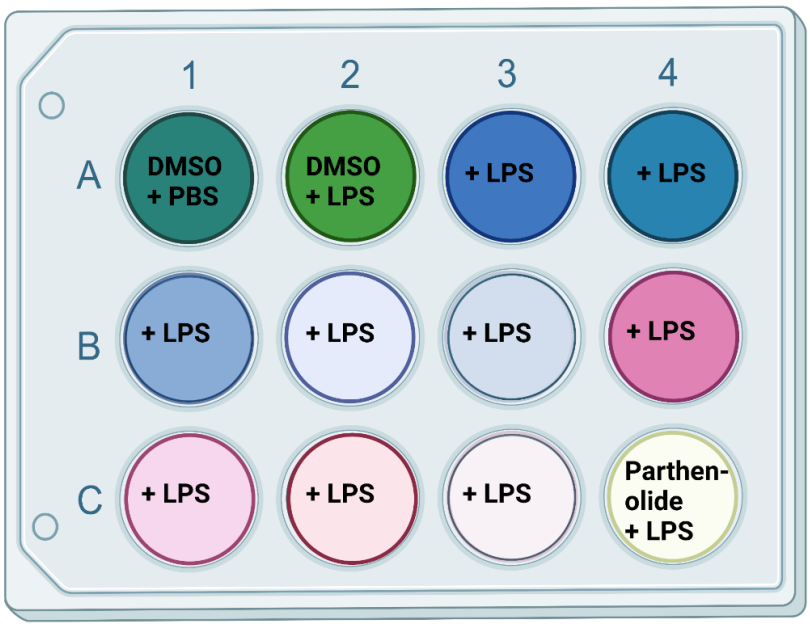

Figure 14: Schematic illustration of the 12-well plate seeded with J774A.1 macrophages after compound treatment and stimulation with LPS in the Griess assay.
The vehicle controls were DMSO 0.1% plus PBS and DMSO 0.1% plus LPS. Parthenolide 1 µM plus LPS was used as positive control. The J774A.1 cells were treated with different concentrations of the tested compounds and were stimulated with LPS. Illustration created in BioRender.com

On the third day, the Griess reagents were freshly prepared. Therefore, 2 ml 85% H_3PO_4 and 32 ml distilled H_2O were mixed to produce 5% H_3PO_4. This solution then served as solvent for the Griess reagent sulfanilamide at a concentration of 1%. The second Griess reagent N-naphtyl-ethylenediamine was solved in distilled H_2O at a concentration of 0.1%. The two reagents were mixed 1:1 immediately before using.

The 12-well plate was removed from the incubator and via TECAN Spark® Microplate Reader pictures of the cells were taken to determine their overall viability and the cell density.

Then 100 µl of the supernatant from each well were pipetted in a 96-well plate in eight wells to obtain technical octuplicates. Subsequently, 100 µl of the 1:1 mixture of the Griess reagents were added in each well of the 96-well plate, respectively. The absorbance of the stable azo compound at 550 nm was measured via TECAN Spark® Microplate Reader. The statistical analysis was conducted by using one-way-ANOVA analysis of the program GraphPad Prism 6.01.

Table 7: Materials used in the Griess assay.

Material	**Ingredients**	**Source**
Griess reagent	N-naphtyl-ethylenediamine 0,1% solved in distilled H_2O	Sigma-Aldrich (Vienna, Austria)
	Sulfanilamide 1% solved in 5% H_3PO_4	Sigma-Aldrich (Vienna, Austria)

5 Luciferase assay

The luciferase assay is commonly used to examine if a compound or protein affects the gene expression. Thereby, the amount of the gene product is coherent to the emitted light. Luciferase is an enzyme, which catalyzes a bioluminescence reaction. It is naturally produced by different organisms, like the fireflies. (93) In the luciferase assays, the regulatory region of the target gene is coupled to the reporter gene of the firefly luciferase from *Photinus pyralis*. The used cell line was transfected with this specific plasmid. Thus, when the ligand activates a signal pathway, which affects the target gene, the reporter protein will be expressed and can be detected by a bioluminescence reaction. (93, 94) For the examination of the viability and the transfection efficacy of the cells, the HEK293 cells were transfected with the DNA of

the green fluorescent protein (GFP) and the HEK293/ NF-κB-luc cell line was treated with cell tracker green (CTG). By working with TGR5-Epac-HEK or Epac-HEK cell lines the Epac-based FRET biosensor was used as an internal viability marker.

The expressed luciferase enzyme catalyzes the bioluminescence reaction, where luciferin is converted in presence of ATP, O_2 and Mg^{2+} to oxyluciferin plus CO_2, AMP, pyrophosphate (PP_i) and light (560 nm). (94, 95) The released light can be measured and is directly proportional to the amount of expressed luciferase. (93) The reaction is illustrated in **Figure 15**. Coenzym A (CoA) was also added to the reaction in the lysis buffer, due to the enhanced sensitivity of the assay, which can be traced back to a longer and persistent measurable signal. (96)

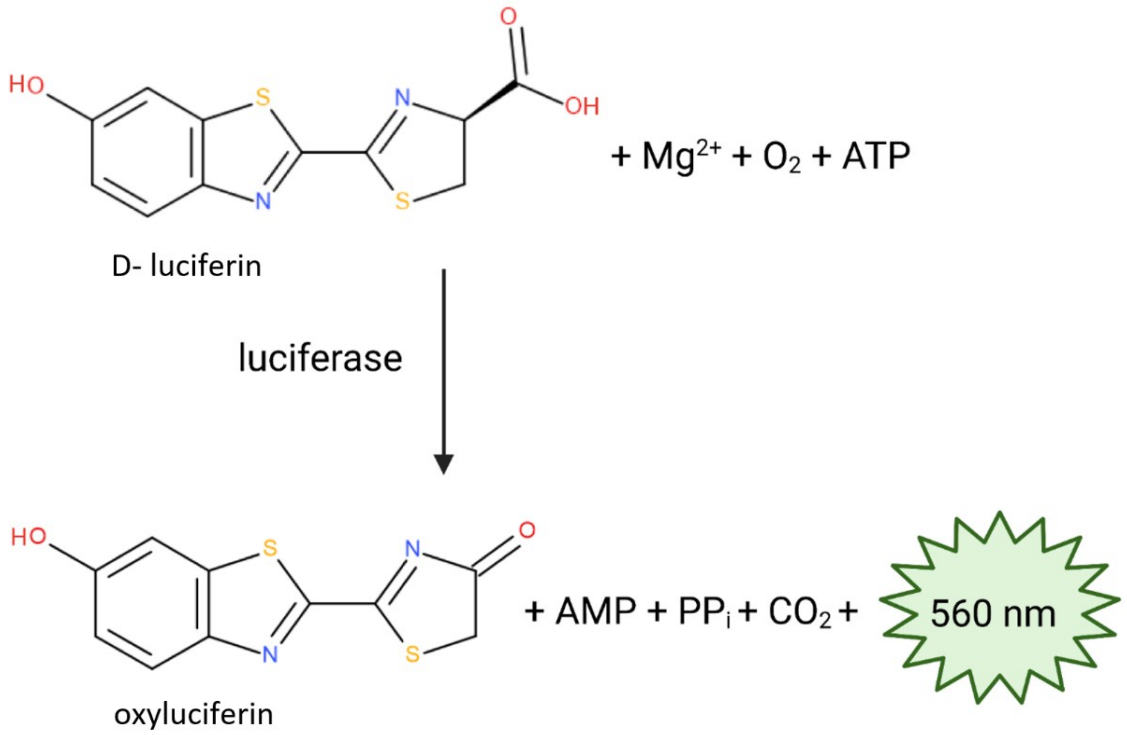

Figure 15: Illustration of the luciferase assay reaction.
The firefly luciferase catalyzes the reaction of luciferin in the presence of Mg^{2+}, O_2 and ATP to oxyluciferin plus AMP, PP_i and CO_2. Hereby, the emitted light at 560 nm can be detected. (94, 95) Illustration created in BioRender.com

Three different types of luciferase assays were conducted: the CRE-luciferase assay, the farnesoid X receptor (FXR)-Gal4-luciferase assay, and the NF-κB-luciferase assay. The first experimental parts of the CRE-luciferase assay and the NF-κB luciferase assay differed in their

methods, because of that they are described separately in the chapters [5.1 Conduction of the CRE- and FXR-Gal4- luciferase assay] and [5.2 Conduction of the NF-κB luciferase assay].

5.1 Conduction of the CRE- and FXR-Gal4-luciferase assay

The aim of the CRE-luciferase experiment was primarily to confirm the results of the target-based and the phenotypic screenings obtained by the Epac-based FRET biosensor (described previously in the chapter [3 Epac-based FRET biosensor assay]) with a more sensitive and quantitative method. For the determination of a potential effect of a tested compound on the cAMP/CRE pathway the plasmid CRE-luciferase was used for transfections. However, it is worth noting that this assay is only an indirect method of measuring the effect on the cAMP/CRE pathway. (93) To assess that the tested compound is TGR5 selective, also a FXR-Gal4-luciferase assay was conducted.

On a 150 mm dish the appropriate cells were seeded with a density of 8×10^6 cells and embedded in 20 ml CM. For the CRE-luciferase assay, either the cell lines TGR5-Epac-HEK or Epac-HEK were used depending on the verification of the positive results of the target-based or the phenotypic screening. In the FXR-Gal4-luciferase assay, the wildtype HEK293 cells were taken. Furthermore, untransfected wildtype HEK293 cells were always needed as control group. However, wildtype HEK293 cells were also seeded on a separate dish which served as control plate, to ensure that the positive results from the screenings can be traced back to the agonistic activity on TGR5 or on the PDE inhibitory activity. On this second control dish an amount of 8×10^6 HEK293 cells was transferred and covered in 20 ml CM. The cells were incubated at 37°C and 5% CO_2 for around four hours after seeding.

After four hours, the cells adhered to the ground of the dish. The transfection was conducted with the calcium phosphate precipitation technique. Therefore, a volume of 1500 µl transfection mixture was needed, and the exact composition of the transfection mixture is listed in **Table 8**. First, ddH2O, HEPES-buffered-saline (2x HBS) and a CRE-luciferase plasmid (10 µg) or a FXR-Gal4 fusion construct (5 µg) as well as a tk-Luc reporter plasmid (5 µg) were added to an Eppendorf tube and vortexed very thoroughly. After the dropwise adding of $CaCl_2$ (2 M), the mixture was vortexed and subsequently, incubated for 20 min at room temperature. In that time, the $Ca_3(PO_4)_2$-DNA co-precipitates were formed. In case the wildtype HEK293 cell line was used as control, the GFP plasmid (3 µg) was also added to the

transfection mixture. Instantly after the incubation, the mixture was pipetted dropwise on the incubated cell culture dish. The cells were incubated at 37°C and 5% CO_2 overnight.

The next morning, the medium change was done immediately due to the toxicity of the precipitates. Therefore, in the first step the old CM was removed from the dish and the cells were washed with 10 ml PBS. After the first step was completed, they were covered in 20 ml CM and incubated again.

Five hours after the medium change, the cells were passaged and treated with the testing compounds. For the preparation of the substance treatment, the dilution factor was 1:250 by using SM. Then, 50 µl of each dilution was pipetted to four wells of a sterile 96-well plate. It is significant to note that four wells were left empty for the seeding of the untransfected cells later. A schematic illustration of the 96-well plate used in the luciferase assay is illustrated in **Figure 16**. In these assays, DMSO 0.1% was always the negative control and roflumilast 1 µM or LCA 10 µM were used as positive controls (**Table 6**).

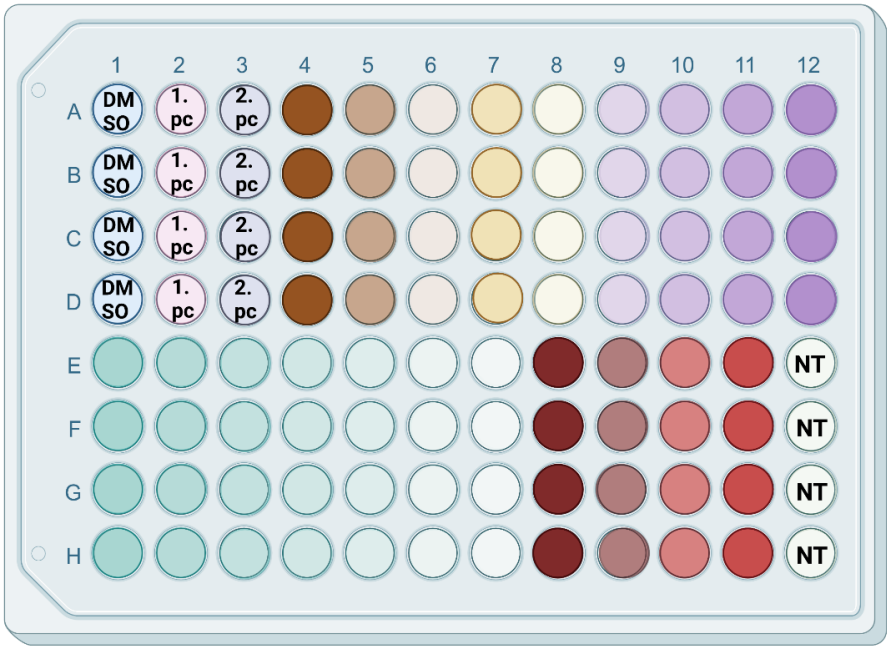

Figure 16: Schematic illustration of the 96-well plate used in the CRE- and FXR-Gal4-luciferase assay. To confirm the results of the target-based or the phenotypic screening the cell line TGR5-Epac-HEK or Epac-HEK was used. The vehicle control was always DMSO 0.1%. The selected positive controls depended on the assay. So, LCA, forskolin or CDCA (10 µM) were applied in the assays. Different concentrations of the tested compounds were added to the wells A4 to H11. pc= positive control; NT= not transfected cells. Illustration created in BioRender.com

Finally, the plate was gently pre-warmed in the incubator at 37°C and 5% CO_2. Subsequently, the old CM was discarded from the incubated dishes, and they were washed with 10 ml PBS.

The trypsinization with 4 ml trypsin/EDTA lasted 5 min and was inactivated by addition of 8 ml CM. The detached cells were transferred to a Falcon Tube and centrifugated at 1400 rpm for 4 min. As soon as the centrifugation was completed, the supernatant was removed from the cell pellet and the cells were resuspended in 11 ml SM. Afterwards, the cell count and the cell viability were determined by using ViCell^{TM} XR Cell Viability Analyzer. An amount of 5 x 10^4 cells per well in 150 µl SM was transferred to each well of the pre-warmed 96-well plate. Hence, the dilution factor of the compounds was totally 1:1000. The same working steps were conducted with the untransfected HEK293 cells and the specific cell amount in 200 µl SM was transferred to the four empty wells. The cells were again incubated overnight. On the third day, the viability of the treated cells was examined with the Olympus CKX31 light microscope. The supernatant above the cells was removed with vacuum and subsequently the plate was frozen at -70°C for at least 30 minutes.

Table 8: Materials for the transfection mixture for the luciferase assays and the composition of 2x HBS.

Material	Ingredients	Amount	Source
Transfection mixture for stably transfected cell lines	$CaCl_2$ (2 M)	94 µl	Sigma-Aldrich (Vienna, Austria)
(TGR5-Epac-HEK and Epac-HEK cells)	pGL4.29[luc2P/CRE/Hygro] Vector	10 µg	Promega (Madison, Wi, USA)
	or		
	FXR-Gal4	5 µg	Prof. Daniel Merk (Ludwig-Maximilians-University, Munich, Germany)
Ad FXR-Gal4:	tk(MH1000)4x LUC	5 µg	Dr. Ronald Evans (Salk Institute for Biological Studies, CA, USA)
	2x HBS	750 µl	
	ddH_2O	ad 1500 µl	
Transfection mixture for wildtype HEK293 cells			
Constituents like above with addition of:	peGFP-N1	3 µg	Clontech (San Jose, CA, USA)
2x HBS (pH 7.05)	NaCl (280 mM)	750 µl	Sigma-Aldrich (Vienna, Austria)
	KCl (10 mM)		Sigma-Aldrich (Vienna, Austria)
	Na_2HPO_4 (1.5 mM)		Carl-Roth (Karlsruhe, Germany)
	HEPES (50 mM)		Sigma-Aldrich (Vienna, Austria)
	Dextrose (12 mM)		Sigma-Aldrich (Vienna, Austria)

5.2 Conduction of the NF-κB luciferase assay

The aim of the NF-κB-luciferase assay was to determine if specific compounds, which have shown an activity in the phenotypic screening as potential PDE-inhibitors, have an impact on the NF-κB pathway through the enhanced cAMP levels. Here, the stably transfected NF-κB-luc cell line was used.

During the cell splitting, two culture flasks with a density of 6 x 10^6 HEK293/ NF-κB-luc cells were prepared and incubated for two days. One of the two culture flasks was stained with cell tracker green (CTG) in order to detect viable HEK293/ NF-κB-luc cells afterwards. Therefore, 3 µl CTG (2 µM) were added to 15 ml DMEM serum-free in a Falcon tube. DMEM serum-free contained 5 ml glutamine solution, 5 ml penicillin/streptomycin solution and 500 ml DMEM without phenol red. The old CM was removed from one culture flask of the HEK293/ NF-κB-luc cells and replaced with the CTG/DMEM serum-free mixture. The cells were incubated for one hour at 37°C and 5% CO_2.

After one hour, the color of the incubated HEK293/ NF-κB-luc cells and of the medium should have changed to green. Through the use of trypsin, the CTG stained cells and the unstained HEK293/ NF-κB-luc cells were splitted. Therefore, the medium was discarded, the cells were washed with 10 ml PBS and detached via the treatment with 2 ml trypsin/EDTA for 2 min. By adding 8 ml CM to the cells, the trypsinization was stopped. Next, the suspended cells were transferred to a Falcon tube and centrifugated at 1400 rpm for 8 min. Afterwards, the supernatant above the cell pellet was discarded and the cells were resuspended in 11 ml DMEM serum-free. The cell count was examined by using ViCell^{TM} XR Cell Viability Analyzer.

In the majority of the wells of the 96-well plate an equal amount of 4 x 10^4 CTG stained HEK293/ NF-κB-luc cells were seeded in 100 µl DMEM serum-free, only four wells were left empty to seed the same amount of unstained NF-κB-HEK293 cells. A schematic graphic of the 96-well plate is shown in **Figure 17**. To foster cell growth, the 96-well plate was incubated overnight. For a further cultivation of the HEK293/ NF-κB-luc cells, 6 x 10^6 unstained cells were transferred to two culture flasks and covered with 20 ml CM. Subsequently, the 96-well plate was deposited overnight in the incubator at 37°C and 5% CO_2.

On the following day, the density, the attachment, and the staining of the cells were checked by using the fluorescence microscope. Under the laminar air flow, the compound dilutions

were established. 1 µl compound was diluted in 399 µl DMEM serum-free (1:400) and an amount of 80 µl of each compound dilution was pipetted to four wells of the 96-well plate to receive quadruplicates. DMSO 0.1% was used as vehicle control and parthenolide 1 µM (**Table 6**), which inhibits the transcription factor NF-κB, was employed as positive control. (97) Following the previous steps, 100 µl DMEM serum-free was added to the unstained HEK293/ NF-κB-luc cells. The cells were again incubated for one hour at 37°C and 5% CO_2. In the meantime, 4 µl TNFα (PeproTech US, Cranbury, USA; #300-01A) were diluted in 2 ml DMEM serum-free to a final concentration of 2 ng/ml TNFα. After one hour, 20 µl TNFα dilution was added to each well except for the wells with the unstained cells. Therefore, the total dilution factor of the compounds was 1:1000. The 96-well plate was again incubated for around 3,5 to 4 hours. Then the medium was removed by using vacuum and the plate was frozen at -70°C for at least one hour.

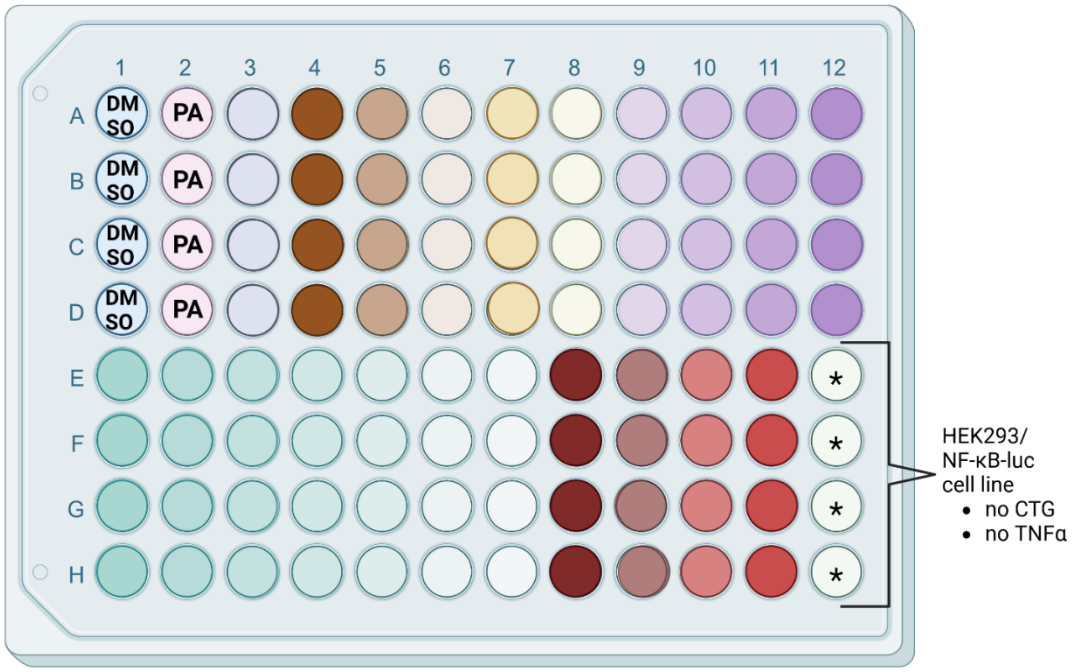

Figure 17: Schematic illustration of the 96-well plate used in the NF-κB assay.
The HEK293/ NF-κB-luc cell line was treated with different concentrations of the compounds LRK071 and AH-17. The vehicle control was DMSO 0.1% and parthenolide 1 µM was used as positive control. After an incubation time of one hour, the cells were stimulated with TNFα except the cells in the row 12 from E to H. Also, the cells in row 12 E to H were not stained with CTG. PA= parthenolide. Illustration created in BioRender.com

5.3 Measurement of the luciferase assays

The lysis of the cells has to be conducted for an appropriate detection of the bioluminescence reaction. Therefore, a lysis buffer was prepared and the components are listed in **Table 9.**

Table 9: Compounds of the lysis buffer for one 96-well plate and reagents for the luciferase-reaction.

Material	**Ingredients**	**Amount (for one 96-well plate)**	**Source**
Lysis buffer	ddH_2O	4,8 ml	
	5x lysis buffer	1,2 ml	Promega (Wi, USA)
	Coenzyme A (CoA)	2 µl, 270 mM	Sigma- Aldrich (Vienna, Austria)
	Dithiothreitol (DTT)	6 µl, 1 M	Fluka (Vienna, Austria)
ATP		50 µl/well	Carl Roth (Karlsruhe, Germany)
D-luciferin		50 µl/well	Synchem (Flesberg, Germany)

The frozen 96-well plate was removed from the freezer and 50 µl lysis buffer was added to each well. The plate was placed on the Multi-MicroPlate Genie™ shaker for 10 min. Afterwards, 40 µl of the liquid was transferred to a black 96-well plate and through a slight movement of the plate the equal distribution of the liquid was warranted.

The measurement was conducted via the TECAN Spark® Microplate Reader. Hereby, the fluorescence and the luminescence were measured. The specific parameters are shown in **Table 10**. For measuring the luminescence, the injection module of the microplate reader was used, which injected ATP and luciferin right before starting the measurement. As soon as luciferin came into contact with the enzyme luciferase, the bioluminescence reaction started and was directly quantified.

By using Microsoft office excel the mean values of the quadruplicates were calculated. Before determination of the ratio of relative luminescence units to relative fluorescence units (RLU/RFU), the mean values of the untransfected cells (background) were subtracted. Afterwards, the ratio was normalized to the negative control DMSO 0.1%. Statistical analysis was conducted by using the One-way-ANOVA analysis of the program GraphPad Prism 6.01.

Table 10: Parameters of the fluorescence and luminescence measurement with TECAN Spark® Microplate Reader.

Mode	**Top Reading Fluorescence Intensity**
Excitation wavelength	485 nm
Excitation bandwidth	20 nm
Emission wavelength	520 nm
Emission bandwidth	20 nm
Integration time	1000 µs
Settle time	0 ms
Mode	**Well**
Injector A & B	
Volume	50 µl
Speed	150 µl/sec
Mode	**Luminescence**
Settle time	50 ms
Integration time	2000 ms
Output	Counts/s
Attenuation	None

Table 11: Devices used in the luciferase assay.

Device	**Source**
HERAsafe®KS18	Thermo Fisher Scientific Inc. (Waltham, CA, USA)
Julabo® SW23	Julabo GmbH (Allentown, PA, USA)
HERAcell® 150 Incubator	Thermo Fisher Scientific Inc. (Waltham, CA, USA)
VM-3000 Mini Vortexer	VWR International (Radnor, PA, USA)
Olympus CKX31 light microscope	Olympus Europa GmbH (Hamburg, Germany)
Fluorescence microscope	
Multi-MicroPlate Genie™ shaker	Scientific Industries (New York, USA)
TECAN Spark® Microplate Reader	Tecan Group Ltd. (Maennedorf, Switzerland)

6 Fluorescence polarization assay

To examine potential PDE4B2 inhibitor activities of specific compounds, the PDE4B2 assay kit (catalog number: #60343) from BPS Bioscience was used. This assay is a cell-free based assay. The inhibitor activities are identified by measuring the fluorescence polarization of the fluorescent dye carboxyfluorescein (FAM), which is linked to cAMP. Since the free dye-labeled cAMP rotates very fast, it emits light with random orientations and low polarization. By adding PDE4B2 the phosphodiester bond of FAM-cAMP gets hydrolyzed. The emerging phosphate group provides a binding site for phosphate binding beads, which immobilize the AMP. Hence this bead-bound FAM-nucleotide rotates slower and emits light with high polarization. In contrast, if a compound inhibits the PDE4B2 enzyme, FAM-cAMP would not be hydrolyzed, and low polarized light would be detected.

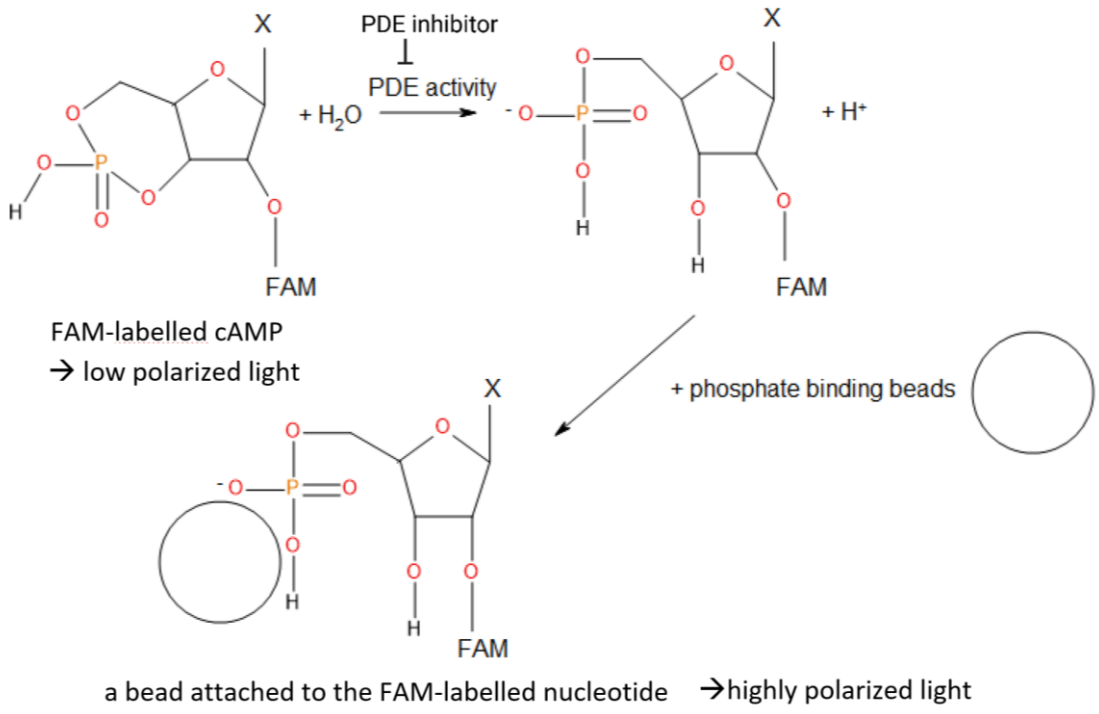

Figure 18: Mechanism of the PDE4B2 assay.
The PDE4B2 enzyme induces the hydrolysis of the phosphodiester bond of the FAM-labelled cAMP. By adding the phosphate binding beads, the beads attach to the phosphate groups of the FAM-labelled nucleotides. If a compound inhibits the PDE activity, the hydrolysis could not be catalysed by PDE and thus, the phosphate binding beads could not attach to the phosphate group. The FAM-labelled cAMP rotates very fast and emits light with low polarization. In contrast, the FAM-labelled nucleotide-bead complex rotates slowly and hence, emits light with high polarization. X= adenine.

The principle of the fluorescence polarization measurement is that linearly polarized light excites the fluorophore. This light occurs when monochromatic light passes an excitation polarizer. The polarized fluorescence of the fluorophore is measured with a parallel and a perpendicular orientated polarizer to the excited light´s plane. Because the sensitivity of the detection of the two polarizers is not equal and is dependent on the used device, the G-factor has to be assessed. So, to determine the fluorescence polarization (FP), the difference between the intensity with polarizers in parallel position ($I_{||}$) and the intensity with polarizers in perpendicular position ($I_{\perp}$) has to be calculated and normalized by the total intensity with consideration of the G-factor. (98, 99) The formula is given in **Figure 19**.

$$FP = 1000 * \frac{(I\| - G * I\perp)}{(I\| + G * I\perp)}$$

Figure 19: Formula for the calculation of the fluorescence polarization (FP).
The intensity with polarizers in parallel position ($I_{||}$), the intensity with polarizers in perpendicular position ($I_{\perp}$) and the G-factor (G) was considered. (98, 99)

6.1 Conduction of the PDE4B2 fluorescence polarization assay

According to the manufacturer´s protocol from BPS Bioscience, the PDE4B2 assay kit consisted of two steps and was conducted in a non-sterile surrounding. In the first step, the testing compounds, FAM-cAMP and PDE4B2 enzyme were incubated for one hour. This reaction mix initiate the first part of the reaction - the hydrolysis of FAM-cAMP. In the next step, beads were added to the reaction mix and again incubated for one hour. Now the fluorescence polarization changes due to the binding of the beads to the phosphate group. After the incubation time, the measurement was conducted.

To receive the intended dilutions of the testing compounds, it was necessary to undertake two sequential dilution steps. Firstly, the compound was diluted 1:1000 by using DMSO 100% (Sigma-Aldrich, Vienna, Austria). Secondly, PDE assay buffer was added to obtain another 1:10 dilution. Because of the addition of the compound dilution to the volume prepared in the 96-well plate, a final third dilution step is achieved with a dilution factor of 1:10.

Starting with the preparation of the experiment, the PDE4B2 assay kit from BPS Bioscience provided a 20 µM stock of FAM-cAMP. 50 µl of this stock was diluted (1:100) in 4950 µl PDE assay buffer to obtain a concentration of 200 nM. Aliquots of this dilution were prepared and

frozen at - 70°C. Before starting the experimental part, also the PDE4B2 enzyme was diluted in two steps to an end concentration of 7,5 pg/µl by using PDE-assay buffer. It is noteworthy that the enzyme is very sensitive to freeze/thaw cycles, because of this, aliquots of the enzyme dilution were frozen at - 70°C.

On a black, low binding 96-well plate 25 µl of FAM-cAMP (200 nM) were pipetted to the wells "positive control", "substrate control" and "test inhibitor". Subsequently, 20 µl PDE-assay buffer was added to the wells "substrate control" and 45 µl buffer was pipetted to the well "blank". To the denoted wells "test inhibitor" and "substrate control" 5 µl of the 10x compound dilutions, which were previously described, were added. For each labeled well "positive control" and "blank" 5 µl of the prepared dilution of PDE-assay buffer plus DMSO 10% (final concentration 1% in the well) were added. Because of the high sensitivity of the PDE4B2 enzyme, it was thawed on ice. 20 µl of PDE4B2 are pipetted to the denoted wells "test inhibitor" and "positive control". The contents of the different liquids are listed in **Table 12**. Immediately, the hydrolysis reaction started. The 96-well plate was incubated for 1 hour at room temperature and protected from light by aluminum foil.

Table 12: Overview of the composition of the different liquids in the PDE4B2 assay.

Ingredients	**Positive control**	**Blank**	**Substrate control**	**Test inhibitor**
FAM-cAMP	25 µl		25 µl	25 µl
PDE-assay buffer		45 µl	20 µl	
PDE4B2 enzyme	20 µl			20 µl
Inhibitor dilution				5 µl
Compound dilution	5 µl	5 µl	5 µl	

For the second part, the binding agent dilution was prepared, before the end of the incubation time was reached. Therefore, the binding agent was vortexed thoroughly and diluted 1:100 in binding agent diluent. Subsequently, after the end of the incubation time, 100 µl binding agent dilution was pipetted to each well, respectively. Again, an incubation period was needed for 1 hour at room temperature. During this time the 96-well plate was shaking very slowly by using Multi-MicroPlate Genie™ shaker and it was again covered with aluminum foil.

The measurement of the fluorescence polarization was conducted with TECAN Spark® Microplate Reader. Therefore, the dye-labeled molecules got excited with monochromatic light of 485 nm ± 20 nm and the emission wavelength was measured at 535 nm ± 20 nm. In

every single measurement the G-factor had to be calculated by the microplate reader. Therefore, the well position of the "blank" and of the "substrate control" were specified in the adjustments. The analysis of the data and the illustration of graphs were performed by using GraphPad Prism 6.01, more precisely, the One-way-ANOVA analysis. Dose-response curves and IC_{50} values were generated by non-linear regression for a better interpretation of the data.

Table 13: Devices used in the PDE4B2 assay.

Device	**Source**
VM-3000 Mini Vortexer	VWR International (Radnor, PA, USA)
Multi-MicroPlate Genie™ shaker	Scientific Industries (New York, USA)
TECAN Spark® Microplate Reader	Tecan Group Ltd. (Maennedorf, Switzerland)

D. Results

1 Results of the Epac-based FRET biosensor assay

The high-throughput screenings, which encompass the phenotypic and the TGR5 target-based screening, as well as the kinetic measurement were conducted with the Epac-based FRET biosensor assay. In both high-throughput screenings, numerous substances of the DNTI project as well as synthesized compounds were tested. This assay made it possible to analyze the influence of tested compounds on the intracellular levels of the second messenger cAMP. The FRET mechanism was used for the direct measurement of cAMP and the measured fluorescence intensity, which corresponds with the cAMP concentration, was specified in the fluorescence emission ratio of CFP to Venus.

1.1 Results of the TGR5 target-based screening

For the TGR5 target-based screening the stably transfected TGR5-Epac-HEK cell line was used. The aim of this screening was the identification of potential TGR5 agonists. It was expected that the intracellular cAMP levels should increase after activation of the TGR5 as TGR5 is coupled to Gαs. To prove the potential TGR5 activation, a minimum of two to three independent measurements were conducted, and the statistical significance of the observed effects was determined. Since DMSO 0.1% served as solvent of the tested compounds, it was used as vehicle control in the screenings. LCA, the endogenous ligand of TGR5, as well as forskolin, a potent stimulator of the adenylate cyclase, served as positive controls.

For the analysis, the measured data is expressed in percent of the fluorescence emission ratio of CFP to Venus normalized to DMSO 0.1%, which represents the basal levels of cAMP.

1.1.1 Leoligin derivatives (3162, 3163)

The leoligin derivatives 3162 and 3163 were tested in the TGR5 target-based screening. A significant increase of the cAMP levels in TGR5-Epac-HEK cells could be detected during the treatment with 3162 at a concentration of 30 µM as well as during the treatment with 3163 at a concentration of 30 µM and 10 µM (**Figure 20**). The increase can be led back on a potential activation of the TGR5 receptor. The leoligin derivatives 3162 and 3163 were also screened in the phenotypic screening in Epac-HEK cells. However, no significant increase of the cAMP levels could be observed in this control assay indicating a TGR5-specific effect (data not shown). Interestingly, an increase of the cAMP levels was detected in prior phenotypic screenings of another leoligin derivative 2743. (67)

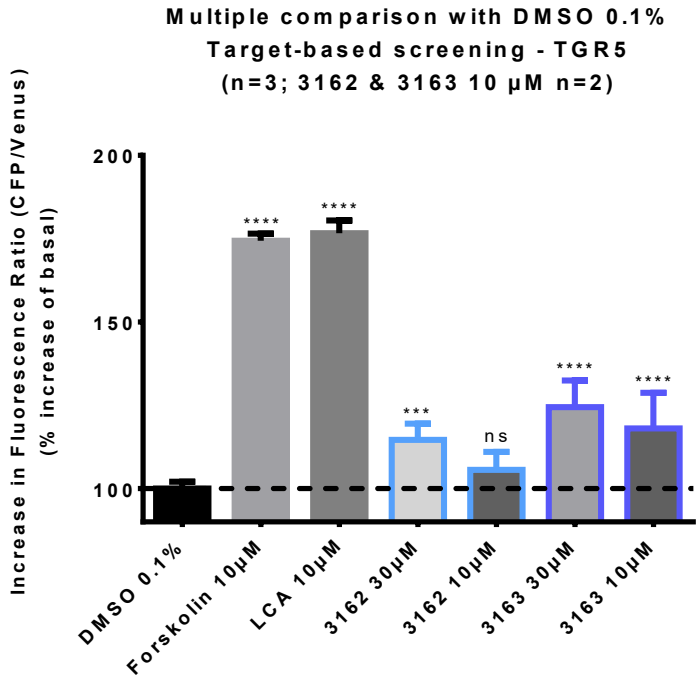

Figure 20: The influence of the DNTI compounds 3162 and 3163 on the intracellular cAMP levels in the TGR5 target-based screening.
The dilutions of the stock compounds (1:1000) were prepared using the CBI buffer. Afterwards, the TGR5-Epac-HEK cells were treated with the compound dilutions. After an incubation time of 10 min, the fluorescence intensity was measured, which is presented as the fluorescence emission ratio of CFP to Venus. The results are expressed in percent normalized to the vehicle control DMSO 0.1%. The data of the tested compounds are shown as mean values ± standard deviation (SD) of 2-3 biological replicates measured in technical triplicates. The statistical analysis was done by using the one-way-ANOVA analysis to examine statistical significance. Furthermore, the mean value of each column was compared to the mean value of the control column (DMSO 0.1%) by using the Dunnett´s post-hoc test. In the graph, DMSO 0.1% indicates the basal levels of cAMP. The mean of this column (100%) is also marked by a horizontal line. Statistical significance of p-values: ****: $p \leq 0.0001$; ***: $p \leq 0.001$; **: $p \leq 0.01$; *: $p \leq 0.05$; ns: $p > 0.05$

1.1.2 Helioxanthin (2644)

A significant increase of the intracellular cAMP levels was detected by testing the compound helioxanthin (2644) in comparison to DMSO 0.1%. The fluorescence emission ratio reached a mean value of 140.73% in three independent measurements. However, the standard deviation of this effect was very high (**Figure 21**).

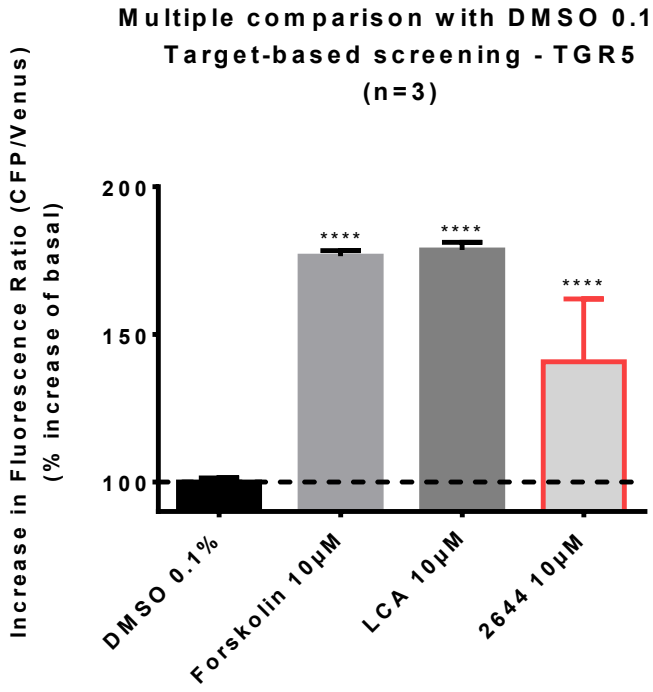

Figure 21: The influence of helioxanthin (DNTI 2644) on the intracellular cAMP levels in the TGR5 target-based screening.
The dilutions of the stock compounds (1:1000) were prepared using the CBI buffer. Afterwards, the TGR5-Epac-HEK cells were treated with the compound dilutions. After an incubation time of 10 min, the fluorescence intensity was measured, which is presented as the fluorescence emission ratio of CFP to Venus. The results are expressed in percent normalized to the vehicle control DMSO 0.1%. The data of the tested compounds are shown as mean values ± SD of three biological replicates measured in technical triplicates. The statistical analysis was done by using the one-way-ANOVA analysis to examine statistical significance. Furthermore, the mean value of each column was compared to the mean value of the control column (DMSO 0.1%) by using the Dunnett´s post-hoc test. In the graph, DMSO 0.1% indicates the basal levels of cAMP. The mean of this column (100%) is also marked by a horizontal line. Statistical significance of p-values: ****: $p \leq 0.0001$; ***: $p \leq 0.001$; **: $p \leq 0.01$; *: $p \leq 0.05$; ns: $p > 0.05$

1.1.3 Notopterol (1055)

Another compound, which caused an increase of the cAMP levels in the TGR5 target-based screening is the coumarin notopterol. In four independent measurements, it was observed that notopterol with a concentration of 8.5 µM effectuated a significant increase of the cAMP levels in TGR5-Epac-HEK cells. (**Figure 22**)

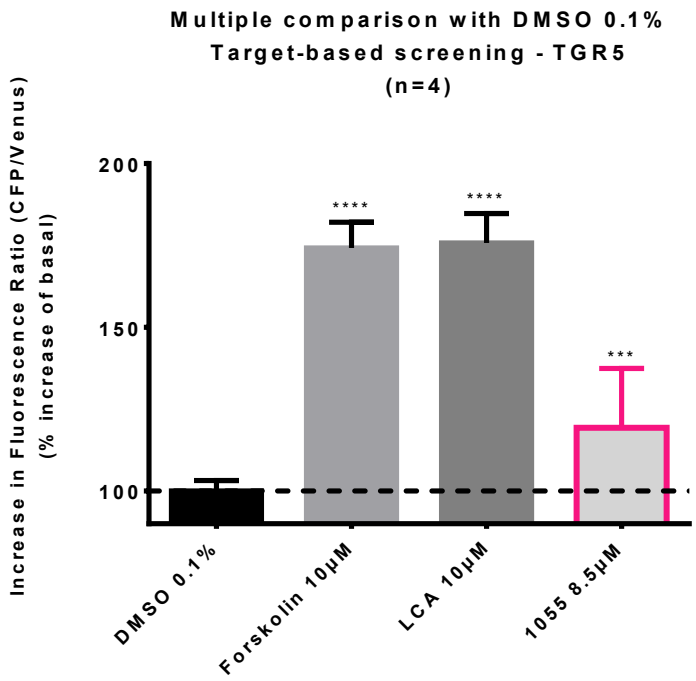

Figure 22: The influence of notopterol (DNTI 1055) on the intracellular cAMP levels in the TGR5 target-based screening.
The dilutions of the stock compounds (1:1000) were prepared using the CBI buffer. Afterwards, the TGR5-Epac-HEK cells were treated with the compound dilutions. After an incubation time of 10 min, the fluorescence intensity was measured, which is presented as the fluorescence emission ratio of CFP to Venus. The results are expressed in percent normalized to the vehicle control DMSO 0.1%. The data of the tested compounds are shown as mean values ± SD of four biological replicates measured in technical triplicates. The statistical analysis was done by using the one-way-ANOVA analysis to examine statistical significance. Furthermore, the mean value of each column was compared to the mean value of the control column (DMSO 0.1%) by using the Dunnett´s post-hoc test. In the graph, DMSO 0.1% indicates the basal levels of cAMP. The mean of this column (100%) is also marked by a horizontal line. Statistical significance of p-values: ****: $p \leq 0.0001$; ***: $p \leq 0.001$; **: $p \leq 0.01$; *: $p \leq 0.05$; ns: $p > 0.05$

1.2 Results of the phenotypic screening

The aim of the phenotypic screening was the identification of compounds which enhance the intracellular cAMP levels after independent stimulation of a Gαs receptor, i.e. the beta2-adrenergic receptor (ADRB2). In theory, this effect can be traced back to a potential PDE inhibitory activity of the tested compounds. Therefore, the stably transfected Epac-HEK cell line was pre-treated for 30 min with certain concentrations of the testing compounds. Subsequently, the cells were stimulated with the unspecific beta-adrenergic agonist isoprenaline (10 nM) to trigger an initial increase of the cellular cAMP levels. The measurement with a microplate reader was conducted half an hour later to allow the desensitization process to take place. After that time, the cAMP levels were measured. A minimum of two to three independent measurements were performed and the statistical significance was determined. The data of the measurements was stated in percent of the fluorescence emission ratio of CFP to Venus normalized to DMSO 0.1%, which represents the basal levels of cAMP. DMSO 0.1% was used as vehicle control, because it served as solvent of the tested compounds. The specific PDE4 inhibitor roflumilast (1 µM) as well as the adenylate cyclase stimulator forskolin (10 µM) served as positive controls.

1.2.1 LRK077

The magnolol derivative LRK077 (**Figure 23**) was tested in the phenotypic screening in different concentrations ranging from 10 µM to 1 nM. This was done to establish a concentration-response dependency. A significant enhancement of the cAMP levels compared to DMSO 0.1% was observed of LRK077 at the concentrations of 10 µM, 3 µM and 1 µM (**Figure 24**). This result indicates a potential PDE inhibitory activity. Also, a dose-response curve was generated to determine the half maximal inhibitory concentration (IC_{50}) of LRK077. **Figure 25** shows the dose-response curve from which a dose-dependent effect can be inferred and the IC_{50} is determined at 3.4 µM.

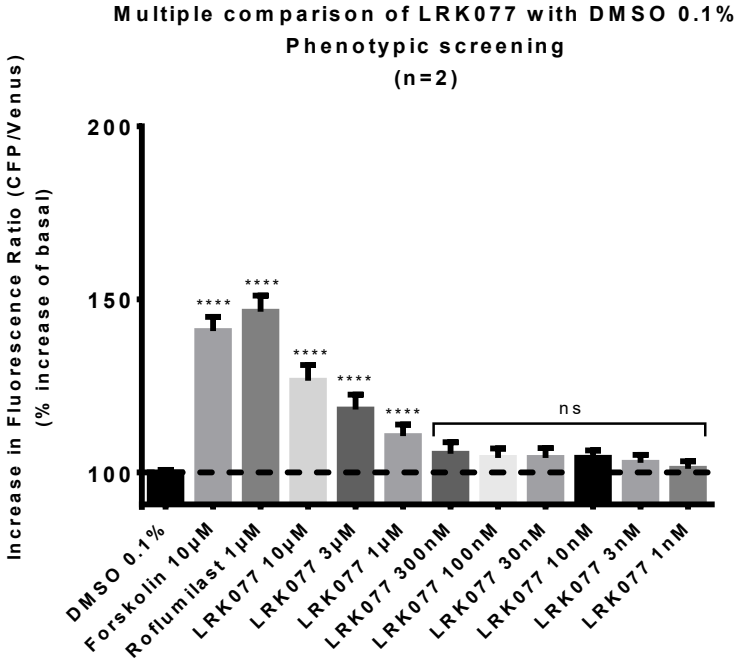

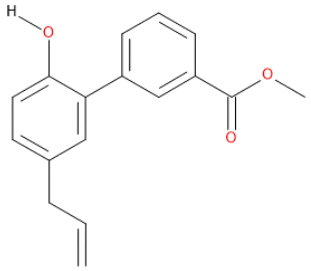

Figure 23: Structure of LRK077.

Figure 24: The influence of LRK077 on the intracellular cAMP levels in the phenotypic screening.
The stably transfected Epac-HEK cell line was treated with different concentrations of LRK077 (10 µM to 1 nM) and was incubated for 30 min. After that time, the cells were stimulated with isoprenaline (10 nM). Half an hour later, the fluorescence intensity was measured, which is presented as the fluorescence emission ratio of CFP to Venus. The results are expressed in percent normalized to the vehicle control DMSO 0.1%.
The data of the tested compounds are shown as mean values ± SD of two biological replicates measured in technical triplicates. The statistical analysis was done by using the one-way-ANOVA analysis to examine statistical significance. Furthermore, the mean value of each column was compared to the mean value of the control column (DMSO 0.1%) by using the Dunnett´s post-hoc test. DMSO 0.1% indicates the basal levels of cAMP and serves as vehicle control. The mean of this column (100%) is also marked by a horizontal line. Statistical significance of p-values: ****: $p \leq 0.0001$; ***: $p \leq 0.001$; **: $p \leq 0.01$; *: $p \leq 0.05$; ns: $p > 0.05$

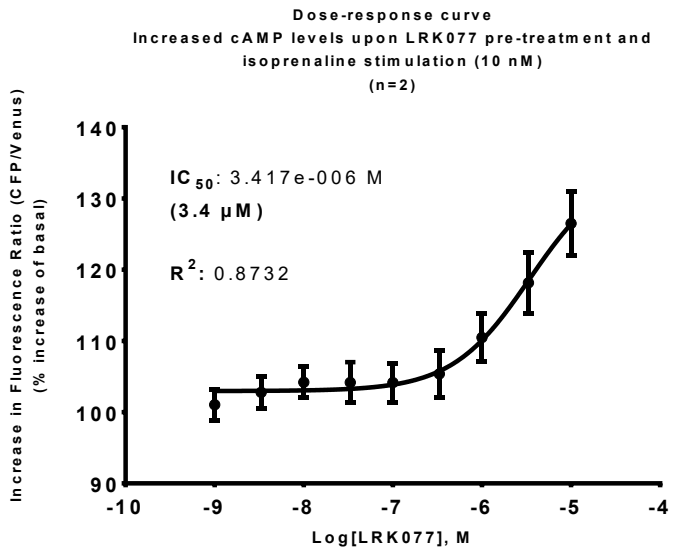

Figure 25: Dose-response curve of LRK077.
The dose-response curve was generated with the data of two independent phenotypic screenings. A dose-dependent effect from LRK077 in different concentrations on the cAMP levels was determined. The fluorescence intensity was measured, which is presented as the fluorescence emission ratio of CFP to Venus. The results are expressed in percent normalized to the vehicle control DMSO 0.1%. The software GraphPad Prism 6.01 was used for the nonlinear regression analysis to calculate IC_{50} and R^2 values.

1.2.2 Determination of a potential additive effect of LRK071 plus forskolin

The influence of the leoligin derivative LRK071 on the intracellular cAMP levels in Epac-HEK cells was already previously observed in the master´s thesis of the student Nourhan Elbeialy[67] in the working group of Univ.-Prof. Dr. Dirsch (University of Vienna). The increase of the cAMP levels was led back to a potential PDE inhibitory activity of LRK071. (67) To investigate this theory further, LRK071 would have an additive effect as potential PDE inhibitor on the intracellular cAMP levels with forskolin, a maximal stimulator of the adenylate cyclase, because of different points of action in the cAMP pathway. To determine this, the Epac-HEK cells were pre-treated with different concentrations of LRK071 (10 µM to 300 pM) and the selective PDE4 inhibitor roflumilast (3 µM to 100 pM), which was utilized as a positive control, following the instructions of the workflow of the phenotypic screening. Instead of treating the cells with isoprenaline (10 nM), the cells were stimulated with forskolin (final concentration 10 µM) after 30 min incubation. Hereby, the vehicle control was DMSO 0.1% plus forskolin 10 µM, which stands for the maximal increase of the cAMP levels caused by forskolin alone. Another positive control was the PDE4 inhibitor rolipram 10 µM plus forskolin 10 µM, which showed a significant additive increase of the cAMP levels compared to the vehicle control DMSO 0.1% plus forskolin 10 µM (**Figure 26**).

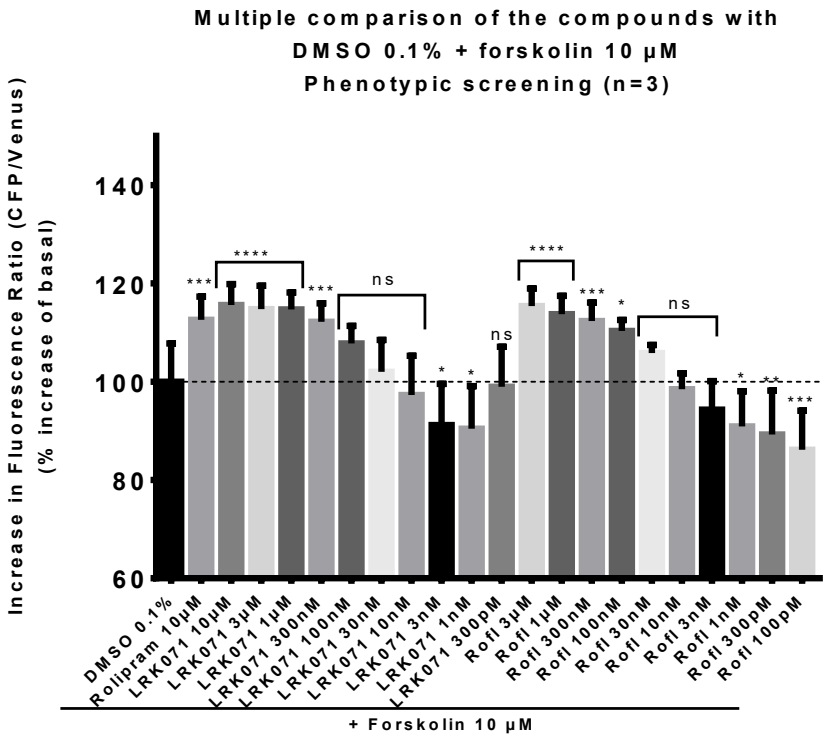

Figure 26: Determination of an additive effect of LRK071 plus forskolin 10 µM and roflumilast plus forskolin 10 µM in the phenotypic screening.
The stably transfected Epac-HEK cell line was treated with different concentrations of LRK071 (10 µM to 300 pM) and roflumilast (1 µM to 100 pM) and was incubated for 30 min. After that time, the cells were stimulated with forskolin (10 µM). Half an hour later, the fluorescence intensity was measured, which is presented as the fluorescence emission ratio of CFP to Venus. The results are expressed in percent normalized to the vehicle control DMSO 0.1%.
The data of the tested compounds are shown as mean values ± SD of three biological replicates measured in technical triplicates. The statistical analysis was done by using the one-way-ANOVA analysis to examine statistical significance. Furthermore, the mean value of each column was compared to the mean value of the control column (DMSO 0.1% plus forskolin 10 µM) by using the Dunnett´s post-hoc test. DMSO 0.1% plus forskolin 10 µM indicates the increase of the cAMP levels by forskolin 10 µM and serves as vehicle control. The mean of this column (100%) is also marked by a horizontal line. Statistical significance of p-values: ****: $p \leq 0.0001$; ***: $p \leq 0.001$; **: $p \leq 0.01$; *: $p \leq 0.05$; ns: $p > 0.05$

The higher concentrations of LRK071 (10 µM to 300 nM) plus forskolin 10 µM as well as the higher concentrations of roflumilast (3 µM to 100 nM) plus forskolin 10 µM showed a significant additive effect, which is illustrated in **Figure 26**. The very low concentrations of LRK071 as well as of roflumilast (LRK071 3 nM, 1 nM + forskolin 10 µM; roflumilast 1 nM, 300 pM, 100 pM + forskolin 10 µM) were also ranked as significant, however, this cannot be traced back to an additive effect. This result of an additive effect underpins the theory that LRK071 could be a PDE inhibitor rather than influencing beta-adrenergic signaling. Also, dose-response curves were generated to determine the IC_{50} value of LRK071 plus forskolin 10 µM

(IC_{50}: 35.21 nM) and roflumilast plus forskolin 10 µM (IC_{50}: 14.14 nM). **Figure 27** illustrates both dose-response curves and depicts the dose-dependent effect.

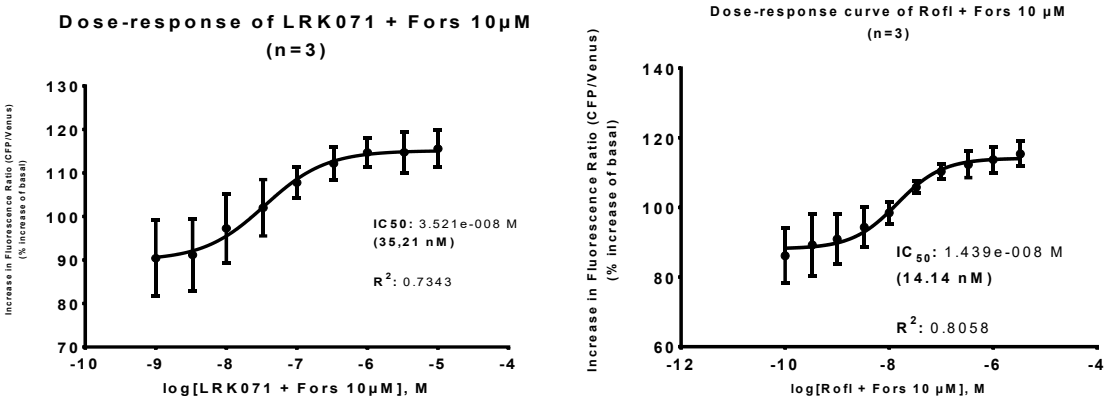

Figure 27: Dose response curves of LRK071 + forskolin 10 µM and of roflumilast + forskolin 10 µM. A dose-dependent effect of LRK071 + forskolin 10 µM and roflumilast + forskolin 10 µM in different concentrations on the cAMP level was determined in three independent measurements in the phenotypic screening. The fluorescence emission was measured, which is presented as the fluorescence emission ratio of CFP to Venus. The results are expressed in percent normalized to the vehicle control DMSO 0.1%. It was observed that both dose-response curves showed an effect on the cAMP levels in a dose-dependent manner. The software GraphPad Prism 6.01 was used for the nonlinear regression analysis to calculate IC_{50} and R^2 values.

1.3 Results of the kinetic cAMP measurement via FRET assay

In this assay, the changes of the intracellular cAMP levels, which are caused by a compound, can be observed over a certain time period. Therefore, the Epac-HEK cell line was used, because the changes in the intracellular cAMP levels were detected by the Epac-based FRET biosensor. The fluorescence emission was measured continuously over time and the fluorescence emission ratio of CFP to Venus was calculated.

1.3.1 Determination of the change of the cAMP levels caused by LRK071, AH-17 and 2743 after isoprenaline stimulation

The magnolol derivatives LRK071 and AH-17 as well as the leoligin derivative 2743 caused an increase in the cAMP levels in previous phenotypic screenings. This could be due to a potential PDE inhibitory activity. To support this theory, kinetic cAMP measurements were conducted with these three compounds. So, the Epac-HEK cells were treated and incubated for 30 min with the compounds of interest, namely, LRK071, AH-17 and 2743 (each concentration was 10 µM). Subsequently, due to the stimulation of the β-adrenergic receptor with the agonist isoprenaline (10 nM/ 10 µM), the cAMP levels were increased. Because of a stronger increase of the cAMP levels with a higher concentration of isoprenaline and hence, a better detection

of a possible effect, the concentration of isoprenaline was enhanced from 10 nM to 10 µM in a second measurement. The cAMP levels were observed over a timeframe of 15 min and, in this time, a total of 55 emission spectra were recorded. The results are presented in the fluorescence emission ratio of CFP to Venus. In theory, if the compound of interest was a PDE-inhibitor, the cAMP levels would be stabilized and the metabolization of cAMP would be impeded. DMSO 0.1% served as vehicle control and roflumilast 1 µM, a specific PDE4 inhibitor, was utilized as positive control.

As shown in **Figure 28**, it was observed that the cAMP levels in the cells, which were treated with DMSO 0.1%, firstly raised due to the isoprenaline stimulation, only to fall shortly thereafter due to desensitization of the receptor and/or metabolization by PDEs. In contrast, the treatment of the cells with roflumilast stabilized the cAMP levels and after a while, the cAMP levels decreased very slowly. The results of the compounds LRK071, AH-17 and 2743 were similar to the effects of roflumilast. To conclude, the obtained results maintain the theory of a potential PDE inhibitory activity of LRK071, AH-17 and 2743.

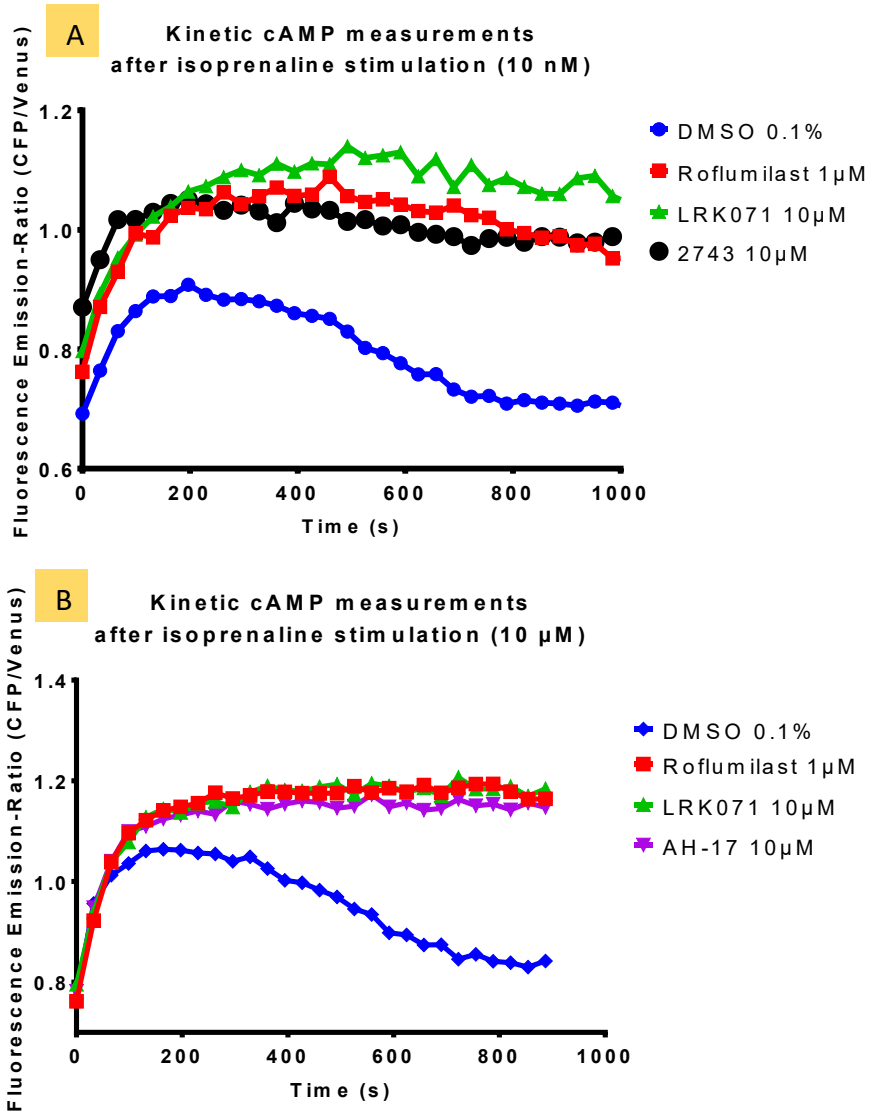

Figure 28: Kinetic cAMP measurements of the compounds LRK071, AH-17 and 2743.
The stably transfected Epac-HEK cell line was incubated with the compounds LRK071, AH-17 and 2743 (each at a concentration of 10 µM) for 30 min. After that time, the cells were stimulated with isoprenaline (10 nM or 10 µM). Over a period of 15 min, 55 fluorescence emission spectra were measured at different time points, and the data is presented as the fluorescence emission ratio of CFP to Venus over time (s).
Graph A illustrates the data of LRK071 as well as of 2743. In this measurement, the concentration of isoprenaline was at 10 nM. Graph B shows the results of the measurement of LRK071 and AH-17. Hereby, the isoprenaline concentration was at 10 µM.

1.3.2 Kinetic cAMP measurement with LRK071 stimulation

LRK071 increased the intracellular cAMP levels in the phenotypic screening and stabilized the cAMP levels in the kinetic cAMP measurement after isoprenaline stimulation. However, the elevation of the cAMP levels could also be elicited through a Gαs-coupled receptor stimulation by LRK071. For this reason, a kinetic cAMP measurement was conducted without compound pre-treatment of the cells and following receptor stimulation by isoprenaline. Instead, LRK071

100 µM as well as DMSO 1% were directly injected into the specific well and thus, a final dilution step took place to achieve a final concentration of LRK071 at 10 µM and DMSO 0.1%. Subsequently, the measurement of the fluorescence emission started for 15 min. The data, which are measured at different time points, are specified in the fluorescence emission ratio of CFP to Venus.

As expected, the evaluated data showed that DMSO 0.1% did not activate a receptor and thus, did not elevate the cAMP levels (**Figure 29**). Similar results were obtained of the evaluated data from LRK071. The height of the cAMP levels was equal after the treatment with LRK071 compared to DMSO 0.1%. This concludes that LRK071 might not stimulate a receptor, which increases the intracellular cAMP levels.

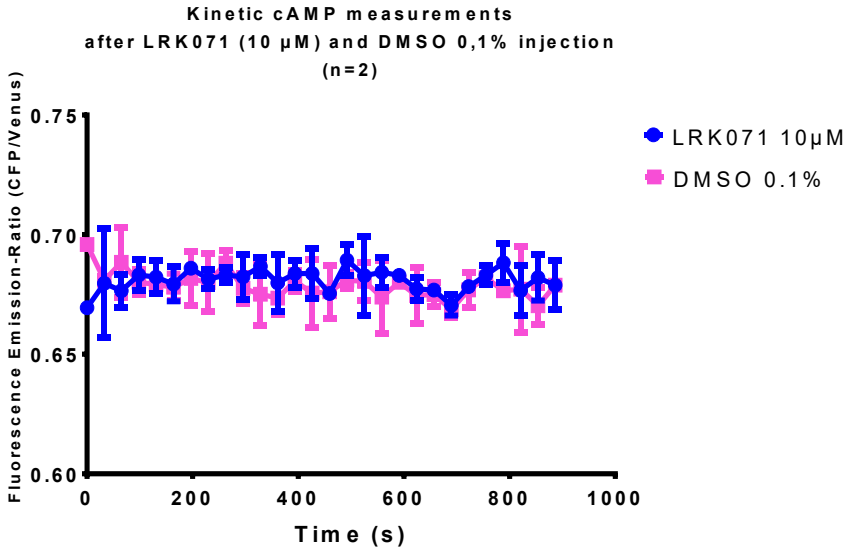

Figure 29: Kinetic cAMP measurement with injection of LRK071 (10 µM) or DMSO 0.1%.
In this measurement, the stably transfected Epac-HEK cell line was used. The compounds LRK071 (final concentration 10 µM) as well as DMSO (final concentration 0.1%) were directly injected into the specific well. No compound pre-treatment or isoprenaline stimulation were performed in this assay. Over a period of 15 min, 55 fluorescence emission spectra were measured at different time points, and the data is presented as the fluorescence emission ratio of CFP to Venus over time (s). Two measurements of each compound were conducted in the same experiment.

2 Results of the Griess assay

The Griess assay was performed to determine whether the NO production is decreased in murine J774A.1 macrophages after the treatment with the compounds LRK071, AH-17 and 2743. A decrease of the NO production indicates an anti-inflammatory effect of the tested compound.

To stimulate the NO production in murine J774A.1 macrophages, the cells were treated with LPS 1 µg/ml. This bacterial cell membrane structure binds to the TLR4 on macrophages and thus, the NF-κB signal pathway is activated. The transcription factor NF-κB modulates the gene expression and different chemokines as well as cytokines, such as TNF-α or interferon-α, are secreted. The reaction of the macrophages to the cytokines is a respiratory burst, in which different microbicide molecules, such as NO or H_2O_2, are released. (3) Dependent on the reaction conditions NO oxidizes to nitrite or nitrate. Nitrite reacts with the Griess reagents naphthylendiamine and sulfanilamide to a stable azo compound, and therefore, nitrite can be measured quantitatively in this assay. (90, 91, 92) The absorbance of the azo compound was detected at 550 nm via a microplate reader. Parthenolide 1 µM, a NF-κB inhibitor, was used as positive control and decreased the NO production significantly. While DMSO 0.1% + PBS 0.1% did not stimulate the NO production, DMSO 0.1% + LPS 1 µg/ml enhanced the NO production and served as vehicle control. For determination of the significance, DMSO 0.1% + LPS 1 µg/ml is utilized as control column.

2.1 Effects of LRK071 in the Griess assay

Different concentrations of LRK071 (10 µM to 100 nM) were tested in the Griess assay to determine if LRK071 decreases the NO production (**Figure 30**). In theory, the second messenger cAMP impedes the NF-κB signal pathway via inhibition of IKK. (47) Thus, the NF-κB signal pathway and in the following the NO production should be inhibited through the elevation of the cAMP levels by LRK071 as well as by the PDE4 inhibitor roflumilast, which was used as a positive control in the experiments.

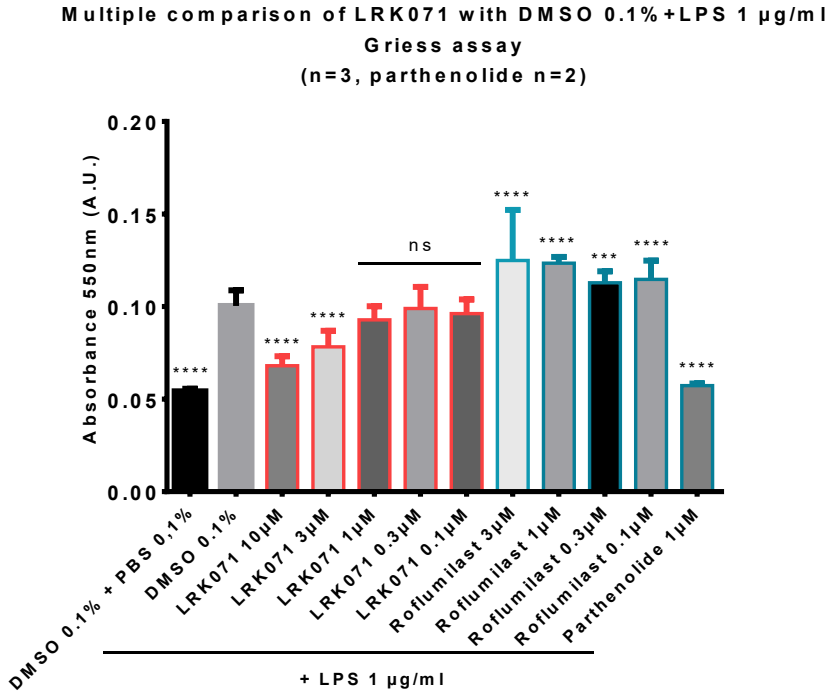

Figure 30: Results of the Griess assay after the treatment with LRK071 and roflumilast.
The murine J774A.1 macrophages were treated with different concentrations of LRK071 (10 µM- 100 nM) as well as roflumilast (3 µM- 100 nM) for 30 min. Subsequently, the cells were stimulated with LPS (1 µg/ml) and incubated overnight. On the next day, the Griess reagents were added and the absorbance was detected at 550 nm (A.U.: arbitrary unit).
The data of the tested compounds are shown as mean values ± SD of 2-3 biological replicates measured in technical octuplicates. The statistical analysis was done by using the one-way-ANOVA analysis to examine statistical significance. Furthermore, the mean value of each column was compared to the mean value of the control column by using the Dunnett´s post-hoc test. The control column was DMSO 0.1% + LPS 1 µg/ml. Statistical significance of p-values:
****: $p \leq 0.0001$; ***: $p \leq 0.001$; **: $p \leq 0.01$; *: $p \leq 0.05$; ns: $p > 0.05$

The evaluated data in **Figure 30** showed a significant decrease of the NO production of LRK071 at the concentrations 10 µM and 3 µM. In comparison, no decrease could be observed in different concentrations of roflumilast. A dose-response curve of LRK071 was generated and a dose-dependent tendency for a decrease in the NO production could be seen. The IC_{50} value was determined at 4.6 µM (**Figure 31**).

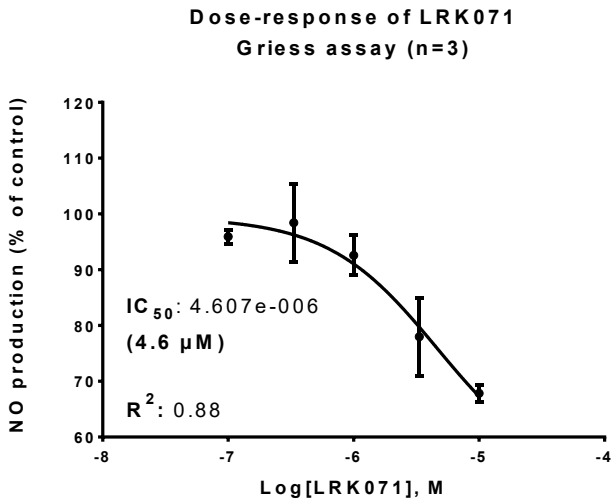

Figure 31: Dose-response curve of LRK071 in the Griess assay.
A dose-dependent effect of LRK071 in different concentrations on the decrease of the NO production was determined in three independent measurements. The data is given in percent of the absorbance normalized to the vehicle control DMSO 0.1% + LPS 1 µg/ml. The software GraphPad Prism 6.01 was used for the nonlinear regression analysis to calculate IC_{50} and R^2 values.

2.2 Effects of AH-17 in the Griess assay

A significant decrease of the NO production in J774A.1 macrophages after treatment with different concentrations of AH-17 (10 µM – 100 nM) was observed in three independent measurements (**Figure 33**). The results indicated a potential anti-inflammatory effect of the compound AH-17. Also, a dose-response curve was generated. The IC_{50} value of AH-17 was calculated at 11 µM (**Figure 34**). The structure of the magnolol derivative AH-17 is illustrated in **Figure 32**.

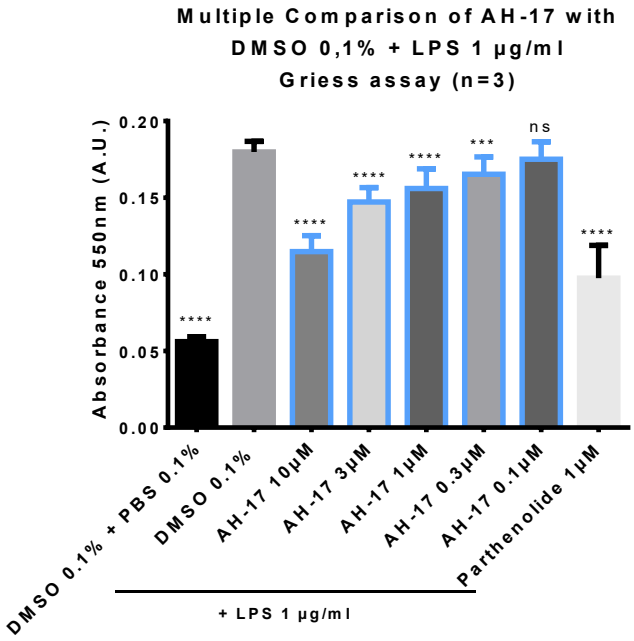

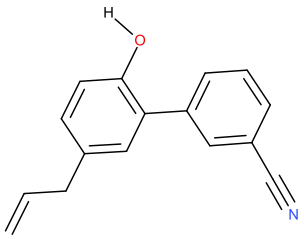

Figure 32: Structure of AH-17.

Figure 33: Results of the Griess assay after the treatment with AH-17.
The murine J774A.1 macrophages were treated with different concentrations of AH-17 (10 µM-100 nM) for 30 min. Subsequently, the cells were stimulated with LPS (1 µg/ml) and incubated overnight. On the next day, the Griess reagents were added and the absorbance was detected at 550 nm (A.U.: arbitrary unit).
The data of the tested compounds are presented as mean values ± SD of three biological replicates measured in technical octuplicates. The statistical analysis was done by using the one-way-ANOVA analysis to examine statistical significance. Furthermore, the mean value of each column was compared to the mean value of the control column by using the Dunnett´s post-hoc test. The control column was DMSO 0.1% + LPS 1 µg/ml. Statistical significance of p-values:
****: $p \leq 0.0001$; ***: $p \leq 0.001$; **: $p \leq 0.01$; *: $p \leq 0.05$; ns: $p > 0.05$

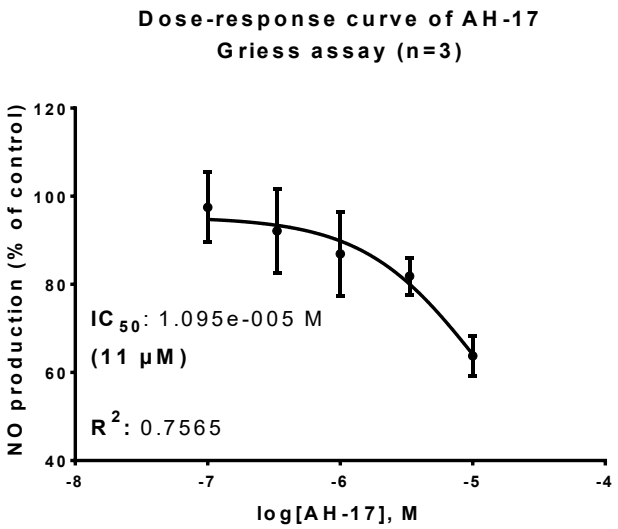

Figure 34: Dose response curve of AH-17 in the Griess assay.
A dose-dependent effect of AH-17 on the decrease of the NO production was determined in three independent measurements. The data is given in percent of the absorbance normalized to the vehicle control DMSO 0.1% + LPS 1 µg/ml. The software GraphPad Prism 6.01 was used for the nonlinear regression analysis to calculate IC_{50} and R^2 values.

2.3 Effects of 2743 in the Griess assay

Different concentrations ranging from 30 µM to 1 µM of the leoligin derivative 2743 were tested in the Griess assay. A significant decrease of the NO production in J774A.1 macrophages after stimulation with LPS (1 µg/ml) could be observed after the treatment with 2743 in a dose-dependent manner (**Figure 35**). Also, a dose-response curve was generated. The IC_{50} value of 2743 was determined at 1.9 µM (**Figure 36**).

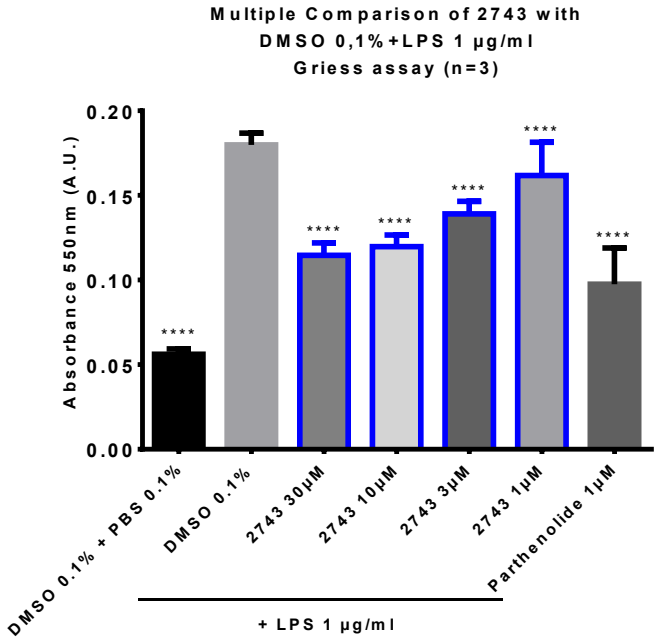

Figure 35: Results of the Griess assay after the treatment with 2743.
The murine J774A.1 macrophages were treated with different concentrations of 2743 (30 µM-1 µM) for 30 min. Subsequently, the cells were stimulated with LPS (1µg/ml) and incubated overnight. On the next day, the Griess reagents were added and the absorbance was detected at 550 nm (A.U.: arbitrary unit).
The data of the tested compounds are shown as mean values ± SD of three biological replicates measured in technical octuplicates. The statistical analysis was done by using the one-way-ANOVA analysis to examine statistical significance. Furthermore, the mean value of each column was compared to the mean value of the control column by using the Dunnett´s post-hoc test. The control column was DMSO 0.1% + LPS 1 µg/ml. Statistical significance of p-values:
****: $p \leq 0.0001$; ***: $p \leq 0.001$; **: $p \leq 0.01$; *: $p \leq 0.05$; ns: $p > 0.05$

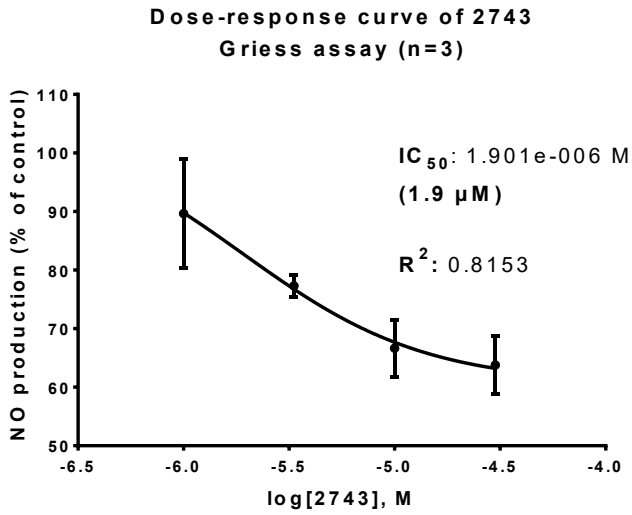

Figure 36: Dose-response curve of 2743 in the Griess assay.
A dose-dependent effect of 2743 in different concentrations on the decrease of the NO production was determined in three independent measurements. The data is given in percent of the absorbance normalized to the vehicle control DMSO 0.1% + LPS 1 µg/ml. The software GraphPad Prism 6.01 was used for the nonlinear regression analysis to calculate IC_{50} and R^2 values.

3 Results of the luciferase assay

3.1 Results of the NF-κB luciferase assay

First and foremost, it was observed that the magnolol derivatives LRK071 and AH-17 did not only increase the cAMP levels in the phenotypic screening, but also, decreased the NO production in LPS-stimulated J774A.1 macrophages. In addition, the NF-κB signal pathway might be impeded by these two substances. Because on the one hand, increased cAMP levels inhibit the NF-κB signal pathway (47), and on the other hand, the NF-κB signal pathway plays a crucial role in the production of NO in macrophages (3), which decreased considerably after the treatment with LRK071 and AH-17 in the Griess assay. So, to determine if the compounds LRK071 and AH-17 might inhibit the NF-κB signal pathway, a NF-κB luciferase assay was performed.

In the NF-κB luciferase assay, parthenolide 1 µM, a NF-κB inhibitor, was used as positive control, whereas DMSO 0.1% served as vehicle control. Besides the testing of different concentrations of LRK071 (10 µM to 30 nM) and of AH-17 (10 µM to 100 nM), also different concentrations of roflumilast (3 µM to 10 nM) were tested. Roflumilast was added, because it increases the intracellular cAMP levels through its PDE4 inhibitory activity and hence, the NF-κB signal pathway should be inhibited via the enhanced cAMP levels. The evaluated data is provided in fold activation normalized to the vehicle control (DMSO 0.1%).

None of the compounds LRK071, AH-17 and roflumilast showed a dose-dependent inhibition of the NF-κB signal pathway in three independent measurements (**Figure 37**). A significant inhibition of the NF-κB signal pathway could only be observed at the highest tested concentration of LRK071 at 10 µM and of AH-17 at 10 µM. Questionably, also the positive control parthenolide 1 µM did not significantly inhibit the NF-κB pathway. So, it seems as if LRK071 and AH-17 might not inhibit the NF-κB signal pathway, however, further tests have to be conducted.

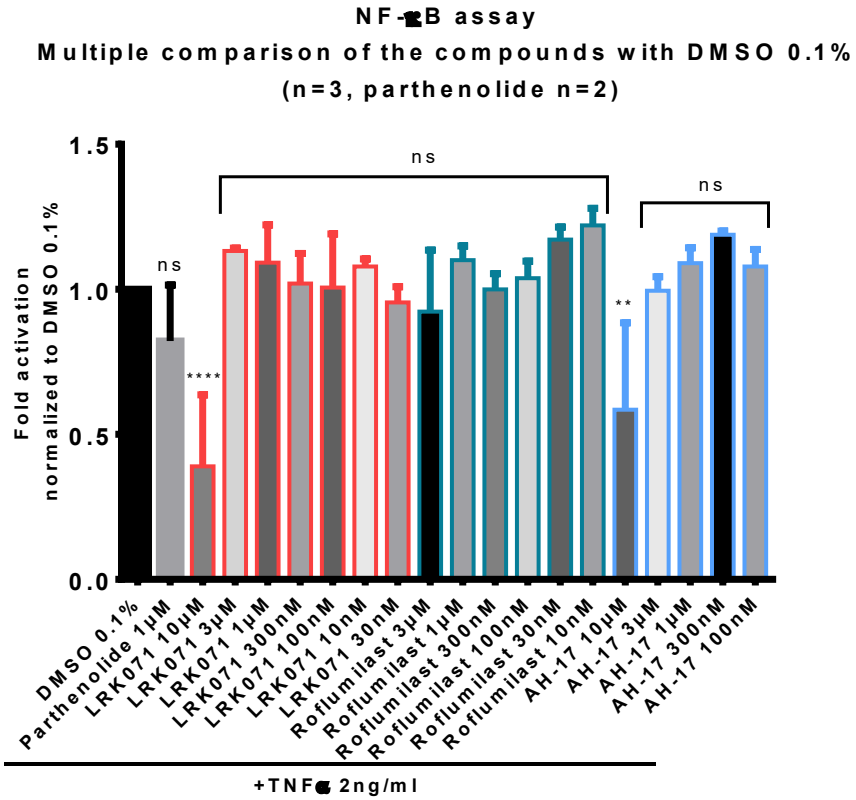

Figure 37: Results of the NF-κB assay after treatment with LRK071, AH-17 and roflumilast.
The NF-κB-luc cell line was stained with CTG. After the compound treatment of the cells and an incubation period of 4.5 h, the cells were stimulated with TNFα (2 ng/ml). Subsequently, the lysis of the cells and the measurement of the fluorescence and luminescence were conducted. The evaluated data, which is referred to as fold activation, is the ratio of RLU/RFU normalized to the vehicle control DMSO 0.1%. Every column stands for the mean value ± SD of 2-3 biological replicates measured in technical quadruplicates. The statistical analysis was done by using the one-way-ANOVA analysis to examine statistical significance. Furthermore, the mean value of each column was compared to the mean value of the control column by using the Dunnett´s post-hoc test. Statistical significance of p-values: ****: $p \leq 0.0001$; ***: $p \leq 0.001$; **: $p \leq 0.01$; *: $p \leq 0.05$; ns: $p > 0.05$

3.2 Results of the CRE-luciferase assay: LRK071 plus H-89

During the workflow the question arose, if LRK071 act as a PKA inhibitor and hence, the cAMP levels would persist on a higher level, because PKA regulates amongst other mechanisms also the downregulation of GPCRs. (45) To answer this question, a CRE-luciferase assay was performed to compare the effect of different concentrations of LRK071 and roflumilast on the cAMP levels with and without co-treatment of the PKA inhibitor H-89 after receptor stimulation with isoprenaline 100 nM. In theory, if PKA could not downregulate the GPCR because of the inhibition by H-89 and potentially by the compounds, the cAMP levels would stay increased due to further stimulation of the receptor.

The Epac-HEK cell line was transfected with the CRE-luc plasmid (10 µg). On the next day, the compound dilutions were prepared and the compounds were diluted (1:1000) by using SM plus H-89 (final concentration 300 nM) to generate the compound dilutions with H-89 (300 nM). For the compound dilutions without H-89, H-89 (300 nM) was replaced by DMSO 100% as comparison control and was diluted (1:1000) with SM to a final concentration of DMSO 0.1%. Additionally, on the 96-well plate in row 1 A-D 1 µl DMSO 100% was added to the SM-plus-DMSO 0.1%-medium and was diluted (1:1000) to a concentration of DMSO 0.1%. So finally, the final concentration of the vehicle control DMSO was 0.2%. Pure SM was added to the wells isoprenaline and to the untransfected cells (**Figure 38**). During a 30 min incubation period in the incubator at 37°C and 5% CO_2, the isoprenaline dilution was made in two steps by using SM to achieve a concentration of 200 nM isoprenaline. Subsequently, the cells were stimulated with 100 µl isoprenaline 200 nM (final concentration 100 nM) and were incubated again for 6 h. After that time, the lysis of the cells and the measurements of the fluorescence and luminescence were conducted.

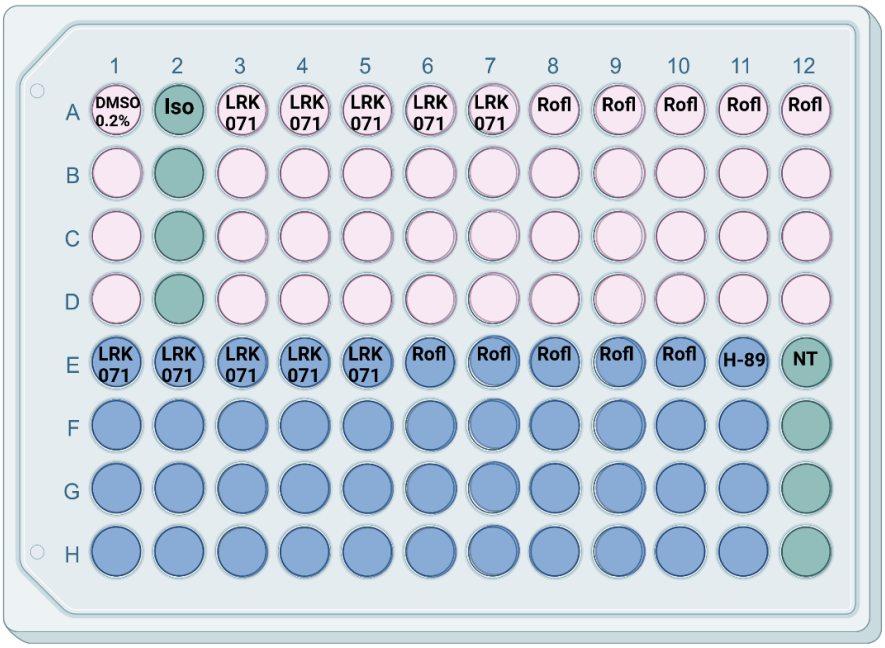

Figure 38: Schematic illustration of the 96-well plate used in the CRE- luciferase assay for the determination of a potential PKA inhibitory activity of LRK071.
In this assay, different concentrations of LRK071 and the comparison control roflumilast were tested with and without co-treatment with H-89 (300 nM). Therefore, different media were used. The wells, which contain the SM plus H-89 (300 nM) are illustrated in blue. The wells, which comprise the SM plus DMSO 0.1% are coloured in pink. Finally, the wells, which contain pure SM are illustrated in green. Iso= isoprenaline; Rofl= roflumilast; NT= not transfected cells. Illustration created in BioRender.com

As expected, in comparison with the vehicle control DMSO 0.2%, isoprenaline 100 nM enhanced the fold activation due to receptor stimulation, whereas H-89 300 nM decreased the fold activation due to receptor desensitization after isoprenaline stimulation. Furthermore, the evaluated data showed a dose-dependent increase in the fold activation of the columns, which were treated with different concentrations of LRK071 (10 µM to 100 nM) and roflumilast (300 nM to 3 nM) without H-89 (300 nM). Firstly, comparing these columns to the columns with LRK071 + H-89 (300 nM) and roflumilast + H-89 (300 nM), the fold activation was much more increased by the compounds without H-89 (300 nM). Secondly, comparing LRK071 + H-89 (300 nM) and roflumilast + H-89 (300 nM) to the well H-89 300 nM, the different concentrations of LRK071 + H-89 (300 nM) and roflumilast + H-89 (300 nM) had a slightly enhanced fold activation in a dose-dependent manner. The data of the measurement is shown in **Figure 39**. To sum up, the columns of LRK071 with and without H-89 (300 nM) showed the same tendency in the fold activation as roflumilast with and without H-89 (300 nM). No column of the different concentrations of LRK071 + H-89 (300 nM) had a lower fold activation than H-89 300 nM, which would indicate an additive PKA inhibition. This

experiment showed that LRK071 might not have a PKA inhibitory activity and supports the theory that LRK071 might be a potential PDE-inhibitor.

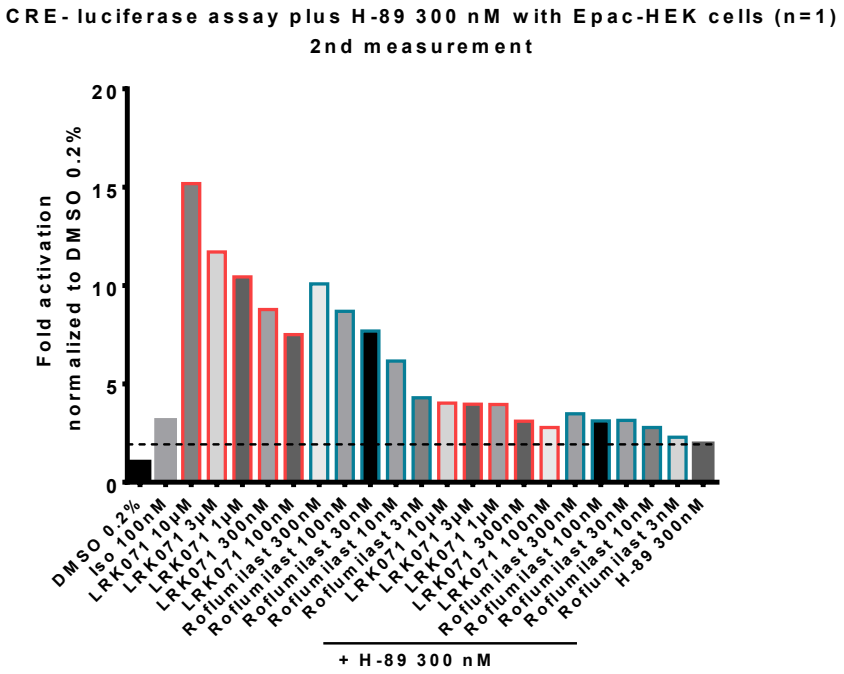

Figure 39: Results of the CRE-luciferase assay after stimulation with isoprenaline (100 nM): treatment with LRK071 and roflumilast with and without H-89 (300 nM).
The Epac-HEK cell line was transfected with the CRE-luc plasmid. The cells were treated with different concentrations of LRK071 (10 µM- 100 nM) and roflumilast (300 nM- 3 nM) with and without H-89 300 nM. After an incubation period of 30 min, the cells were stimulated with isoprenaline 100 nM. The measurement took place 6 h after the treatment. Subsequently, the lysis of the cells and the measurements of the fluorescence and luminescence were conducted. The evaluated data, which is represented as fold activation, is the ratio of RLU/RFU normalized to the vehicle control DMSO 0.2%. In the graph, the value of the column of H-89 300 nM is marked with a horizontal line for a better comparison.

3.3 Follow-up analysis of the results of the TGR5 target-based screening by luciferase assay

The aim of these luciferase assays was to confirm the initial results of the TGR5 target-based screening by using a more sensitive method.

3.3.1 Confirmation of the results of the TGR5 target-based screening via CRE-luciferase assay

An increase of the cAMP levels in in the TGR5 target-based screening was observed for the first time of the leoligin derivatives 3162 and 3163, of the coumarin notopterol as well as of helioxanthin, heliobuphthalmin and dehydroheliobuphthalmin. To determine whether the

compounds affect the CRE/cAMP signal pathway in another assay, the CRE-luciferase assay was conducted.

Therefore, the TGR5-Epac-HEK cell line was transfected with the CRE-luc plasmid (10 µg). Similar to the TGR5 target-based screening, DMSO 0.1% served as vehicle control and the positive controls were LCA 10 µM as well as forskolin 10 µM. Additionally, CDCA 10 µM was also utilized as positive control, which is important for the comparison especially in the FXR-Gal4-luciferase assay, because CDCA is the most potent agonist of the bile acids on FXR. (100) Different concentrations of 3162 (10 to 3 µM), 3163 (10 to 3 µM), 1055 (8.5 to 0.3 µM), 2644 (10 µM to 30 nM), 2641 (10 to 3 µM) and 2640 (10 to 3 µM) were tested.

In line with the results of the TGR5 target-based screening, a significant increase of the fold activation of each substance was observed at least in the highest concentrations. To specify this, a significant increase was detected of 3162 at 10 µM, 3163 at 10 µM and 3 µM, 1055 at 8.5 µM, 2641 at 10 µM and of 2640 at 10 µM. The analyzed data are presented in **Figure 40**. These results substantiated the observed results of the TGR5 target-based screening in a way that all the compounds may affect the cAMP/CRE pathway via the TGR5 receptor. The evaluated cell viability of this luciferase assay is shown in **Figure 53** in the Appendix.

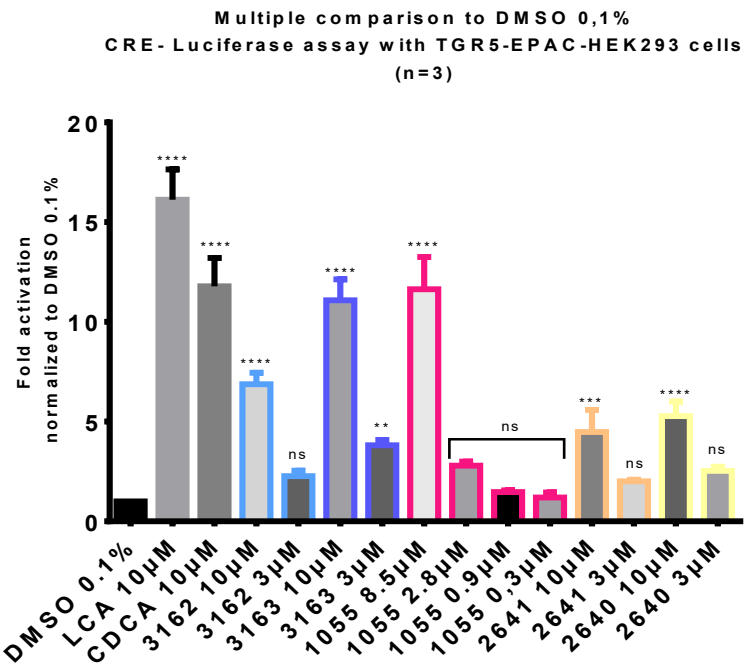

Figure 40: Confirmation of the results of the TGR5 target-based screening in the CRE-luciferase assay of 3162, 3163, 1055, 2641 and 2640.
The TGR5-Epac-HEK cell line was transfected with the CRE-luc plasmid. The cells were treated with different concentrations of 3162, 3163, 1055, 2641 and 2640. After the lysis of the cells, the measurements of the fluorescence and luminescence were conducted. The evaluated data, which is referred to as fold activation, is the ratio of RLU/RFU normalized to the vehicle control DMSO 0.1%. Every column stands for the mean value ± SD of three biological replicates measured in technical quadruplicates. The statistical analysis was done by using the one-way-ANOVA analysis to examine statistical significance. Furthermore, the mean value of each column was compared to the mean value of the control column DMSO 0.1% by using the Dunnett´s post-hoc test. Statistical significance of p-values: ****: $p \leq 0.0001$; ***: $p \leq 0.001$; **: $p \leq 0.01$; *: $p \leq 0.05$; ns: $p > 0.05$

A significant increase in the fold activation was also detected of the substance 2644 (helioxanthin) at 10 µM, which is illustrated in **Figure 41**. After the analysis of the viability of the cells, it was assessed that 2644 is cytotoxic in higher concentrations from 10 µM to 1 µM (**Figure 42**) and thus, the effect observed on the cAMP/CRE pathway in TGR5-Epac-HEK cells might be biased by cytotoxic effects of the compound.

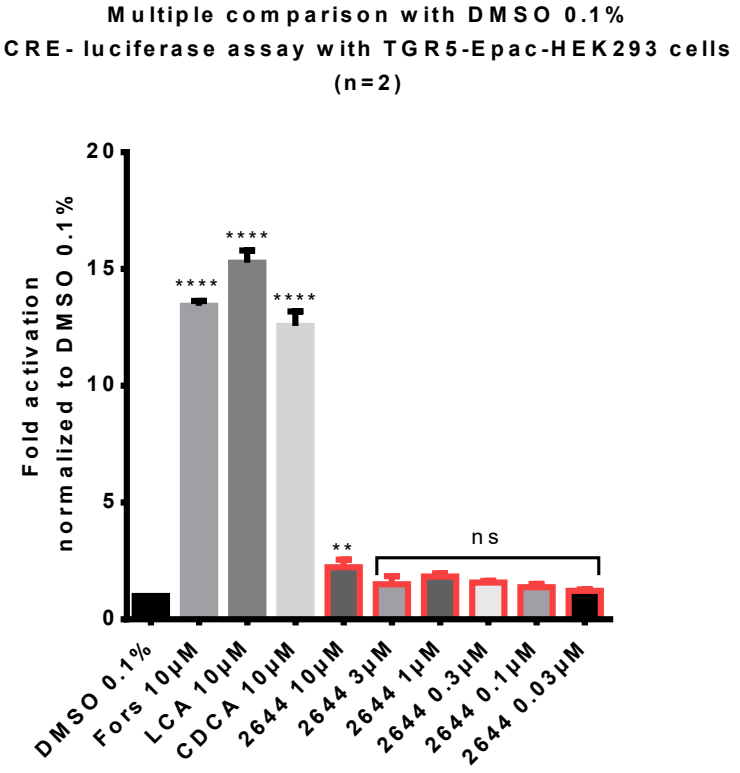

Figure 41: Confirmation of the results of the TGR5 target-based screening in the CRE-luciferase assay of 2644.
The TGR5-Epac-HEK cell line was transfected with the CRE-luc plasmid. The cells were treated with different concentrations of 2644 (10 µM - 0.3 µM). After the lysis of the cells, the measurements of the fluorescence and luminescence were conducted. The evaluated data, which is referred to as fold activation, is the ratio of RLU/RFU normalized to the vehicle control DMSO 0.1%. Every column stands for the mean value ± SD of two biological replicates measured in technical quadruplicates. The statistical analysis was done by using the one-way-ANOVA analysis to examine statistical significance. Furthermore, the mean value of each column was compared to the mean value of the control column DMSO 0.1% by using the Dunnett´s post-hoc test. Statistical significance of p-values: ****: $p \leq 0.0001$; ***: $p \leq 0.001$; **: $p \leq 0.01$; *: $p \leq 0.05$; ns: $p > 0.05$

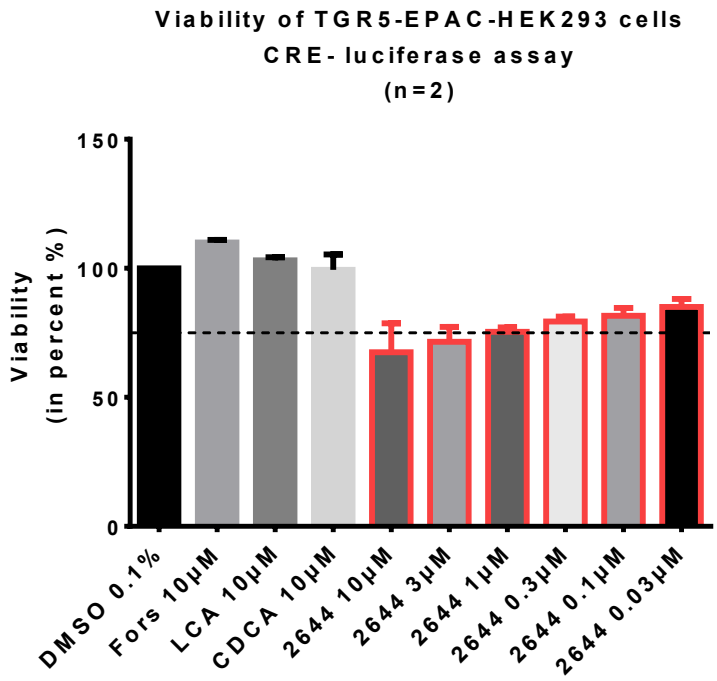

Figure 42: Determination of the viability of the TGR5-Epac-HEK cells in the CRE-luciferase assay after treatment with different concentrations of 2644.
The viability of the TGR5-Epac-HEK cells is determined by measuring the GFP fluorescence, which is a surrogate parameter for the viability. A viability higher than 75% relative to the control is referred to as non-toxic. This threshold is marked with a horizontal line. The data represents the measurement of two biological replicates, which are measured in quadruplicates.

3.3.2 Control of the results of the TGR5 target-based screening in the CRE-luciferase assay with wildtype HEK293 cells

To determine if the effect of the CRE-luciferase assay in TGR5-Epac-HEK cells can be traced back to the specific activation of the TGR5 receptor, a CRE-luciferase assay with wildtype HEK293 cells was conducted, because HEK293 cells do not endogenously express the TGR5 receptor. The same compounds with the same concentrations as in the previously described CRE-luciferase assay with TGR5-Epac-HEK cells were tested.

As expected, the endogenous ligands of the TGR5 receptor, LCA and CDCA, showed no effect in wildtype HEK293 cells. Interestingly, also no increase in the fold activation with the treatment of the compounds 3162, 3163 and 1055 was observed. All of them had the same fold activation like the vehicle control DMSO 0.1%. This concludes that the effect of 3162, 3163 and 1055 on the cAMP/CRE pathway might be TGR5-dependent. Furthermore, high concentrations of 2644 (10 µM, 3 µM, 1 µM), 2641 (10 µM) as well as 2640 (10 µM) showed a significant increase in the fold activation in wildtype HEK293 cells. The data is illustrated in **Figure 43**. However, this might also be traced back on the cytotoxicity of these substances at

high concentrations. The viability graphic can be found in the appendix (**Figure 54**). Further viability tests with a resazurin assay would be necessary to investigate this.

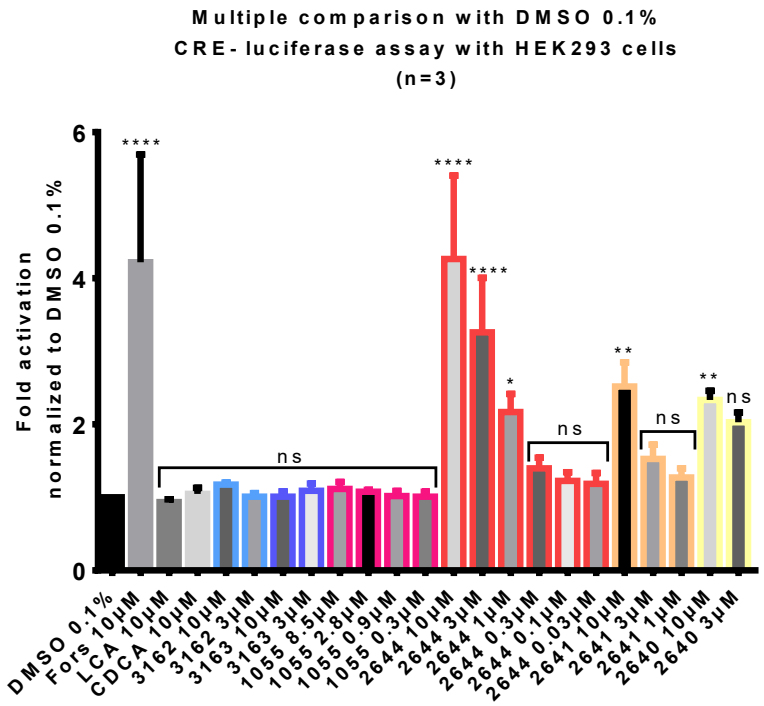

Figure 43: Results of the CRE-luciferase assay in HEK293 cells after the treatment with different concentrations of 3162, 3163, 1055, 2644, 2641 and 2640.
Wildtype HEK293 cells were transfected with the CRE-luc plasmid. The cells were treated with different concentrations of 3162, 3163, 1055, 2644, 2641 and 2640. After the lysis of the cells, the measurements of the fluorescence and luminescence were conducted. The evaluated data, which is referred to as fold activation, is the ratio of RLU/RFU normalized to the vehicle control DMSO 0.1%. Every column stands for the mean value ± SD of three biological replicates measured in technical quadruplicates. The statistical analysis was done by using the one-way-ANOVA analysis to examine statistical significance. Furthermore, the mean value of each column was compared to the mean value of the control column DMSO 0.1% by using the Dunnett´s post-hoc test. Statistical significance of p-values: ****: $p \leq 0.0001$; ***: $p \leq 0.001$; **: $p \leq 0.01$; *: $p \leq 0.05$; ns: $p > 0.05$

3.3.3 FXR-Gal4-luciferase assay: Determination of TGR5 selectivity

Bile acids are not only agonists of the TGR5 receptor, but they can also bind and activate the nuclear receptor FXR. (49) CDCA is the most potent agonist of the FXR of the bile acids. However, also LCA as well as DCA can activate the FXR. (100) Thus, CDCA 10 µM is used as a positive control besides LCA 10 µM and forskolin 10 µM. In this assay, the wildtype HEK293 cells were transfected with an FXR-Gal4 fusion construct and a tk-Luc reporter plasmid. Different concentrations of the compounds 3162, 3163, 1055, 2641 and 2640 were tested. Because of the cytotoxicity of helioxanthin, this compound was not further tested.

The potent FXR agonist CDCA 10 µM showed a significant increase in the fold activation in comparison to DMSO 0.1%. No increase could be observed with the compounds 3162, 3163 as well as with 1055. (**Figure 44**) This suggests that these substances might not activate the FXR receptor. However, the well-known albeit weak FXR agonist LCA 10 µM also showed no significant increase in the fold-activation, which questions the reliability and sensitivity of this assay. Furthermore, a significant increase of the fold activation was reached with the substances 2641 (10 µM, 3 µM) and 2640 (10 µM, 3 µM). In this context, also the viability was determined, which is illustrated in the appendix in **Figure 55**, and thus, all cells are viable. So, 2641 and 2640 might bind to the FXR.

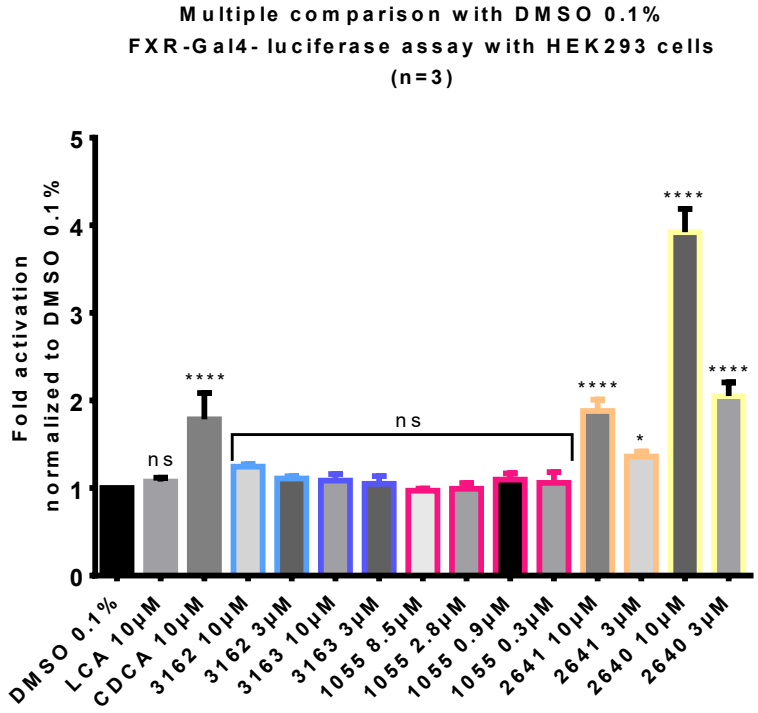

Figure 44: Results of the FXR-Gal4-luciferase assay after the treatment with different concentrations of 3162, 3163, 1055, 2641 and 2640.
The HEK293 cell line was transfected with the FXR-Gal4 fusion construct and a tk-Luc reporter plasmid. The cells were treated with different concentrations of 3162, 3163, 1055, 2641 and 2640. After the lysis of the cells, the measurement of the fluorescence and luminescence was conducted. The evaluated data, which is referred to as fold activation, is the ratio of RLU/RFU normalized to the vehicle control DMSO 0.1%. Every column stands for the mean value ± SD of three biological replicates measured in technical quadruplicates. The statistical analysis was done by using the one-way-ANOVA analysis to examine statistical significance. Furthermore, the mean value of each column was compared to the mean value of the control column DMSO 0.1% by using the Dunnett´s post-hoc test. Statistical significance of p-values: ****: $p \leq 0.0001$; ***: $p \leq 0.001$; **: $p \leq 0.01$; *: $p \leq 0.05$; ns: $p > 0.05$

4 Results of the fluorescence polarization assay

The magnolol derivatives LRK071 as well as AH-17 and the leoligin derivative 2743 increased the cAMP levels in the phenotypic screening. This effect may indicate a potential PDE inhibitory activity. To examine this further, a cell-free PDE4B2 assay was conducted. The PDE4B2 enzyme was chosen, since it can be found in HEK cells as well as in macrophages (40), with which the experiments were conducted. In the PDE4B2 assay the fluorescence polarization was measured as described in [C. Materials and Methods] in the chapter [6 Fluorescence polarization assay]. Low polarized light stands for an inhibition of the PDE4B2 enzyme, whereas the detection of high polarized light stands for no inhibition of this enzyme. Different concentrations of the specific PDE4 inhibitor roflumilast were used, on the one hand, to confirm the functional efficiency of this assay and, on the other hand, to compare its effect with the effect of the tested compounds. The positive control (uninhibited enzyme activity) in this assay was the dye-labeled FAM-cAMP plus the dilution of DMSO 1% (final concentration) in an inhibitor buffer as well as the PDE4B2 enzyme. The FAM-cAMP alone was measured in the designated well 'substrate control' to define its auto-fluorescence polarization, which was included in the calculation of the G-factor.

4.1 PDE4B2 assay: Results of LRK071

To determine the potential PDE inhibitory activity of LRK071, different concentrations from 1 µM to 30 pM were tested in the PDE4B2 assay. Also, different concentrations of roflumilast (100 nM to 3 pM) were added, which served as comparison and to confirm the reliability of this assay. Three independent measurements were conducted. However, because the data of the third measurement showed huge fluctuations in every second concentration, it was excluded from the Dunnett´s post-hoc analysis and will be discussed later on. In the following, the data of the first and second measurement will be analyzed. The fluorescence polarization was normalized to the positive control and is given in percent of enzyme activity of the positive control.

A tendency for a potential inhibition of the PDE4B2 enzyme could be detected at different concentrations of roflumilast (**Figure 45**). However, the measured data showed high standard deviations. As illustrated in **Figure 46**, a dose-response curve of roflumilast was generated by using the software GraphPad Prism 6.01. The IC_{50} was determined at 104.3 pM with a low R^2 of 0.46. Also, a slight tendency towards a PDE inhibitory activity of LRK071 in different concentrations (1 µM – 30 pM) could be observed (**Figure 45**). With the obtained data it was not possible to generate a dose-response curve of LRK071 by using GraphPad Prism 6.01.

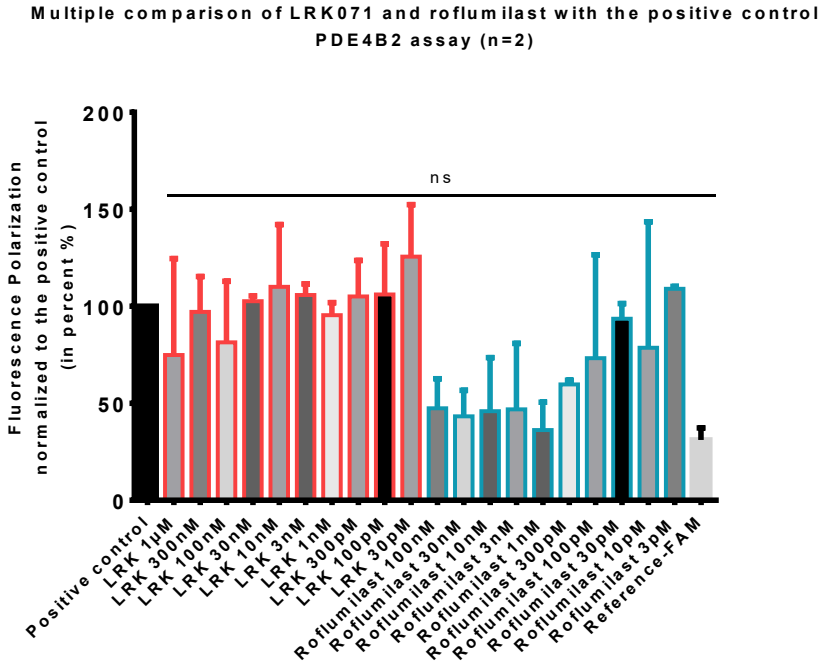

Figure 45: Fluorescence polarization with recombinant PDE4B2 assay of LRK071 and roflumilast.
After the dilution of the different concentrations of LRK071 and roflumilast, the dye-labelled FAM-cAMP was added and incubated for 1 h at room temperature. Beads were added to the reaction mix, which caused changes in the fluorescence polarization depending on the amount of hydrolysed FAM-cAMP. Again, an incubation period of 1 h at room temperature was performed and afterwards, the fluorescence polarization was measured. The data is given in percent of the fluorescence polarization normalized to the positive control.
The data of the tested compounds are shown as mean values ± SD of two biological replicates. The statistical analysis was done by using the one-way-ANOVA analysis to examine statistical significance. Furthermore, the mean value of each column was compared to the mean value of the positive control by using the Dunnett´s post-hoc test. Statistical significance of p-values: ****: $p \leq 0.0001$; ***: $p \leq 0.001$; **: $p \leq 0.01$; *: $p \leq 0.05$; ns: $p > 0.05$

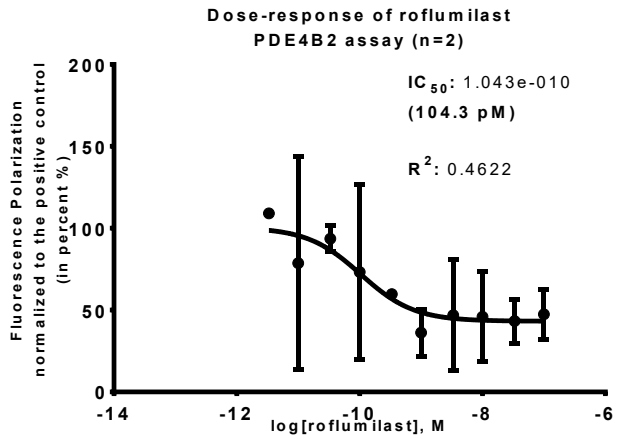

Figure 46: Dose-response curve of roflumilast in the PDE4B2 assay.
A slight dose-dependent effect of roflumilast (100 nM to 3 pM) on the inhibition of the PDE4B2 enzyme was determined in two independent measurements. The software GraphPad Prism 6.01 was used for the nonlinear regression analysis to calculate IC_{50} and R^2 values.

As mentioned before, the data of the third measurement of the PDE4B2 assay with the compounds LRK071 and roflumilast showed a major variability in the detection of the fluorescence polarization. As illustrated in **Figure 47**, every second column, which are marked in the colors red or green, was higher than the in between columns. This effect could be caused by a pipetting error or because other plates were used in the third measurement, which disturbed the measurement with the TECAN Spark® Microplate Reader. By observing only every second value in **Figure 47**, a tendency of a potential PDE inhibitory activity of roflumilast as well as of LRK071 was detected. The data is specified in the fluorescence polarization.

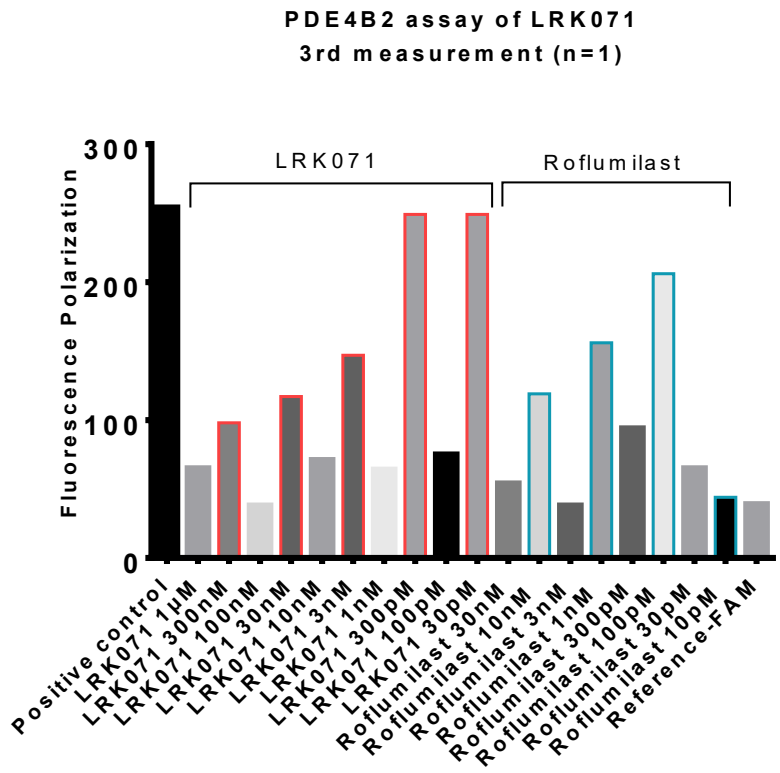

Figure 47: The third measurement of LRK071 and roflumilast in the PDE4B2 assay.
After the dilution of the different concentrations of LRK071 and roflumilast, the dye-labelled FAM-cAMP was added and incubated for 1 h at room temperature. Beads were added to the reaction mix, which caused changes in the fluorescence polarization depending on the amount of hydrolysed FAM-cAMP. Again, an incubation period of 1 h at room temperature was performed and afterwards, the fluorescence polarization was measured.
The data of the tested compounds are shown of one biological replicate. The statistical analysis was done by using the one-way-ANOVA analysis. Every second value is marked either with the color red or green.

4.2 PDE4B2 assay: Results of AH-17

The obtained results of the PDE4B2 assay with AH-17 were comparable to the results of LRK071. A slight tendency towards the inhibitory activity at different concentrations of AH-17 (1 µM- 1 nM) could be observed in two independent measurements. Also, different concentrations of roflumilast (30 nM – 10 pM) showed a tendency towards the inhibitory activity of the PDE4B2 enzyme, which is illustrated in **Figure 48**. High standard deviations need to be taken into account again in this evaluation. This challenges the reliability of the PDE4B2 assay. Dose-response curves were created to determine the IC_{50} and R^2. The IC_{50} value of roflumilast was at 1.64 nM and of AH-17 at 97 nM (**Figure 49**).

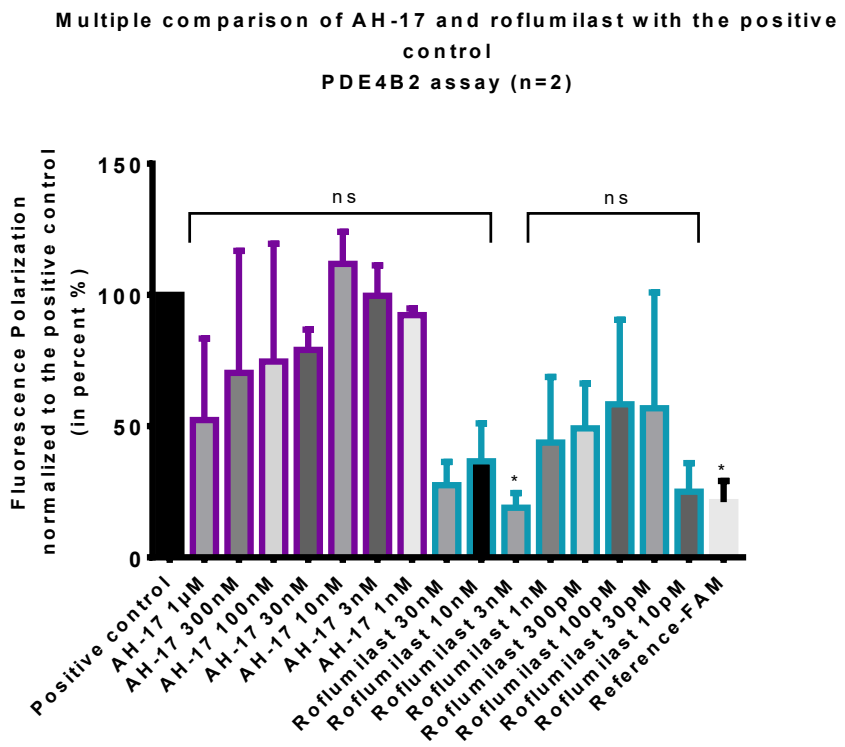

Figure 48: Fluorescence polarization with recombinant PDE4B2 assay of AH-17 and roflumilast.
After the dilution of the different concentrations of AH-17 and roflumilast, the dye-labeled FAM-cAMP was added and incubated for 1 h at room temperature. Beads were added to the reaction mix, which caused changes in the fluorescence polarization depending on the amount of hydrolysed FAM-cAMP. Again, an incubation period of 1 h at room temperature was performed and afterwards, the fluorescence polarization was measured. The data is given in percent of the fluorescence polarization normalized to the positive control.
The data of the tested compounds are shown as mean values ± SD of two biological replicates. The statistical analysis was done by using the one-way-ANOVA analysis to examine statistical significance. Furthermore, the mean value of each column was compared to the mean value of the positive control by using the Dunnett´s post-hoc test. Statistical significance of p-values: ****: $p \leq 0.0001$; ***: $p \leq 0.001$; **: $p \leq 0.01$; *: $p \leq 0.05$; ns: $p > 0.05$

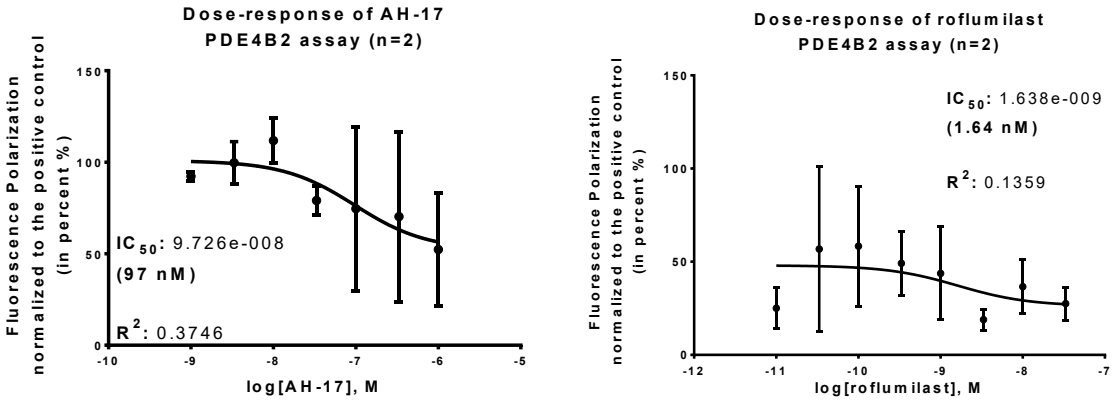

Figure 49: Dose-response curve of AH-17 and roflumilast.
A potential dose-dependent effect of AH-17 and roflumilast in different concentrations on the inhibition of the PDE4B2 enzyme was determined. The software GraphPad Prism 6.01 was used for the nonlinear regression analysis to calculate IC_{50} and R^2 values.

4.3 PDE4B2 assay: Results of 2743

As regards the results of 2743, the leoligin derivative was tested in the PDE4B2 assay in only one measurement. Hence, the interpretation of the data was very preliminary. A marginal tendency of a PDE4B2 inhibitor activity of 2743 could be interpreted in **Figure 50**. The PDE4 inhibitor roflumilast showed a clearer tendency for the inhibition of PDE4B2, but the data included again fluctuations. In addition, dose-response curves of 2743 and of roflumilast were generated, which also showed a slight tendency towards the inhibitory activity of the PDE4B2 enzyme in a dose-dependent manner (**Figures 51 and 52**). However, further measurements have to be conducted to obtain reliable results.

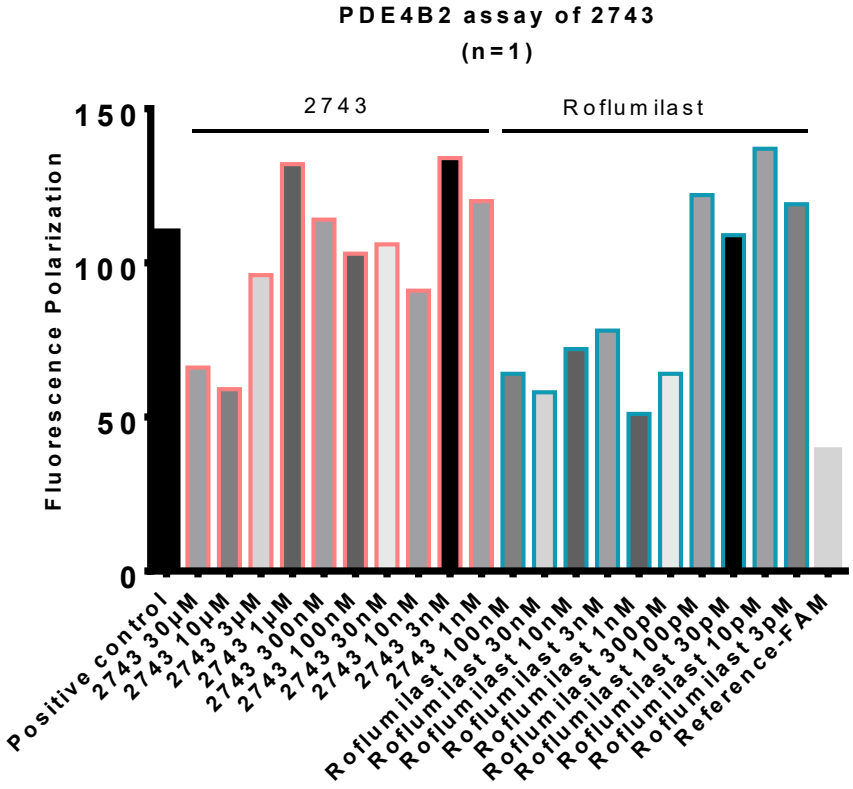

Figure 50: PDE4B2 assay of 2743 and roflumilast.
After the dilution of the different concentrations of LRK071 and roflumilast, the dye-labeled FAM-cAMP was added and incubated for 1 h at room temperature. Beads were added to the reaction mix, which caused changes in the fluorescence polarization depending on the amount of hydrolysed FAM-cAMP. Again, an incubation period of 1 h at room temperature was performed and afterwards, the fluorescence polarization was measured.
The data of the tested compounds are shown of one biological replicate. The statistical analysis was done by using the one-way-ANOVA analysis.

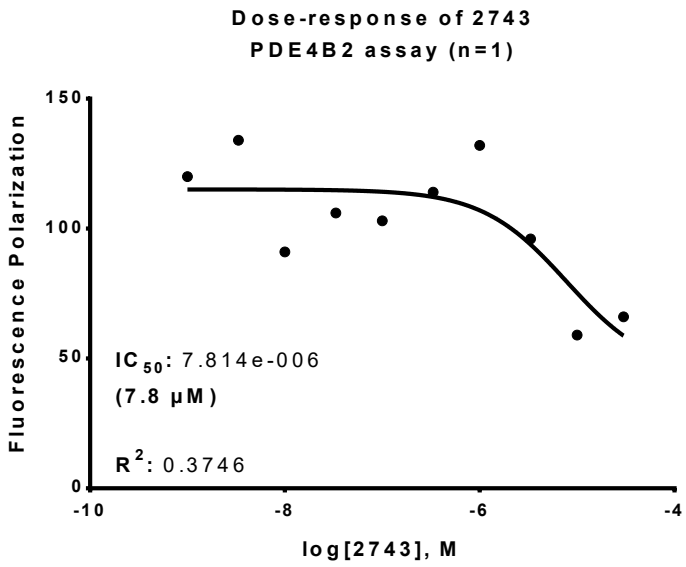

Figure 51: Dose-response curve of 2743 in the PDE4B2 assay.
A slight dose-dependent effect of 2743 (30 µM – 1 nM) on the inhibition of the PDE4B2 enzyme was determined in one measurement. The data is expressed in the fluorescence polarization. The software GraphPad Prism 6.01 was used for the nonlinear regression analysis to calculate IC_{50} and R^2 values.

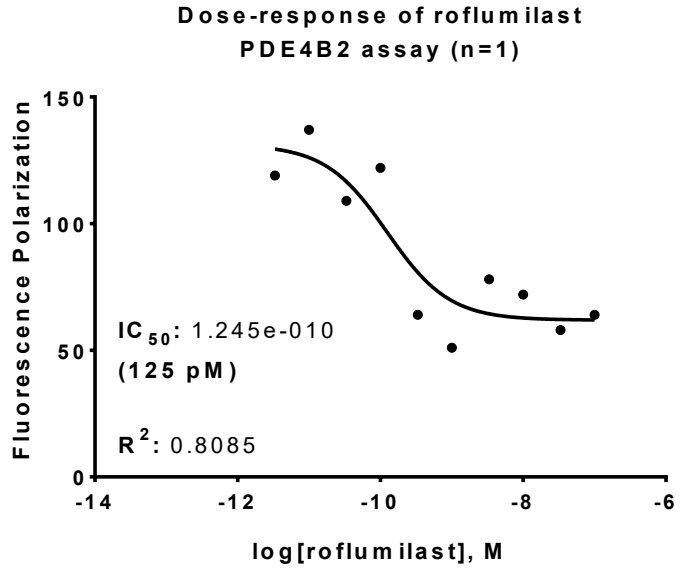

Figure 52: Dose-response curve of roflumilast in the PDE4B2 assay.
A slight dose-dependent effect of roflumilast (100 nM to 3 pM) on the inhibition of the PDE4B2 enzyme was determined in one measurement. The data is expressed in the fluorescence polarization. The software GraphPad Prism 6.01 was used for the nonlinear regression analysis to calculate IC_{50} and R^2 values.

E. Discussion and conclusion

The second messenger cAMP plays a pivotal role in the innate as well as in the adaptive immune system. Because of its anti-inflammatory and immunomodulatory effect, different therapeutic drugs were developed, such as the PDE4 inhibitors roflumilast and apremilast, which affect the intracellular cAMP levels. (57) So, the discovery of new substances which modulate the cAMP levels is of great interest for further therapeutic strategies. In this study, numerous natural products as well as synthesized compounds were screened to examine their effect on the intracellular cAMP levels in modified HEK293 cells by using the Epac-based FRET biosensor assay. Two different high-throughput screenings were conducted. Firstly, the effect of different compounds on the cAMP levels was investigated in TGR5-Epac-HEK cells to identify potential TGR5 agonists via the target-based screening. Secondly, the phenotypic screening was conducted to examine the effect of several compounds on the cAMP levels in Epac-HEK cells, where changes can be traced back to a potential PDE inhibitory activity.

A limiting factor of the high-throughput screenings was the age of the DNTI compounds. The DNTI project took place in the year 2016. However, since then the stock of the substances was frozen at -70 °C and the dilutions of the compounds were stored at -20 °C. Due to the freeze and thaw cycles as well as the age of the substances, the chemical structure could have changed, which has to be checked with nuclear magnetic resonance (NMR) spectroscopy or mass spectrometry (MS), for instance.

For the first time a significant increase of the cAMP levels was detected in the TGR5 target-based screening of the leoligin derivatives 3162 and 3163, of the coumarin notopterol (1055) as well as of helioxanthin (2644). To confirm these results with a more sensitive method and to determine their effect on the CRE/cAMP pathway, a CRE-luciferase assay was performed. The results of the CRE-luciferase assay with TGR5-Epac-HEK cells showed a significant effect on the cAMP/CRE pathway of 3162 at 10 µM, 3163 at 10 µM and 3 µM, 1055 at 8.5 µM and 2644 at 10 µM. The compounds 2641 and 2640 were also tested in the CRE-luciferase assay, because of the detection of an increase in the cAMP levels in the TGR5 target-based screening in one measurement (data not shown). The fold-activation in the CRE-luciferase assay was significantly increased by treatment with 2641 at 10 µM and of 2640 also at 10 µM. However, it was observed that 2644 was significantly cytotoxic in the CRE-luciferase assays in the concentrations ranging from 10 to 1 µM.

To determine if the increase of the cAMP levels could be traced back to a potential TGR5 agonistic activity, the substances were also tested in a CRE-luciferase assay in wildtype HEK293 cells. No significant increase of the fold-activation was detected of the leoligin derivatives 3162 and 3163 as well as of the coumarin notopterol. This result supports the theory that these compounds act as TGR5-agonists. A FXR-Gal4-luciferase assay was performed to assess TGR5 selectivity. Also, no significant increase of the fold-activation of the compounds 3162, 3163 and 1055 was observed. However, it is noteworthy that the potent FXR agonist CDCA showed a significant effect at 10 µM, whereas the less potential FXR-agonist LCA 10 µM showed no effect. (100) So, it is important to repeat the test in higher as well as in different concentrations of the substances to exclude a covered effect and possibly to establish dose-response curves.

Furthermore, 2644, 2640 as well as 2644 showed a significant effect in higher concentrations in a CRE-luciferase assay in wildtype HEK293 cells as well as in a FXR-Gal4-luciferase assay in Epac-HEK cells. After determination of the cell viability, it was observed that 2644 in the concentrations of 10 µM to 1 µM is cytotoxic in HEK293 cells. The increase in the fold-activation might be traced back to the cytotoxicity, hence, assays for the determination of the toxicity are of fundamental importance, such as the resazurin assay. 2644 has a similar scaffold as the cytostatic drug podophyllotoxin. Hence, the observed cytotoxic activity might arise due to the similarity of the structures. Both substances have a central isobenzofuranon as well as a benzodioxol structure. The benzodioxol structure is also part of the substances 2640 and 2641. The researchers Chen and Xie [(101)] found out that podophyllotoxin activates the CRE gene expression via PKA activation in a cAMP independent manner. (101) Hence, it would be interesting, if the compounds 2644, 2640 as well as 2641 also might utilize this pathway.

The magnolol derivative LRK071 was tested in previous phenotypic screenings and an increase of the cAMP levels was detected. In this study, another synthesized magnolol derivative LRK077 was screened for the first time in the phenotypic screening and an increase of the cAMP levels was observed. To compare the effect of LRK077 with LRK071, different concentrations of LRK077 were tested in the phenotypic screening, and a dose-response curve was established. The IC_{50} of LRK077 was determined at 3.4 µM and thus, LRK077 is less potent than LRK071, whose IC_{50} was observed at 350 nM in previous phenotypic screenings. (67)

Like LRK071, also the magnolol derivative AH-17 and the leoligin derivative 2743 increased the cAMP levels in prior phenotypic screenings. A potential PDE inhibitory effect was hypothesized as an underlying molecular mechanism. In addition, a kinetic cAMP measurement was performed to support this theory. All three compounds increased and stabilized the intracellular cAMP levels in Epac-HEK cells similar to the PDE4 inhibitor roflumilast. Furthermore, to specify the analysis of the potential PDE inhibitory effect, a fluorescence polarization assay was conducted. The PDE4B2 enzyme was chosen in this assay, because of its expression in macrophages and HEK cells. (40) The obtained data of all three compounds was very unspecific and not significant. Roflumilast was taken as comparison, because it is a selective PDE4 inhibitor and inhibits the subtype PDE4B2 with an IC_{50} of 0.2 nM. (102) Only a clearer tendency towards an inhibitory effect of PDE4B2 with roflumilast could be observed in the fluorescence polarization assay. This concludes that further tests need to be performed to obtain more accurate data.

Furthermore, after the treatment with LRK071, AH-17 and 2743, a significant decrease in the NO production in LPS-stimulated murine J774A.1 macrophages was determined. This implies anti-inflammatory properties of these compounds. Interestingly, roflumilast did not show a decrease of the NO production in LPS-induced J774A.1 macrophages, whereas the working group of Kwak detected a decrease of the NO production in LPS-stimulated RAW264.7 macrophages via heme-oxygenase 1 and carbon monoxide. (103)
Since cAMP inhibits the NF-κB signal pathway and additionally, a decrease in the NO production was determined in the Griess assay, which might be traced back to the inhibition of the NF-κB signal pathway, a NF-κB luciferase assay was performed with different concentrations of LRK071 and AH-17. A significant decrease was only observed in the highest concentration of LRK071 at 10 µM as well as of AH-17 at 10 µM. However, the positive control parthenolide 1 µM had no significant effect because of high standard deviations. To conclude, the substances LRK071 as well as AH-17 did not show a dose-dependent inhibition of the NF-κB signal pathway and hence, it seems like both compounds do not inhibit the NF-κB pathway.

LRK071 was also tested to identify if the increase of the cAMP levels can be traced back to a potential PKA inhibitory activity, a potential adenylate cyclase stimulatory activity or even to a stimulation of another Gαs-coupled receptor. To examine the PKA inhibitory theory a

CRE-luciferase assay was performed. The treatment of Epac-HEK cells with different concentrations of LRK071 with and without the PKA inhibitor H-89 (300 nM) was compared to roflumilast with and without H-89 (300 nM). If LRK071 had a PKA inhibitory activity, an additive inhibitory effect in combination with H-89 (300 nM) would be detected. However, no additive inhibitory effect of LRK071 in combination with H-89 (300 nM) was observed. The observed effect of the co-treatment and single treatment groups of LRK071 was similar to the effect of both groups of roflumilast. A phenotypic screening with stimulation by forskolin was conducted to determine the potential adenylate cyclase stimulation of LRK071. Therefore, the cells were treated with LRK071 and roflumilast with and without the strong adenylate cyclase stimulator forskolin (10 µM). In this experiment, no additive effect would be detected in combination with forskolin, if LRK071 was a stimulator of the adenylate cyclase. Hereby, an additive effect of roflumilast and LRK071 in combination with forskolin (10 µM) was detected. Both results of LRK071 are similar to the ones of roflumilast, which refute the theories that LRK071 might be a PKA inhibitor or an adenylate cyclase stimulator. However, it supports the theory that LRK071 might be a PDE inhibitor. To test the theory that LRK071 might stimulate another GPCR, which increases the cAMP levels, a kinetic cAMP measurement was performed. Instead of stimulating the Epac-HEK cells with isoprenaline, they were directly treated with the compound LRK071. No increase of the cAMP levels was examined, which refutes the theory of the receptor stimulation.

The working group of Burgin[(104)] worked on designing partial allosteric PDE4 modulators, because of reduced side effects in contrast to full agonists, in particular emesis. The key elements of the pharmacophore model are a planar scaffold with a hydrogen bond acceptor, a linker as well as two aromatic substituents, which provide a clamp to bind the UCR2 region in the closed confirmation. (104) The magnolol derivatives LRK071 as well as AH-17 provide a very similar scaffold to the required structure's key features. So, it is assumable that the magnolol derivatives also might affect the enzyme PDE4.

To summarize the results of LRK071, different signal pathways were examined to identify the mechanism of action especially of LRK071. However, it is still unclear, which mechanism is responsible for the increase of the cAMP levels in the phenotypic screening. All results of the performed experiments support the PDE-inhibitory theory. So, it is of paramount importance to conduct further experiments to assess the exact mechanism of action of LRK071.

F. Appendix

1 Abbreviations

A	ADRB2	Beta2- adrenergic receptor
	AMP	Adenosine monophosphate
	ATP	Adenosine triphosphate
	A.U.	Arbitrary unit
C	CA	Cholic acid
	cAMP	Cyclic adenosine monophosphate
	CBI	Complete induction buffer
	CD	Cluster of differentiation
	CDCA	Chenodeoxycholic acid
	CFP	Cyan fluorescent protein
	cGMP	Cyclic guanine monophosphate
	CM	Complete medium
	CNG	cyclic nucleotide-gated channel
	CoA	Coenzyme A
	CRE	cAMP responsive element
	CREB	cAMP response element - binding protein
	CTG	Cell tracker green
D	DCA	Deoxycholic acid
	ddH_2O	Double-distilled water
	DMEM	Dulbecco´s Modified Eagle´s Medium
	DMSO	Dimethyl sulfoxide
	DNTI	Drugs from nature targeting inflammation
E	EC_{50}	Half maximal effective concentration
	Epac	Exchange protein directly activated by cAMP
	ERK	Extracellular-signal regulated kinase
F	FAM	Carboxyfluorescein

	FBS	Fetal bovine serum
	FP	Fluorescence polarization
	FRET	Förster/ Fluorescence resonance energy transfer
	FURA-buffer	
	FXR	Farnesoid X receptor
G	GEF	Guanine-nucleotide exchange factor
	GFP	Green fluorescent protein
	GLP-1	Glucagon-like peptide 1
	GPCR	G-protein coupled receptor
	G-protein	Guanine nucleotide-binding regulatory protein
	GRK	G-protein coupled kinase
	GTP	Guanosine triphosphate
H	HCN	Hyperpolarization-activated cyclic nucleotide-gated channel
	HEK293	Human embryonic kidney 293 cells
	HBS	Hepes-buffered-saline
I	IBMX	3-isobutyl-1-methylxanthine
	IC_{50}	Half maximal inhibitory concentration
	Ig	Immunoglobulin
	IL	Interleukin
	IP3	Inositol-1,4,5-trisphosphate
L	LCA	Lithocholic acid
	LPS	Lipopolysaccharide
M	MS	Mass spectrometry
	Mcp-1	Monocyte chemoattractant protein 1
	MHC	Major histocompatibility complex
N	NF-κB	Nuclear factor kappa-light-chain-enhancer of activated B cells
	NK cells	Natural killer cells
	NMR	Nuclear magnetic resonance

P	PAMP	Pathogen-associated molecular pattern
	PBS	Phosphate buffered saline
	PDE	Phosphodiesterase
	PP_i	Pyrophosphate
	PRR	Pattern-recognition receptor
R	RFU	Relative fluorescence units
	RLU	Relative luminescence units
	rpm	Revolutions per minute
S	SD	Standard deviation
	SM	Stripped medium
	Sr-a	Scavenger receptor a
T	TCR	T cell receptor
	TGR5	Takeda-G-protein coupled receptor
	TLCA	Taurolithocholic acid
	TNFα	Tumor necrosis factor α
	Tregs	Regulatory T cells
U	UCR	Upstream conserved region

2 Figures

3 Tables

4 References

1. Faller A, Schünke M. Der Körper des Menschen. 17th ed. New York: Thieme; 2016. 139-144 p.
2. Delves PJ, Roitt IM. The immune system. N. Engl. J. Med. 2000; 343(1):37-49.
3. Müller-Esterl W. Biochemie. Eine Einführung für Mediziner und Naturwissenschaftler. München: Elsevier GmbH; 2004. 70-475 p.
4. Abdulkhaleq LA, Assi MA, Abdullah R, Zamri-Saad M, Taufiq-Yap YH, Hezmee MN. The crucial roles of inflammatory mediators in inflammation: A review. Vet. World. 2018; 11(5):627-635.
5. Pahwa R, Goyal A, Jialal I. Chronic inflammation [Internet]. Treasure Island (FL): StatPearls; 2022 [cited 2022 July 29th]. Available from: https://www.ncbi.nlm.nih.gov/books/NBK493173/
6. Falk E. Pathogenesis of atherosclerosis. J. Am. Coll. Cardiol. 2006; 47(8):C7-C12.
7. Lundstrom K. An overview on GPCRs and drug discovery: Structure-based drug design and structural biology on GPCRs. Methods Mol. Biol. 2009; 552:51-66.
8. Rohrer DK, Kobilka KK. G-protein coupled receptors: Functional and mechanistic insights through altered gene expression. Physiol. Rev. 1998; 78(1):35-52.
9. Lefkowitz RJ, Hausdorff WP, Caron MG. Role of phosphorylation in desensitization of the β-adrenoceptor. Trends Pharmacol. Sci. 1990; 11(5):190-194.
10. Strader CD, Fong TM, Tota MR, Underwood D. Structure and Function of G protein-coupled receptors. Annu. Rev. Biochem. 1994; 63:101-132.
11. Lohse MJ, Engelhardt S, Eschenhagen T. What is the role of β-adrenergic signaling in heart failure? Circ. Res. 2003; 93(10):896-906.
12. Yokoyama U, Iwatsubo K, Umemura M, Fujita T, Ishikawa Y. The prostanoid EP4 receptor and its signaling pathway. Pharmacol. Rev. 2013; 65(3):1010-1052.
13. Torphy TJ. β-adrenoceptors, cAMP and airway smooth muscle relaxation: challenges to the dogma. Trends Pharmacol. Sci. 1994; 15(10):370-374.
14. Balogh J, Wihlborg A-K, Isackson H, Joshi BV, Jacobson KA, Arner A, et al. Phospholipase C and cAMP-dependent positive inotropic effects of ATP in mouse cardiomyocytes via P2Y11-like receptors. J. Mol. Cell. Cardiol. 2005; 39(2):223-230.

15. Rossi AG, McCutcheon JC, Roy N, Chilvers ER, Haslett C, Dransfield I. Regulation of macrophage phagocytosis of apoptotic cells by cAMP. J. Immunol. 1998; 160(7):3562-3568.
16. Rowe J, Finlay-Jones JJ, Nicholas TE, Bowden J, Morton S, Hart PH. Inability of histamine to regulate TNF-α production by human alveolar macrophages. Am. J. Respir. Cell Mol. Biol. 1996; 17(2):218-226.
17. De Rooji J, Zwartkruis FJ, Verheijen MH, Cool RH, Nijman SM, Wittinghofer A, et al. Epac is a Rap1 guanine-nucleotide-exchange factor directly activated by cyclic AMP. Nature. 1998; 396(6710):474-477.
18. Zufall F, Firestein S, Shepherd GM. Cyclic nucleotide-gated ion channels and sensory transduction in olfactory receptor neurons. Annu. Rev. Biophys. Biomol. Struct. 1994; 23(1):577-607.
19. Biel M, Michalakis S. Cyclic nucleotide-gated channels. In: Schmidt HH, Hofman F, Stasch JP, editors. cGMP: Generators, effectors and therapeutic implications [Internet]. Berlin, Heidelberg: Springer; 2009. [2022 May 17] p. 111-136. Available from: https://doi.org/10.1007/978-3-540-68964-5_7
20. Kawasaki H, Springett GM, Mochizuki N, Toki S, Nakaya M, Matsuda M, et al. A family of cAMP-binding proteins that directly activate Rap1. Science. 1998; 282(5397):2275-2279.
21. Gelinas JN, Banko JL, Peters MM, Klann E, Weeber EJ, Nguyen PV. Activation of exchange protein activated by cyclic-AMP enhances long-lasting synaptic potentiation in the hippocampus. Learn. Mem. 2008; 15:403-411.
22. Murray AJ, Shewan DA. Epac mediates cyclic AMP-dependent axon growth, guidance and regeneration. Mol. Cell Neurosci. 2008; 38:578-588.
23. Yokoyama U, Patel HH, Lai NC, Aroonsakool N, Roth DM, Insel PA. The cyclic AMP effector Epac integrates pro- and anti-fibrotic signals. Proc. Natl. Acad. Sci. U.S.A. 2008; 105:6386-6391.
24. Bos JL. Epac: a new cAMP target and new avenues in cAMP research. Nat. Rev. Mo. Cell Biol. 2003; 4(9):733-738.
25. Kaupp BU, Seifert R. Cyclic nucleotide-gated ion channels. Physiol. Rev. 2002; 82(3):769-824.
26. Halliwell JV, Adams PR. Voltage-clamp analysis of muscarinic excitation in hippocampal neurons. Brain Res. 1982; 250(1):71-92.

27. Bader CR, Macleish PR, Schwartz EA. A voltage-clamp study of the light response in solitary rods of the tiger salamander. The Journal of Physiology. 1979; 296(1):1-26.
28. Pape HC. Queer current and pacemaker: The hyperpolarization-activated cation current in neurons. Annu. Rev. Physiol. 1996; 58:299-327.
29. Hofmann F, Biel M, Kaupp BU. International union of pharmacology. LI. Nomenclature and structure-function relationships of cyclic nucleotide-regulated channels. Pharmacol. Rev. 2005; 57:455-462.
30. Lugnier C. Cyclic nucleotide phosphodiesterase (PDE) superfamiliy: A new target for the development of specific therapeutic agents. Pharmacol. Ther. 2006; 109(3):366-398.
31. Stoclet JC, Keravis T, Komas N, Lugnier C. Section Review: Cardiovascular & renal: Cyclic nucleotide phosphodiesterases as therapeutic targets in cardiovascular diseases. Expert Opin. Invest. Drugs. 1995; 4(11):1081–1100.
32. Beavo JA. Cyclic nucleotide phosphodiesterases: Functional implications of multiple isoforms. Physiol. Rev. 1995; 75(4):725-748.
33. Richter W, Menniti FS, Zhang HAT, Conti M. PDE4 as a target for cognition enhancement. Expert Opin. Ther. Targets. 2013; 17(9):1011-1027.
34. Butcher RW, Sutherland EW. Adenosine 3´, 5´-phosphate in biological materials. The Journal of Biological Chemistry. 1962; 237(4):1244-1250.
35. Boswell-Smith V, Spina D. PDE4 inhibitors as potential therapeutic agents in the treatment of COPD-focus on roflumilast. Int. J. Chron. Obstruct. Pulmon. Dis. 2007; 2(2):121-129.
36. Zheng J, Yang J, Zhou X, Zhao L, Hui F, Wang H, Bai C, et al. Roflumilast for the treatment of COPD in an Asian population: a randomized, double-blind, parallel-group study. Chest. 2014; 145(1):44-52.
37. Houslay MD. PDE4 cAMP-specific phosphodiesterases. Prog. Nucleic Acid Res. Mol. Biol. 2001; 69:249-315.
38. Boolell M, Gepi-Attee S, Gingell JC, Allen MJ. Sildenafil, a novel effective oral therapy for male erectile dysfunction. Br. J. Urol. 1996; 78(2):257-261.
39. Schmidt B, Roberts RS, Davis P, Doyle LW, Barrington KJ, Ohlsson A, et al. Caffeine therapy for apnea of prematurity. N. Engl. J. Med. 2006; 354(20):2112-2121.

40. Tenor H, Hatzelmann A, Kupferschmidt R, Stanciu L, Djukanovic R, Schudt C, et al. Cyclic nucleotide phosphodiesterase isoenzyme activities in human alveolar macrophages. Clin. Exp. Allergy. 1995; 25(7):625-633.Schett
41. Bailie G, MacKenzie SJ, Houslay MD. Phorbol 12-myristate 13-acetate triggers the protein kinase A-mediated phosphorylation and activation of the PDE4D5 cAMP phosphodiesterase in human aortic smooth muscle cells through a route involving extracellular signal regulated kinase (ERK). Mol. Pharmacol. 2001; 60(5):1100-1111.
42. Housay MD, Schafer P, Zhang KY. Keynote review: Phosphodiesterase-4 as a therapeutic target. Drug Discovery Today. 2005; 10(22):1503-1519.
43. Shepherd MC, Bailie GS, Stirling DI, Houslay MD. Remodelling of the PDE4 cAMP phosphodiesterase isoform profile upon monocyte-macrophage differentiation of human U937 cells. Br. J. Pharmacol. 2004; 142(2):339-351.
44. Rajagopal S, Shenoy SK. GPCR desensitization: acute and prolonged phases. Cell. Signalling. 2018; 41:9-16.
45. Sibley DR, Peters JR, Nambi P, Caron MG, Lefkowitz RJ. Desensitization of turkey erythrocyte adenylate cyclase. J. Biol. Chem. 1984; 259(15):9742-9749.
46. Sibley DR, Strasser RH, Caron MG, Lefkowitz RJ. Homologous desensitization of adenylate cyclase is associated with phosphorylation of the beta-adrenergic receptor. J. Biol. Chem. 1985; 260(7):3883-3886.
47. Perino A, Schoonjans K. TGR5 and immunometabolism: Insights from Physiology and Pharmacology. Trends Pharmacol. Sci. 2015; 36(12):847-857.
48. Pols TW, Nomura M, Harach T, Lo Sasso G, Oosterveer MH, Thomas C, et al. TGR5 activation inhibits atherosclerosis by reducing macrophage inflammation and lipid loading. Cell Metab. 2011; 14:747-757.
49. Guo C, Chen WD, Wang YD. TGR5, not only a metabolic regulator. Front. Physiol. 2016; 7:646.
50. Kawamata Y, Fujii R, Hosoya M, Harada M, Yoshida H, Miwa M, et al. A G protein-coupled receptor responsive to bile acids. J. Biol. Chem. 2003; 278(11):9435-9440.
51. Kirchweger B, Kratz JM, Ladurner A, Grienke U, Langer T, Dirsch VM, et al. In silico workflow for the discovery of natural products activating the G protein-coupled bile acid receptor 1. Front. Chem. 2018; 6:242.

52. Horiba T, Katsukawa M, Mita M, Sato R. Dietary obacunone supplementation stimulates muscle hypertrophy, and suppresses hyperglycemia and obesity through the TGR5 and PPARγ pathway. Biochem. Biophys. Res. Commun. 2015; 463(4):846-852.
53. Piotrowski DW, Futatsugi K, Warmus JS, Orr ST, Freeman-Cook KD, Londregan AT, et al. Identification of tetrahydropyrido[3,4-d]pyrimidine amides as a new class of orally bioavailable TGR5 agonists. ACS Med. Chem. Lett. 2013; 4(1):63-68.
54. Kumar DP, Asgharpour A, Mirshahi F, Park SH, Liu S, Imai Y, et al. Activation of transmembrane bile acid receptor TGR5 modulates pancreatic islet α cells to promote glucose homeostasis. J. Biol. Chem. 2016;291(13):6626-6640.
55. Guo C, Su J, Li Z, Xiao R, Wen J, Li Y, et al. The G-protein-coupled bile acid receptor Gpbar1 (TGR5) suppresses gastric cancer cell proliferation and migration through antagonizing STAT3 signaling pathway. Oncotarget. 2015; 6(33):34402-34413.
56. Serasanambati M, Chilakapati SR. Function of nuclear factor kappa B (NF-κB) in human diseases – A review. South Indian Journal of Biological Sciences. 2016; 2(4):368-387.
57. Raker VK, Becker C, Steinbrink K. The cAMP pathway as therapeutic target in autoimmune and inflammatory diseases. Front. Immunol. 2016; 7:123.
58. Serezani CH, Ballinger MN, Aronoff DM, Peters-Golden M. Cyclic AMP: master regulator of innate immune cell function. Am. J. Respir. Cell Mol. Biol. 2008; 39(2):127-132.
59. Lin G, Bornfeldt KE. Cyclic AMP-specific phosphodiesterase 4 inhibitors promote ABCA1 expression and cholesterol efflux. Biochem. Biophys. Res. Commun. 2002; 290(2):663-669.
60. Bulut V, Severn A, Liew FY. Nitric oxide production by murine macrophages is inhibited by prolonged elevation pf cyclic AMP. Biochem. Biophys. Res. Commun. 1993; 195(2):1134-1138.
61. Negreiros-Lima GL, Lima KM, Moreira IZ, Jardim BL, Vago JP, Galvão I, et al. Cyclic AMP regulates key features of macrophages via PKA: recruitment, reprogramming and efferocytosis. Cells. 2020; 9(1):128.
62. Baeuerle PA, Baichwal VR. NF-κB as a frequent target for immunosuppressive and anti-inflammatory molecules. In: Dixon FJ. Advances in Immunology. 65 ed. San Diego: Academic Press; 1997. p. 111-135.

63. Minguet S, Huber M, Rosenkranz L, Schamel WW, Reth M, Brummer T. Adenosine and cAMP are potent inhibitors of the NF-κB pathway downstream of immunoreceptors. Eur. J. Immunol. 2005; 35:31-41.
64. Parry GC, Mackman N. Role of cyclic AMP response element-binding protein in cyclic AMP inhibition of NF-κB-mediated transcription. J. Immunol. 1997; 159(11):5450-5456.
65. Harvey AL. Natural products in drug discovery. Drug Discovery Today. 2008; 13(19-20):894-901.
66. Sarrica A, Kirika N, Romeo M, Salmona M, Diomede L. Safety and toxicology of magnolol and honokiol. Planta Med. 2018; 84(16):1151-1164.
67. Elbeialy N. Screening von Naturstoffen auf deren potenziellen Einfluss auf intrazelluläre cAMP-Levels zur Immunomodulation. Diplomarbeit, Univ. Wien. 2021.
68. Wang L, Ladurner A, Latkolik S, Schwaiger S, Linder T, Hošek J, et al. Leoligin, the major lignan from Edelweiss (Leontopodium nivale ssp. alpinum), promotes cholesterol efflux from THP-1 macrophages. J. Nat. Prod. 2016; 79(6):1651-1657.
69. Safer S, Tremetsberger K, Guo YP, Kohl G, Samuel MR, Stuessy TF, et al. Phylogenetic relationships in the genus Leontopodium (Asteraceae: Gnaphalieae) based on AFLP data. Bot. J. Linn. Soc. 2011; 165(4):364-377.
70. Duwensee K, Schwaiger S, Tancevski I, Eller K, van Eck M, Markt P, et al. Leoligin, the major lignan from Edelweiss, activates cholesteryl ester transfer protein. Atherosclerosis. 2011; 219(1):109-115.
71. Linder T, Liu R, Atanasov AG, Li Y, Geyrhofer S, Schwaiger S. et al. Leoligin-inspired synthetic lignans with selectivity for cell-type and bioactivity relevant for cardiovascular disease. Chem. Sci. 2019; 10:5815-5820.
72. Tanishq C, Sujata D. Immunomodulatory activity of methanolic extract of Ruta graveolens. J. Nat. Prod. Resour. 2016; 2(2):62-64.
73. Asgarpanah J, Khoshkam R. Phytochemistry and pharmacological properties of Ruta graveolens L. J. Med. Plants Res. 2016; 6(23):3942-3949.
74. Li Y, Fu L, Yeo H, Zhu JL, Chou CK, Kou YH, et al. Inhibition of hepatitis B virus gene expression and replication by helioxanthin and its derivative. Antiviral Chem. Chemother. 2005; 16(3):193-201.

75. Hajdu Z, Haskó J, Krizbai IA, Wilhelm I, Jedlinszji N, Fazakas C, et al. Evaluation of lignans from Heliopsis helianthoides var. scabra for their potential antimetastatic effects in the brain. J. Nat. Prod. 2014; 77(12):2641-2650.
76. Wang Q, Zhou X, Yang L, Zhao Y, Chew Z, Xiao J, et al. The natural compound notopterol binds and targets JAK2/3 to ameliorate inflammation and arthritis. Cell Rep. 2020; 32(11):108158.
77. Azietaku JT, Ma H, Yu Xa, Li J, Oppong MB, Cao J, et al. A review of the ethnopharmacology, phytochemistry and pharmacology of notopterygium incisum. J. Ethnopharmacol. 2017; 202:241-255.
78. Chen D, Wang Q, Li Y, Sun P, Kuek V, Yuan J, et al. Notopterol attenuates estrogen deficiency-induced osteoporosis via repressing RANKL signaling and reactive oxygen species. Front. Pharmacol. 2021; 12:664836.
79. Jiang X, Lu H, Li J, Liu W, Wu Q, Xu Z, et al. A natural BACE1 and GSK3β dual inhibitor Notopterol effectively ameliorates the cognitive deficits in APP/PS1 Alzheimer´s mice by attenuating amyloid-β and tau pathology. Clin. Transl. Med. 2020; 10(3):e50.
80. Huang Q, Wang L, Ran Q, Wang J, Wang C, He H, et al. Notopterol-induced apoptosis and differentiation in human acute myeloid leukemia HL-60 cells. Drug Des. Devel. Ther. 2019; 13:1927-1940.
81. Waltenberger B, Atanasov AG, Heiss EH, Bernhard D, Rollinger JM, Breuss JM, et al. Drugs from nature targeting inflammation (DNTI): a successful Austrian interdisciplinary network project. Monatshefte für Chemie. 2016; 147:479-491.
82. Förster T. Zwischenmolekulare Energiewanderung und Fluoreszenz. Ann. Phys. 1948; 437(1-2):55-75.
83. Liu L, He F, Yu Y, Wang Y. Application of FRET biosensors in mechanobiology and mechanopharmacological screening. Front. Bioeng. Biotechnol. 2020; 8:595497.
84. Ponsioen B, Zhao J, Riedl J, Zwartkruis F, van der Krogt G, Zaccolo M, et al. Detecting cAMP-induced Epac activation by fluorescence resonance energy transfer: Epac as a novel cAMP indicator. EMBO Rep. 2004; 5:1176-1180.
85. Miyawaki A. Development of probes for cellular functions using fluorescent proteins and fluorescence resonance energy transfer. Annu. Rev. Biochem. 2011; 80:357-373.
86. Hochreiter B, Garcia AP, Schmid JA. Fluorescent proteins as genetically encoded FRET biosensors in life science. Sensors. 2015; 15:26281-26314.

87. Wieb van der Meer B. Förster Theory. In: Medintz I, Hildebrandt N, editors. FRET-Förster Resonance Energy Transfer. 1st ed. Weinheim: Wiley-VCH; 2013. p. 23-62.
88. Stryer L, Haugland RP. Energy transfer: a spectroscopic ruler. Proc Natl Acad Sci USA. 1967; 58(2):719-726.
89. Sekhar KR, Grondin P, Francis SH, Corbin JD. Design and synthesis of xanthines and cyclic GMP analogues as potent inhibitors of PDE5. In: Schudt C, Dent G, Rabe KF, editors. Phosphodiesterase inhibitors. New York: Academic Press; 1996; p. 136.
90. Feldman PL, Griffith OW, Stuehr DJ. The surprising life of nitric oxide. Chem. Eng. News. 1993; 71(51):26-38.
91. Griess JP. Ber. Dtsch. Chem. Ges. 1879; 12:426.
92. Sun J, Zhang X, Broderick M, Fein H. Measurement of nitric oxide production in biological systems by using Griess reaction assay. Sensors. 2003; 3:276-284.
93. Carter M, Shieh J. Guide to research techniques in neuroscience [Internet]. 2nd ed. ScienceDirect; 2015 [cited 2022 04 13]. p.311-343. Available from: https://doi.org/10.1016/B978-0-12-800511-8.00015-0
94. Hakkila K, Maksimow M, Karp M, Virta M. Reporter genes lucFF, luxCDABE, gfp, and dsred have different characteristics in whole-cell bacterial sensors. Anal. Biochem. 2002; 301:235-242.
95. DeLuca M, McElroy WD. Two kinetically distinguishable ATP sides in firefly luciferase. Biochem. Biophys. Res. Commun. 1984; 123(2):764-770.
96. Smale ST. Luciferase assay. Cold Spring Harbor Protocols. 2010; 2010(5).
97. Bork PM, Schmitz ML, Kuhnt M, Escher C, Heinrich M. Sesquiterpene lactone containing Mexican Indian medicinal plants and pure sesquiterpene lactones as potent inhibitors of transcription factor NF-κB. FEBS Lett. 1997; 402(1):85-90.
98. Owicki JC. Fluorescence polarization and anisotropy in high-throughput screening: perspectives and primer. J. Biomol. Screening. 2000; 5(5):297-306.
99. Lea WA, Simeonov A. Fluorescence polarization assay in small molecule screening. Expert Opin. Drug Discovery. 2011; 6(1):17-32.
100. Rizzo G, Renga B, Mencarelli A, Pellicciari R, Fiorucci S. Role of FXR in regulating bile acid homeostasis and relevance for human diseases. Curr. Drug Targets: Immune, Endocr. Metab. Disord. 2005; 5(3):289-303.

101. Chen YQ, Xie X. Podophyllotoxin induces CREB phosphorylation and CRE-driven gene expression via PKA but not MAPKs. Mol. Cells. 2010; 29:41-50.
102. Hatzelmann A, Morcillo EJ, Lungarella G, Adnot S, Sanjar S, Beume R, et al. The preclinical pharmacology of roflumilast – a selective, oral phosphodiesterase 4 inhibitor in development for chronic obstructive pulmonary disease. Pulm. Pharmacol. Ther. 2010; 23:235-256.
103. Kwak HJ, Song JS, No ZS, Song JH, Yang SD, Cheon HG. The inhibitory effects of roflumilast on lipopolysaccharide-induced nitric oxide production in RAW264.7 cells are mediated by heme oxygenase-1 and its product carbon monoxide. Inflamm. res. 2005; 54: 508-513.
104. Burgin AB, Magnusson OT, Singh J, Witte P, Staker BL, Bjornsson JM, et al. Design of phosphodiesterase 4 (PDE4D) allosteric modulators for enhancing cognition with improved safety. Nat. Biotechnol. 2010; 28(1):63-72.

5 Data of the high-throughput screenings

Table 14: Data of the high-throughput screenings (Epac-based FRET biosensor assays) from compounds of the DNTI project at a concentration of mostly 10 µM to determine their influence on the cAMP level.

The modified HEK cells were treated with the compounds (mostly 10 µM) and incubated for 30 min. After that time, the cells were stimulated with isoprenaline (100 nM). The fluorescence intensity was measured, and the data is provided in the fluorescence ratio of CFP to Venus normalized to DMSO 0.1%, stated in percent. The mean of technical triplicates is given.

DNTI number	**Phenotypic screening:** Increase of the fluorescence ratio (CFP/Venus) normalized to DMSO 0.1% in percentage	**Target-based screening:** Increase of the fluorescence ratio (CFP/Venus) normalized to DMSO 0.1% in percentage
640		106,85
641		108,80
727		106,46
730		103,68
754		107,60
755		108,70
756		102,66
758		101,92
759		99,46
760		102,52
761		104,19
763		108,20
764		106,95
765		108,90
766		107,85
767		111,06
768		108,73
770		108,61
771		104,68
772		101,78
773		98,13
774		98,68
775		99,66
776		97,38
777		98,88
778		98,87
779		99,25
780		97,46
783		99,88

DNTI number	**Phenotypic screening:** Increase of the fluorescence ratio (CFP/Venus) normalized to DMSO 0.1% in percentage	**Target-based screening:** Increase of the fluorescence ratio (CFP/Venus) normalized to DMSO 0.1% in percentage
793		99,70
795		99,11
799		100,15
800		102,05
801		98,12
802		167,27
803		100,56
804		99,90
805		102,70
806		118,86
807		100,09
808		102,08
850		117,78
851		99,17
852		107,69
853		101,79
854		104,70
855		80,30
856		100,83
857	94,89	237,08
931		116,74
964		101,32
965		106,20
966		101,40
967		104,89
968		104,17
969		104,31
992		102,40
1002		102,22

DNTI number	Phenotypic screening: Increase of the fluorescence ratio (CFP/Venus) normalized to DMSO 0.1% in percentage	Target-based screening: Increase of the fluorescence ratio (CFP/Venus) normalized to DMSO 0.1% in percentage
1005		101,84
1006		102,94
1007		98,81
1008		118,81
1009		100,58
1022		102,29
1044		109,21
1045		101,15
1046		95,02
1047		104,54
1048		103,76
1050		103,83
1051		105,51
1054		122,15
1055		147,23
1056		92,43
1073		94,42
1079		100,86
1080		92,80
1081		92,04
1082		91,55
1083		93,01
1088		92,70
1089		92,36
1091		90,38
1094		92,53
1096		92,37
1097		90,80
1098		89,53
1099		90,49
1100		91,66
1101		92,32
1102		90,91
1103		103,85
1140		101,51
1141		102,39
1142		101,37

DNTI number	Phenotypic screening: Increase of the fluorescence ratio (CFP/Venus) normalized to DMSO 0.1% in percentage	Target-based screening: Increase of the fluorescence ratio (CFP/Venus) normalized to DMSO 0.1% in percentage
1143		100,12
1144		99,09
1145		101,20
1146		101,55
1147		102,98
1148		103,97
1150		103,13
1151		103,37
1152		102,67
1153		103,56
1154		102,76
1155		103,10
1213		102,65
1214		103,73
1215		97,35
1216		101,50
1217		98,98
1218		98,93
1219		99,78
1220		99,17
1221		97,51
1222		98,56
1223		106,65
1224		103,18
1225		99,78
1226		100,12
1227		98,53
1228		101,68
1229		97,74
1230		95,43
1231		103,45
1232		97,78
1233		98,95
1234		102,27
1235		100,46
1236		99,02
1237		99,14

DNTI number	Phenotypic screening: Increase of the fluorescence ratio (CFP/Venus) normalized to DMSO 0.1% in percentage	Target-based screening: Increase of the fluorescence ratio (CFP/Venus) normalized to DMSO 0.1% in percentage
1238		104,67
1239		95,10
1240		97,76
1241		103,61
1242		97,86
1329		97,15
1330		101,99
1331		101,15
1332		97,70
1360		96,45
1399		97,75
1400		96,66
1401		113,12
1402		96,66
1415		98,27
1416		97,74
1417		96,77
1418		98,17
1419		105,81
1420		100,07
1441		98,93
1442		99,89
1444		100,15
1445		99,63
1446		99,82
1447		105,32
1448		99,65
1503		99,54
1504		103,29
1507		99,51
1508		100,30
1509		100,25
1510		102,40
1513		102,27
1514		101,16
1516		101,86
1517		103,36

DNTI number	Phenotypic screening: Increase of the fluorescence ratio (CFP/Venus) normalized to DMSO 0.1% in percentage	Target-based screening: Increase of the fluorescence ratio (CFP/Venus) normalized to DMSO 0.1% in percentage
1518		105,65
1519		100,12
1529		100,82
1531		104,72
1532		104,02
1534		105,82
1548		106,09
1555		105,72
1557		103,35
1682		101,34
1684		100,79
1686		101,39
1688		101,55
1689		100,64
1705		104,47
1706		102,19
1707		105,23
1708		103,17
1709		104,32
1710		105,44
1711		104,66
1712		104,72
1713		100,22
1714		98,87
1715		103,80
1716		93,13
1717		103,76
1718		102,80
1719		105,62
1720		104,23
1721		103,41
1739		101,99
1740		100,27
1741		100,31
1742		102,49
1743		103,95
1750		105,59

DNTI number	Phenotypic screening: Increase of the fluorescence ratio (CFP/Venus) normalized to DMSO 0.1% in percentage	Target-based screening: Increase of the fluorescence ratio (CFP/Venus) normalized to DMSO 0.1% in percentage
1751		105,84
1758		104,90
1759		104,48
1763		106,13
1764		104,90
1765		104,81
1766		102,39
1767		100,00
1829		108,13
1831		103,27
1832		122,54
1833		102,57
1834		102,86
1850		101,63
1851		102,24
1852		101,43
1876		99,28
1877		102,67
1878		103,29
1879		105,56
1880		107,09
1881		104,87
1882		105,66
1883		111,84
1884		107,34
1885		105,97
1899		103,91
1916		101,73
1917		101,76
1918		96,20
1919		93,09
1921		93,26
1922		95,23
1923		93,69
1951		92,71
1952		91,70
1953		90,17

DNTI number	Phenotypic screening: Increase of the fluorescence ratio (CFP/Venus) normalized to DMSO 0.1% in percentage	Target-based screening: Increase of the fluorescence ratio (CFP/Venus) normalized to DMSO 0.1% in percentage
1954		93,70
1955		94,71
1956		94,07
1957		93,14
1958		94,85
1959		93,64
2097		92,28
2098		92,02
2099		94,21
2100		93,09
2101		93,92
2102		93,29
2103		100,26
2105		100,58
2123		102,56
2125		100,44
2126		101,58
2127		98,55
2128		98,19
2129		102,24
2130		99,73
2131	102,87	99,79
2132	100,41	101,72
2133	98,78	100,60
2135	100,13	100,63
2136	100,98	102,28
2284		102,20
2285		100,95
2352	100,94	98,42
2353	101,08	100,75
2354	100,81	99,75
2355	102,15	98,63
2356	101,35	100,66
2357	101,11	96,59
2359	96,96	103,94
2360	100,26	102,20
2361	99,34	103,00

DNTI number	Phenotypic screening: Increase of the fluorescence ratio (CFP/Venus) normalized to DMSO 0.1% in percentage	Target-based screening: Increase of the fluorescence ratio (CFP/Venus) normalized to DMSO 0.1% in percentage
2363	103,45	100,00
2364	102,10	102,36
2365	100,29	97,39
2367	102,79	102,22
2368	102,79	203,38
2369	101,79	119,90
2370	101,63	101,82
2371	101,08	101,16
2372	102,32	101,60
2373	101,64	100,82
2412	100,31	100,55
2413	101,35	101,04
2414	100,44	104,85
2415	102,19	99,00
2418	105,20	104,32
2419	102,85	100,94
2422	100,11	100,63
2423	99,98	98,77
2424	100,69	98,88
2445	98,11	100,52
2446	99,48	99,12
2447	101,27	100,38
2448	101,76	100,57
2449	100,99	99,83
2450	102,51	100,74
2451	101,54	98,66
2452	101,39	98,26
2454	102,37	98,34
2455	104,05	97,07
2456	102,70	99,42
2459	100,49	99,37
2460	100,32	99,98
2461	102,14	98,56
2462	100,68	98,93
2538		100,08
2539		102,25
2540		102,17

DNTI number	Phenotypic screening: Increase of the fluorescence ratio (CFP/Venus) normalized to DMSO 0.1% in percentage	Target-based screening: Increase of the fluorescence ratio (CFP/Venus) normalized to DMSO 0.1% in percentage
2541		99,63
2543		97,86
2544		101,83
2545		100,80
2547		102,37
2550		100,13
2551		101,23
2552	106,98	103,18
2553	101,61	98,97
2554	101,33	100,53
2555	101,26	99,12
2556	103,23	101,58
2557	100,65	99,04
2558	101,96	100,18
2559	100,41	101,96
2560	103,31	226,91
2569	102,84	100,49
2570	103,98	100,66
2571	102,81	101,95
2573	101,90	100,49
2574	104,73	101,35
2575	101,88	100,46
2576	100,91	100,05
2626		98,52
2627		100,75
2628		101,97
2630		101,73
2633		100,96
2636		101,43
2637		107,19
2638		98,77
2639		101,48
2640	100,46	110,44
2641	96,89	114,94
2642	98,89	100,29
2643	103,40	100,41
2644	105,12	166,68

DNTI number	**Phenotypic screening:** Increase of the fluorescence ratio (CFP/Venus) normalized to DMSO 0.1% in percentage	**Target-based screening:** Increase of the fluorescence ratio (CFP/Venus) normalized to DMSO 0.1% in percentage
2654	104,32	99,23
2655	102,24	99,71
2656	103,43	99,69
2657	100,37	101,02
2658	101,52	100,17
2659	100,29	100,36
2733	98,91	98,51
2734	105,30	
2795	101,35	
2796	100,07	
2797	101,61	
2798	102,74	
2799	104,58	
2800	102,45	
2802	102,25	
2803	103,30	
2804	103,04	
2805	103,02	
2806	100,73	
2807	101,91	
2808	100,47	
2819	100,53	
2820	101,62	
2822	101,36	
2823	102,67	
2824	103,97	
2825	103,81	
2826	103,11	
2827	103,06	
2828	103,50	
2830	103,40	
2831	102,67	
2832	102,40	
2833	102,73	
2834	103,87	
2835	104,76	
2836	104,90	

DNTI number	**Phenotypic screening:** Increase of the fluorescence ratio (CFP/Venus) normalized to DMSO 0.1% in percentage	**Target-based screening:** Increase of the fluorescence ratio (CFP/Venus) normalized to DMSO 0.1% in percentage
2837	106,07	
2838	105,66	
2839	105,12	
2840	105,44	
2842	104,81	
2843	100,05	
2846	101,12	
2847	101,53	
2848	101,07	
2849	102,04	
2855	104,65	
2856	102,47	
2858	100,86	
2859	101,57	
2864	102,42	
2865	103,07	
2866	100,98	
2867	99,72	
2872	100,49	
2873	99,26	
2876	98,45	
2878	97,69	
2879	98,30	
2881	99,51	
2882	101,52	
2883	100,40	
2884	101,66	
2885	98,98	
2886	99,44	
2887	100,66	
2888	100,62	
2889	99,64	
2890	99,02	
2891	97,30	
2892	101,10	
2893	99,78	
2894	101,06	

DNTI number	**Phenotypic screening:** Increase of the fluorescence ratio (CFP/Venus) normalized to DMSO 0.1% in percentage	**Target-based screening:** Increase of the fluorescence ratio (CFP/Venus) normalized to DMSO 0.1% in percentage
2895	101,89	
2896	99,80	
2897	100,03	
2898	101,13	
2899	99,09	
2900	98,49	
2901	100,36	
2902	98,79	
2903	100,32	
2904	99,47	
2905	101,39	
2906	100,47	
2907	99,71	
2908	100,54	
2909	100,38	
2911	100,46	
2912	99,35	
2913	98,98	
2914	103,00	
2915	103,22	
2916	102,37	
2917	102,85	
2918	101,42	
2919	102,23	
2920	104,31	
2921	101,06	
2922	106,74	
2923	100,53	
2924	97,04	
2926	102,54	
2927	102,67	
2929	102,79	
2930	103,49	
2931	101,55	
2933	102,46	
2934	102,33	
2935	103,71	

DNTI number	**Phenotypic screening:** Increase of the fluorescence ratio (CFP/Venus) normalized to DMSO 0.1% in percentage	**Target-based screening:** Increase of the fluorescence ratio (CFP/Venus) normalized to DMSO 0.1% in percentage
2936	100,36	
2937	100,27	
2938	102,57	
2939	101,45	
2940	100,41	
2941	104,13	
2942	100,62	
2943	98,98	
2944	98,32	
2945	100,35	
2946	99,95	
2947	100,71	
2948	100,61	
2949	101,59	
2950	100,64	
2951	99,80	
2956	100,90	
2957	110,45	
2958	103,93	
2959	100,09	
2960	99,02	
2961	101,48	
2962	103,09	
2963	99,88	
2964	100,88	
2965	102,16	
2966	101,11	
2968	109,20	
2969	96,51	
2970	98,06	
2971	99,63	
2972	101,23	
2976	101,70	
2981	102,92	
2982	101,06	
2983	100,24	
2984	102,80	

DNTI number	**Phenotypic screening:** Increase of the fluorescence ratio (CFP/Venus) normalized to DMSO 0.1% in percentage	**Target-based screening:** Increase of the fluorescence ratio (CFP/Venus) normalized to DMSO 0.1% in percentage
2985	101,24	
2986	100,18	
2987	100,67	
2988	100,21	
2990	99,22	
2991	99,18	
2992	98,03	
2993	99,37	
2994	98,80	
2995	95,59	
2996	101,07	
2997	100,50	
3006	100,85	
3007	99,53	
3008	99,28	
3009	98,89	
3011	98,83	
3012	101,11	
3014	99,74	
3015	99,56	
3016	98,88	
3017	103,84	
3023	105,26	
3024	106,11	
3025	104,78	
3026	106,62	
3027	107,91	
3028	109,28	
3029	105,63	
3030	106,47	
3031	102,64	
3032	102,89	
3033	101,18	
3034	106,12	
3037	105,71	
3039	106,11	
3040	105,66	

DNTI number	**Phenotypic screening:** Increase of the fluorescence ratio (CFP/Venus) normalized to DMSO 0.1% in percentage	**Target-based screening:** Increase of the fluorescence ratio (CFP/Venus) normalized to DMSO 0.1% in percentage
3041	105,71	
3042	105,88	
3043	106,28	
3044	107,17	
3046	102,11	
3047	102,62	
3048	102,63	
3049	101,63	
3050	99,64	
3051	103,95	
3054	105,03	
3079	104,93	
3080	106,15	
3081	106,62	
3082	104,93	
3083	104,77	
3085	103,37	
3086	99,61	
3087	99,54	
3088	103,11	
3099	95,80	
3101	95,57	
3125	99,26	
3126	99,83	
3157	103,73	
3158	102,11	
3159	101,77	
3160	101,62	
3161	103,05	
3162	102,98	
3163	104,35	
3164	100,61	
3165	100,97	
3166	99,92	
3167	100,19	
3168	101,33	
3169	100,26	

DNTI number	**Phenotypic screening:** Increase of the fluorescence ratio (CFP/Venus) normalized to DMSO 0.1% in percentage	**Target-based screening:** Increase of the fluorescence ratio (CFP/Venus) normalized to DMSO 0.1% in percentage
3170	100,31	
3171	101,59	
3172	100,70	
3173	99,97	
3174	100,58	
3175	101,57	

6 Viability data of the luciferase assays

6.1 Viability data of the CRE- luciferase assay in TGR5-Epac-HEK cells

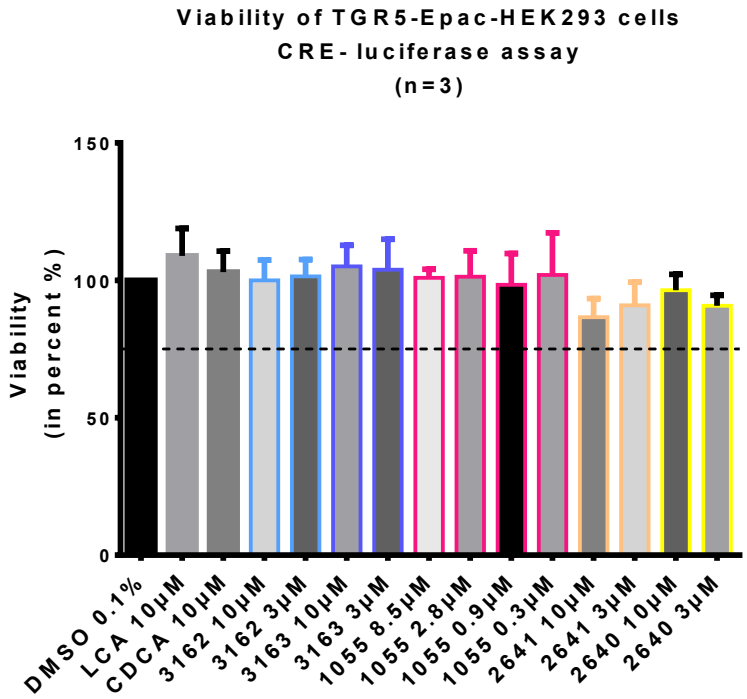

Figure 53: Determination of the viability of the TGR5-Epac-HEK293 cells in the CRE-luciferase assay after treatment with different concentrations of 3162, 3163, 1055, 2641 and 2640.
The viability of the TGR5-Epac-HEK293 cells is determined by measuring the GFP fluorescence, which is a surrogate parameter for the viability. A viability higher than 75% relative to the control is referred to as non-toxic. This threshold is marked with a horizontal line. The data represents the measurement of three biological replicates, which are measured in quadruplicates.

6.2 Viability data of the CRE- luciferase assay in HEK293 cells

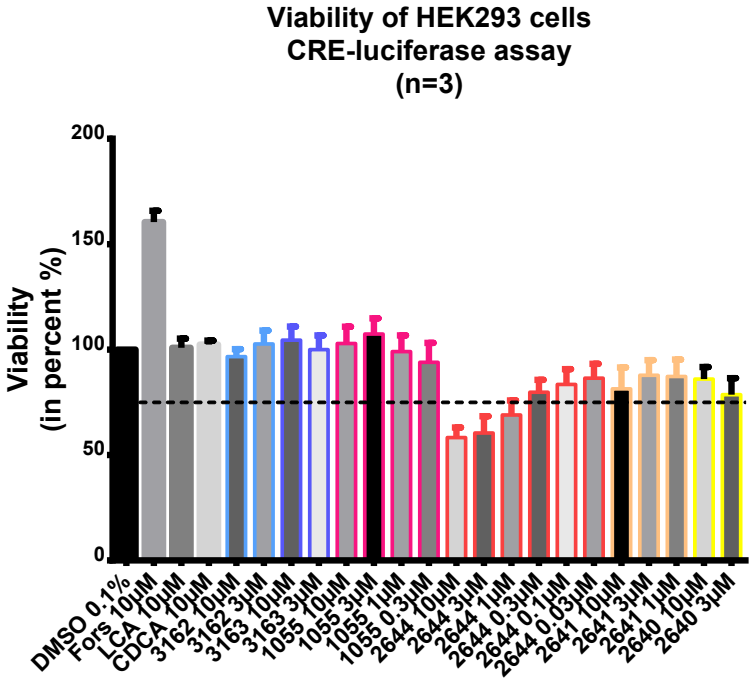

Figure 54: Determination of the viability of the HEK293 cells in the CRE-luciferase assay after treatment with different concentrations of 3162, 3163, 1055, 2644, 2641 and 2640.
The viability of the HEK293 cells is determined by measuring the GFP fluorescence, which is a surrogate parameter for the viability. A viability higher than 75% relative to the control is referred to as non-toxic. This threshold is marked with a horizontal line. The data represents the measurement of three biological replicates, which are measured in quadruplicates.

6.3 Viability data of the FXR-Gal4-luciferase assay in HEK293 cells

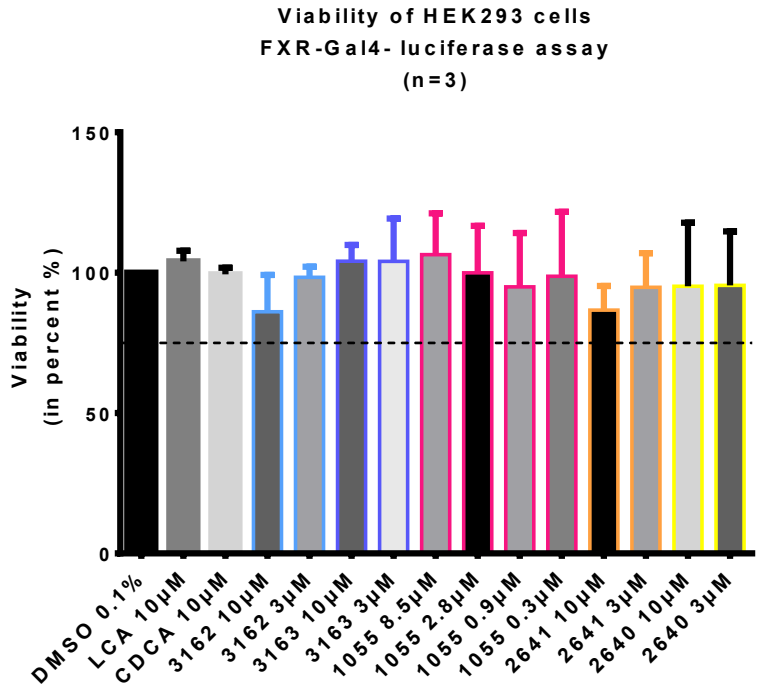

Figure 55: Determination of the viability of the HEK293 cells in the FXR-Gal4-luciferase assay after treatment with different concentrations of 3162, 3163, 1055, 2641 and 2640.
The viability of the HEK293 cells is determined by measuring the GFP fluorescence, which is a surrogate parameter for the viability. A viability higher than 75% relative to the control is referred to as non-toxic. This threshold is marked with a horizontal line. The data represents the measurement of three biological replicates, which are measured in quadruplicates.

7 Acknowledgements

I would like to thank Univ.-Prof. Dr. Dirsch for giving me the opportunity to carry out the research for my master´s thesis in the Molecular Targets group at the Department of Pharmaceutical Sciences at the University of Vienna. By working in the department, I have obtained insights into the scientific working methods, and I am grateful to have gained this invaluable experience. I would also like to thank the team of the Molecular Targets group, which welcomed me very nicely and supported me in my daily work. It was great to be part of the team and I will always remember this time in a good way.

Special thanks go to Mag. Dr. sc. ETH Alexander Perhal, who supervised me during the whole time in the lab and supported me even afterwards during the writing process of my master´s thesis. I would like to thank him for his constant support, his advice, and the kindness.

I would also like to thank my family for their great support and for always standing behind me during the whole time of my study.

Finally, thanks to my friends as well as my fellow students, with whom I could always talk and who encouraged me.